Department of Mechanical Engineering

Characteristics of Multimode Heat Transfer in a Differentially - Heated Horizontal Rectangular Duct

Panitan Wangdhamkoom

This thesis is presented for the Degree of
Master of Engineering
of
Curtin University of Technology

February 2007

Declaration

To the best of my knowledge and belief this thesis contains no material previously published by any other person except where due acknowledgment has been made.

This thesis contains no material which has been accepted for the award of any other degree or diploma in any university.

Signature: …….

Date: ……...

ACKNOWLEDGMENTS

I wish to acknowledge the contribution and support of the people that I have met during my study for the Master Degree at Curtin University of Technology, Australia.

Dr. Ramesh Narayanaswamy, my supervisor, my first advisor to the higher degree study. He is very gentle and kind. His knowledge to the field of my study, combined with his superior support is highly appreciated.

Associate Professor Dr. Tilak T. Chandratilleke, my co-supervisor, who always provides me with invaluable suggestions, understanding and superior supports.

Associate Professor Dr. Ian M. Howard and Dr. Kian K. Teh who both were my class lecturers. They also extended their kindness to me when I went on with the research.

My father, my mother and my little brother who keep sending heartedly, sincerely support to me while I am abroad.

My company, PTT Exploration and Production Plc., who provides financial support throughout the study. Their contribution to encourage their staffs taking further study is highly appreciated. I would like to thank especially to Miss Kancharat Ponghirun, Mr. Preecha Tienchai and Mr. Vuthiphon Thuampoomngam for their understanding and strong support.

And it would not be completed if I never mention my friends, whether whom I have just met in Australia or have already known in Thailand, especially to Mr. Anusak, Mr. Krittanan and Mr. Ponlawat. They always give my study time here enjoyable and having plenty of happiness.

TABLE OF CONTENTS

NOMENCLATURE

a	absorption coefficient, 1/m
A	cross sectional area, m^2
AR	duct aspect ratio, W/H
D_h	hydraulic diameter, $D_h = 2(WH)/(W+H)$
g	gravitational acceleration, m/s^2
Gr	Grashof number, $Gr = g\,\beta(T_h-T_c)\,H^3 / \nu^2$
Gr*	modified Grashof number, $Gr = g\,\beta\,q''H^4 / k\,\nu^2$
h	heat transfer coefficient, $W/m^2{\cdot}K$; enthalpy, J
I	radiation intensity, $W/m^2{\cdot}sr$
H	duct height, m
k	thermal conductivity of air, W/m·K
L	duct length, m
n	refractive index of the medium
Nu	Nusselt number, $Nu = h\,D_h / k$
p	static pressure, Pa
Pr	Prandtl number
Pl	Planck number
q″	heat flux, W/m^2
Ra	Rayleigh number, Ra = GrPr

Re	Reynolds number, $Re = U_{in}D_h/\nu$
S	path length, m
t	time, s
T	temperature, K
T*	dimensionless temperature, $T^* = (T-T_c)/(T_h-T_c)$
u	fluid velocity in the x-coordinate direction, m/s
U	average fluid velocity in the direction of flow, m/s
v	fluid velocity in the y-coordinate direction, m/s
w	fluid velocity in the z-coordinate direction, m/s
W	width of the duct, m
x	x-coordinate, m
y	y-coordinate, m
z	z-coordinate, m
Z	dimensionless z-coordinate, $Z = z/D_h$

Greek Symbols

β	thermal expansion coefficient,1/K
ε	emissivity
ν	kinematic viscosity, m^2/s
Φ	phase function
Ω′	solid angle, sr

σ_s	scattering coefficient, 1/m
σ	Stefan-Boltzmann constant (5.672×10^{-8} W/m $^2 \cdot K^4$)

Subscripts

avg	average
b	bulk mean temperature
c	cooled
con	convection
h	heated, hydraulic
i	inlet
l	local
rad	radiation
tran	transverse

ABSTRACT

This study presents the numerical analysis of steady laminar flow heat transfer in a horizontal rectangular duct with differential heating on the vertical walls. Three heating configurations: one uniform wall temperature (CS1) and two linearly varying wall temperature cases (CS2 and CS3) are analysed. The study considers the combined effects of natural convection, forced convection and radiation heat transfer on the overall heat transfer characteristics. Air, which is assumed to be a non-participating medium, is chosen as the working fluid. A computational fluid dynamics solver is used to solve a set of governing equations for a range of parameters.

For chosen duct aspect ratios, the numerical model simulates the flow and heat transfer for two main effects: buoyancy and radiation heat transfer. Buoyancy effect is represented by Grashof number, which is varied from 2,000 to 1,000,000. The effect of radiation heat transfer is examined by choosing different wall surface emissivity values. The weak and strong radiation effect is represented by the emissivity values of 0.05 and 0.85 respectively. Three duct aspect ratios are considered - 0.5, 1 and 2.

The heat transfer characteristics of all the above heating configurations - CS1, CS2, and CS3 are analysed and compared. The numerical results show that, for all heating configurations and duct aspect ratios, the overall heat transfer rate is enhanced when the buoyancy effect increases. Since buoyancy effect induces natural circulation, this circulation is therefore the main mechanism that enhances heat transfer. Radiation heat transfer is found to significantly influence convection heat transfer in high Grashof numbers.

CHAPTER 1
INTRODUCTION

1.1 Background

The cooling (or heating) passage is basically a channel that is an integral part of a heat exchange system used to exchange heat with its surroundings *via* one or more heat transfer modes. There are several engineering applications that incorporate this concept; for example, the cooling of electronic components in circuitry devices, compact heat exchangers, and gas turbine blade cooling passages. In order to achieve the desired heat exchange duty in any application, it is important to understand the heat transfer mechanisms inside a passage. These mechanisms are driven by a variety of parameters, which mainly are types and conditions of the flow, geometry and material of the passage, properties of fluid, and the thermal boundary conditions.

There are several parameters that can be studied in the area of heat and fluid flow through a cooling/heating passage. Laminar flow in a rectangular passage has received great attention due to its simplicity and the range of applications. Laminar flow in a rectangular duct is not difficult to set up in an experiment, and several studies have been done in this area for both natural and forced convection heat transfer. However, many of the studies have considered convection to be the only mode of heat transfer. Radiation and conduction heat transfer are normally neglected.

In reality, all of the three modes of heat transfer - conduction, convection, and radiation are present in any given physical situation. The boundary conditions on the walls of the duct are also varied. Most of the studies consider uniform heating, which is either uniform temperature or uniform heat flux on the wall boundary conditions. Real applications, however, have non-uniform heating situations. It is therefore interesting to note that research on the heat and fluid flow characteristics of a passage requires considerable attention.

1.2 Research Objective

The aim of the present study is to investigate the heat transfer characteristics of convective heat transfer in a horizontal rectangular duct heated from the vertical side walls with interaction from thermal radiation. The numerical study is carried out for laminar flow of air through a rectangular duct, focusing on the mixed convection flow regime. Radiation heat transfer from the internal walls of the duct is considered. The analysis is performed for a range of thermal and geometric parameters, and boundary conditions. The results of the study are used to obtain further understanding on the effect of the interaction of different modes of heat transfer on the overall heat transfer rates.

1.3 Research Approach

The study is carried out numerically using a CFD software package - FLUENT. The numerical results obtained are analysed and presented in terms of dimensionless parameters. The effects of various parameters on the fluid flow and heat transfer characteristics are brought out by means of several graphs and discussion.

1.4 Structure of the Thesis

The thesis begins with an introduction and aim of the research in the introductory chapter. Chapter 2 is devoted thoroughly to the literature review, which presents the previous studies in the area relevant to the current research. This is then followed by the scope of the present study which is presented at the end of the chapter.

The development of numerical modelling used to solve the research problem is described in detail in Chapter 3. Grid independence study and the validation of numerical modelling are included in this chapter. This validation allows the formulated model to be applied with confidence for detailed analysis of the current work.

Chapters 4 to 6 present the results and discussion from different heating boundary conditions and range of parameters that apply to a horizontal rectangular

duct. Three case studies, each of them representing a specific heating boundary condition, are presented separately in these chapters. Finally, the conclusions drawn from the analysis of results are presented in Chapter 7.

1.5 Closure

This chapter has provided an introduction of the problem and the objectives of the research. The structure of the thesis is also presented to give an overview of the contents of the thesis.

In the next chapter, the literature review and scope of the present work will be presented in detail.

CHAPTER 2
LITERATURE REVIEW

2.1 Introduction

The review of previous studies in the area of laminar flow in a horizontal rectangular channel is presented in this chapter. The development of the knowledge of flow and heat transfer characteristics, important parameters that govern the problem, and boundary conditions are reviewed. This will help develop the ideas of the work scopes in the present work.

A detailed review of literature is presented next. This is followed by a summarised table that provides a concise presentation of the development of studies done in the past. Finally, the scope of work of this thesis is presented.

2.2 Laminar Flow in a Horizontal Rectangular Duct

The geometry of a rectangular duct is more complex than a circular tube. It consists of width and height, which has to be considered in the analysis in every cross sectional plane compared to the radius of a tube in the case of circular tube. This indicates that the flow and heat transfer characteristics of a rectangular duct requires more parameters to model than a circular geometry. As a consequence, heat exchange process in a rectangular duct depends on the aspect ratio as well as the boundary conditions (heating/cooling) that is applied on each side of the duct. Different heating/cooling conditions lead to different fluid flow and heat transfer characteristics, and hence require extensive studies.

Laminar flow in a horizontal rectangular duct has been investigated by many researchers, especially the configuration wherein the flow is heated from the bottom wall. A review of literature relevant to the flow in rectangular ducts that are heated from the bottom wall is given below.

Naito [1] conducted an analytical study for thermal and velocity boundary layer development in the entrance region of parallel plates using Karman-Pohlhausen method. The flow was assumed to be laminar, and both parallel walls had uniform

heat flux boundary conditions. This study also included a case in which one wall was insulated, while the opposite wall was held at the uniform heat flux. The results were presented as variation of thermal boundary thickness and Nusselt numbers for Prandtl number in the range between 0.01 to 1000.

Ozoe et al. [2] studied experimentally the rates of heat transfer for laminar natural convection in a bottom-heated and top-cooled rectangular channel. Air and silicone oil were used as the fluid medium in this study. The aspect ratios (width/height) were varied from 1 to 15.5 in suitable steps, and Rayleigh numbers were varied from 3,000 to 10,000. The channel was also rotated from 0° to 180° to investigate the inclination effect. Correlations were formulated for both maximum and minimum values of average Nusselt number as a function of the aspect ratio.

Incropera and Maughan [3] experimentally studied laminar flow through parallel plates forming a channel which had an aspect ratio of 10, and heated by uniform heat flux from the bottom plate. They studied the variation of the average Nusselt number for Re = 125 to 500, and Gr* = 7000 to 1,000,000 for both horizontal (zero degree) and inclined channel (up to 30°). The onset of thermal instability was detected downstream from the inlet, and was found to eventually enhance the heat transfer. Further study resulted in correlations [15].

Chiu and Rosenberger [4] investigated the entrance effects in the mixed convection flow from two horizontal differentially-heated parallel plates. The study was conducted for nitrogen gas by laser Doppler anemometry in a range of $1368 < Ra < 8300$, and $15 < Re < 170$. Two entrance lengths were deducted from velocity profiles: one for the onset of instability, and one for the full development of the mixed flow. Further study was carried out [5] to obtain fully developed velocity profiles in a range of $2472 < Ra < 8300$, and $15 < Re < 150$. The results showed that transverse velocities of the longitudinal convection rolls were independent of the forced flow.

Smyth and Salman [6] carried out the experiments on the combined free and forced convection of an air flow in the horizontal parallel plates of aspect ratio 5:1. The bottom plate was heated uniformly, while the top plate had both heated and

unheated boundary conditions. The vertical side walls were unheated. Velocity and temperature profiles obtained showed that the secondary flow created by free convection heat transfer caused significant influence on the flow behaviour, and the heat transfer rate from the bottom plate.

Nyce et al. [7] studied mixed convection in a rectangular channel with a bottom-heated wall by using Doppler Anemometry technique for nitrogen as a fluid. At a Rayleigh number of 22200, they reported that unsteady flows were found even for a Reynolds number of 18.75. The heat conduction at the side walls was also included in the study. The results showed that transverse velocities were found to be independent of Re.

Huang and Lin [8] studied mixed convection in a rectangular channel with bottom-heated and top-cooled boundary conditions by using a numerical method. For a wide range of Gr/Re^2, they covered the flow regime from steady laminar longitudinal vortex flow to unsteady chaotic flow. They concluded that the buoyancy induced flow can cause chaotic flow in the downstream for Gr/Re^2 values from 25 to 40, for Re and aspect ratios of 500 and 2 respectively.

Yan [9] conducted a study for combined mixed convection and mass transfer in the horizontal rectangular ducts. Air was used in the simulation study over a range of parameters. The results showed that the distribution of local Nusselt number was characterized by a decay near the inlet, where the forced convection entrance effect dominated. Thereafter, the decay was attenuated by the onset of buoyancy-driven secondary flow.

Lin and Lin [10] performed an experimental study for an airflow in a bottom-heated horizontal rectangular duct. Their results agreed with the previous study that the onset of thermal instability was detected. This instability was found to move upstream for higher Grashof numbers, or to be delayed for a larger Reynolds number. The flow regime map and correlations were presented.

Corcione [11] studied the bottom-heated rectangular duct with aspect ratio from 0.66 to 8, and Rayleigh numbers from 10^3 to 10^6. With the change of adiabatic

boundary condition at the side walls to cooling (or heating) walls, the heat transfer effectiveness at the bottom wall improved.

Wang et al. [12] furthered the study of mixed convection laminar flow in a horizontal rectangular duct heated from the bottom wall by investigating the effect of constant and variable fluid properties. The Boussinesq approximation was applied to the constant properties model, while the state equation of an ideal gas and power law correlations were used to model of the variable properties.

The studies of laminar mixed convection in a horizontal rectangular channel heated from below suggested that the buoyancy forces induced by bottom wall heating increased the heat transfer rate prior to the onset of instability. Moreover, the onset of instability was delayed by reducing the Grashof number or increasing the Reynolds number. Most of the studies had been done using air as the fluid medium.

2.3 Duct with Side Wall Heating

In a different manner, when the heating orientation changed from bottom to side wall heating, the above studies were inappropriate to identify the heat transfer characteristics. The studies of mixed convection for a side wall heated channel conducted in the past were limited to vertical channel configurations, in which the flow either assisted or opposed the natural convection created by heated vertical walls. The conditions are different from side wall heating in a horizontal duct, where the development of natural convection flow is perpendicular to the direction of the flow. There are a few studies on such configurations and has the same potential applications as in the case of bottom wall heating. Some selected studies of mixed convection in a horizontal channel heated from side walls are reviewed below.

Silekens et al. [13] used water as the fluid medium passing through a rectangular duct heated symmetrically from side walls. Their study was carried out by both experimental and numerical methods with Re = 500 and Gr varied around 10^5. Their results showed that the resulting secondary flow induced by buoyancy forces caused a substantial increase in heat transfer.

Gau et al. [14] investigated the mixed convection in the rectangular channel heated from one side while the remaining walls were insulated. They studied the flow conditions for a range of Re from 317 to 2000, and buoyancy parameter Gr/Re^2, from 0 to 20,000. They found that the heated buoyant flow, which accumulated in the upper region of the channel, was thermally stable, and had slower motion which could reduce the heat transfer enhancement by the buoyancy force. Their experimental results were correlated for Nusselt number as a function of buoyancy parameter.

2.4 Radiation Heat Transfer in a Rectangular Duct

In addition to mixed convection heat transfer, radiation heat transfer is always involved in the heat exchange process. Combined convection and radiation heat transfer in the rectangular duct has been studied by several researchers to explore the effects that dominate the combined mode of heat transfer.

Im and Ahluwalia [16] conducted an analytical study to investigate the combined effects of convection and radiation in rectangular ducts. Their sample calculations identified the physical differences between forced convection and gas radiation heat transfer mechanisms. The effects of thermal radiation to field velocity and skin friction were also presented.

Huang et al. [17] investigated the combined effects of radiation and laminar mixed convection in an isothermal rectangular channel. The mixed convection and radiation were formulated by the vorticity-velocity of Navier-Stokes equation and integral formulation for radiation equation. Gray fluid was employed in the mixed convection flow regime. The study reported that buoyancy forces led to significant enhancement in heat transfer in the entrance region.

Yang et al. [18] studied the combined effects of forced convection and radiation heat transfer in rectangular and equilateral isothermal cross sections. The study was extended in [19] for arbitrary shaped ducts. Their numerical results for participating medium reported that the wall emissivity was one of the major parameters that controlled combined heat transfer in the irregular ducts. Furthermore, the total Nusselt number increased as radiation effect increased.

Krishnan et al. [20] proposed a correlation for combined natural convection and radiation between parallel vertical plates. In this experimental study, air was used as the fluid medium between parallel plates. The results were presented in a correlation equation form, and reported that the reduction of non-dimensional temperature excess of the heated plate was due to the effect of radiation heat transfer.

2.5 Non-uniform Heating

The previous sections considered the heated walls as either uniform temperature or heat flux. However, in the area of non-uniform heating, where temperature and heat flux are no longer uniform, few studies are reported.

Ostrach [21] conducted an analytical study of laminar flow through vertical parallel plates with combined forced and natural convection effects. The heated wall temperatures were considered to be linearly varying along the height of plates. The flow entered the channel from bottom and assisted the body forces which were moving upward. Modified Rayleigh number was found to be one of the important parameters of this heating configuration. The solutions obtained were tabulated for simple usage and sufficiently accurate for modified Rayleigh numbers up to 10^4.

Chen et al. [22] performed a numerical study to investigate the flow and heat transfer characteristics of laminar natural convection flow in horizontal, inclined and vertical parallel plates. They considered both variable temperature and variable heat flux as a polynomial function of axial distance. Correlations were proposed on the special condition where temperature or heat flux was uniform.

Basak et al. [23] studied numerically a steady laminar natural convection flow in a square cavity with uniformly and non-uniformly heated bottom wall. They applied a sinusoidal function to the non-uniform temperatures at the bottom wall. The range of Rayleigh ($10^3 \le \mathrm{Ra} \le 10^5$) and Prandtl ($0.7 \le \mathrm{Pr} \le 10$) numbers were considered. Correlations for average Nusselt number as a function of Rayleigh number were proposed.

In the previous paragraphs, several studies that developed the foundation for the present study were presented. The next section summarises these studies in chronological order to give a brief and easy picture of what has been already done.

2.6 Summary of Reviewed Research

The literature review from the previous section is summarised in chronological order to give a brief description of previous studies for the research of flow in a horizontal rectangular channel.

Year	Authors	Remarks
1954	Ostrach	Numerical study of combined forced and natural convection in vertical parallel plates was conducted for linearly variable temperatures profile at the heated plates.
1975	Naito	Formulated an analytical approach for boundary layer development in the entrance region of the parallel plates using Karman-Pohlhausen method.
1975	Ozoe et al.	Proposed correlations from experimental study for laminar flow in bottom-heated and top-cooled channel for a range of aspect ratios and Rayleigh numbers.
1984	Im and Ahluwalia	Analytical study for the combined effect of convection and radiation in rectangular ducts.
1986	Chen et al.	Conducted a study of laminar natural convection in horizontal, inclined and vertical parallel plates heated by either variable temperature or heat flux.
1987	Incropera and Maughan	Reported the experimental study of laminar flow in horizontal and inclined bottom-heated parallel plates. Onset of thermal instability was detected for a range of experimental parameters.

Year	Authors	Remarks
1987	Chiu and Rosenberger	Detailed study of the entrance effect in mixed convection flow through parallel plates heated from below was presented by using laser Doppler anemometry technique. Nitrogen was used as a fluid flow media.
1987	Chiu and Rosenberger	Extended the above study in the region of fully developed velocity profiles.
1990	Incropera and Maughan	Extended their earlier study and successfully proposed correlations.
1990	Huang et al.	Reported the combined effect of radiation in laminar mixed convection flow domain. Buoyancy effect was found to enhance heat transfer in the entrance region.
1991	Smyth and Salman	Conducted the study for mixed convection in horizontal parallel plates heated from bottom for a set of boundary conditions to study the effect of secondary flow to the flow behaviours and heat transfer process of the bottom plate.
1991	Yang et al.	Combined effect of radiation and forced convection in rectangular and equilateral isothermal cross sections was studied by numerical approach.
1992	Nyce et al.	Studied mixed convection using nitrogen in bottom-heated channel. The unsteady flow that occurred for a range of parameters was reported.
1992	Yang and Ebadian	Extended their previous study to arbitary shaped ducts. Some of the parameters, such as emissivity, were investigated to see their effects to the combined flow.

Year	Authors	Remarks
1994	Huang and Lin	Studied the flow regime from steady laminar to the onset of chaotic flow for a range of buoyancy parameters (Gr/Re^2) in bottom-heated channel by using numerical method.
1996	Yan	Investigated the effect of combined mixed convection and mass transfer in a bottom-heated horizontal rectangular duct to thermal buoyancy force, friction factor ratio, Nusselt and Sherwood number.
1996	W.L. Lin and T.F. Lin	The airflow in bottom-heated horizontal rectangular channel was studied to construct the flow regime map and correlations
1998	Silekens et al.	Symmetrically side wall heating was investigated for water flow in a rectangular channel. The results showed substantial increase in heat transfer due to buoyancy forces.
2000	Gau et al.	Studied experimentally the behaviour of the mixed convection flow in a channel heated from one side wall. The flow was found to be thermally stable when heated from a side.
2003	Corcione	Extended the boundary conditions of the bottom - heated rectangular channel to study the heat transfer effectiveness when side walls are under cooling or heating instead of adiabatic boundary condition.
2003	Wang et al.	The effects of constant and variable properties were investigated for mixed convection in channel heated from bottom.

Year	Authors	Remarks
2004	Krishnan et al.	Proposed the correlation for combined natural convection and radiation between vertical parallel plates. Excessive temperature on the heated plate was found to be reduced by radiation heat transfer.
2006	Basak et al.	Presented a study of laminar natural convection flow in a square enclosure where bottom wall was heated by a uniform or a sinusoidal-profile temperature.

2.7 Scope of the Present Work

From a review of published literature, it is clear that side wall heating has received considerably less attention compared to the bottom wall heating, despite the fact that side wall heating is quite common in terms of applications. Regarding the available studies on side wall heating, it is seen that this configuration has potentially enhanced the heat transfer with a benefit of having thermal stability, wherein the bottom wall heating usually becomes thermally unstable for a high buoyancy parameter.

In addition, most of the studies in literature investigated the combined effect of radiation only for gray fluids. Radiation effect that takes place in mixed convection was usually neglected by several researchers due to the assumption that it had small or negligible effects, especially when the problem dealt with air (being a non-participating medium). However, radiation heat transfer effect becomes more important when the flow is under high temperature.

In this study, air is used as the fluid flowing through a rectangular duct. Although air is a non-participating medium, and radiation heat transfer depends only on geometry of the duct and the wall temperatures, the flow is still indirectly affected by radiation heat transfer. This is due to the flow acquiring additional convective thermal energy obtained from the duct walls, which are at a certain temperature.

These walls interact among themselves radiatively exchanging thermal energy. Hence, the effect of radiation heat transfer, in some conditions, cannot be neglected. As a result, it is interesting to include the effect of radiation along with the mixed convection problem. The result of such an analysis would lead to better understanding and prediction of the flow and heat transfer characteristics.

The present study is conducted considering laminar mixed convection of airflow in a horizontal rectangular duct with the combined effect from radiation heat transfer. The problem is studied numerically using a computational fluid dynamics software package. The thermal entrance region is one of the main regions of interests in the study. The airflow is assumed to be hydrodynamically fully developed at the inlet, while developing thermal boundary layers is assumed inside the duct, where heating occurs. A range of parameters - Grashof number, emissivity and duct aspect ratio is used to determine the flow and heat transfer characteristics. Reynolds number is fixed at a constant value to ensure that forced convection is in the laminar flow regime. For all boundary conditions of the side wall heating, the cooled wall, which is opposite to the heated wall, is considered to have an isothermal temperature. The temperature of the cooled wall is always maintained at the fluid inlet temperature. The horizontal walls (top and bottom walls) are insulated.

Three heating configurations are studied. There are one uniform temperature (Case Study 1, CS1), and two linearly varying temperature profiles (Case Study 2, CS2; Case Study 3, CS3). For the linearly varying temperature cases, a linear temperature profile, in which temperature linearly varies from T_h to T_c is applied to the heated wall. There are two heating configurations for linearly varying temperature cases: one that starts with T_h at the bottom and linearly decreases to T_c at the top (case study 2, CS2), and another one that starts with T_c at the bottom and linearly increases to T_h at the top (case study 3, CS3). Figure 2.1 shows the three heating configurations.

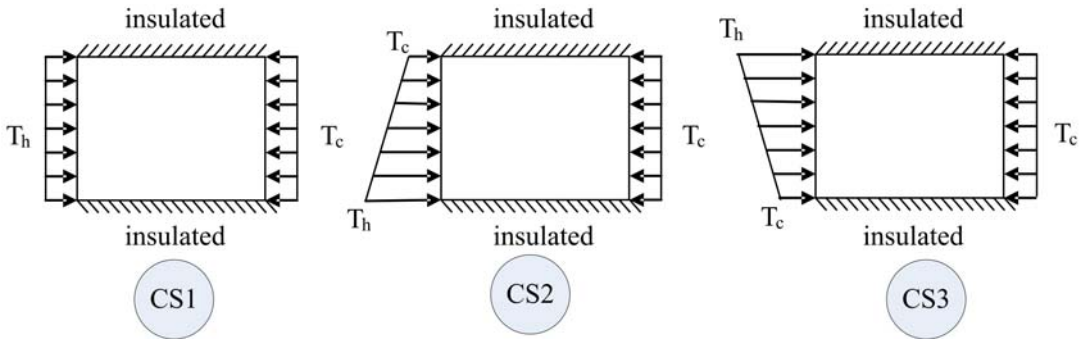

Figure 2.1 Schematic diagram of three heating configurations

The variable temperature heating has the potential application in the study of turbine blade cooling channel, in which the temperatures at leading edge area vary largely from the trailing edge. It is also a simplified form of variable heating, which is common in many engineering applications.

In summary, the present study investigates two main heating scenarios: uniform temperature and variable temperature. The results provide additional knowledge and better understanding of the heat transfer mechanisms applicable for the design of heat exchange systems.

2.8 Closure

This chapter has reviewed several previous studies on flow and heat transfer characteristics of laminar mixed convection in a horizontal rectangular duct. The review has led to the development of the scope of the present study as well as the fundamental knowledge of the phenomena of the flow in a heated duct, which is essential to help formulate the required model in the next chapter.

In the next chapter, the numerical model, which is used to solve the current problem stated in this chapter, is formulated and presented.

CHAPTER 3
NUMERICAL MODELLING

3.1 Introduction

The present study is performed by using a numerical method. In this chapter, the development of numerical modelling is presented. First, the assumptions are stated, followed by modelling of the rectangular duct, in which grid independence study is carried out. Then, appropriate flow models and associated modelling parameters are chosen. Finally, the formulated model is validated by comparing the results obtained with that available in literature.

The model of a rectangular duct is constructed by GAMBIT [27] and then exported to the CFD solver FLUENT [28] where the boundary conditions and other parameters are applied.

3.2 Problem Statement

Considering laminar flow in a horizontal rectangular duct. Hydrodynamically fully-developed flow enters the duct inlet with a temperature T_i, and average velocity U_i. When the fully-developed flow enters the duct, it is heated by one vertical wall which has a heating temperature profile as indicated in each case study. The other vertical wall directly opposite to the heated wall is maintained at a uniform temperature, and equal to the inlet temperature of air. This cooled wall has the same uniform temperature as inlet air temperature ($T_c = T_i$) for all heating configurations considered in the present study. The top and bottom walls of the rectangular duct are insulated, and hence no heat transfer takes place across these two walls. The length of the duct is sufficiently long for the thermal boundary layers to grow and become fully developed. The present study is concentrated in the region of a fully-developed hydrodynamic boundary layer, and a thermally developing boundary layer in the duct. Radiation heat transfer takes place among the inside walls of the duct.

The flow and heating conditions are expressed in terms of dimensionless parameters. Natural convection, forced convection, and radiation heat transfer are the modes of heat transfer considered. The Reynolds number of the flow entering the duct is fixed at 100, while Grashof number is varied from 2,000 to 1,000,000. The Gr/Re^2 ratios are in range from 0.2 to 100 which is adequate to study the flow and heat transfer characteristics from conditions dominated by forced convection, to mixed convection, and eventually to natural convection heat transfer.

The duct sizes are represented by aspect ratios. Three different aspect ratios - 0.5, 1 and 2, are chosen to study the effect of duct size on the heat transfer characteristics. The aspect ratio of the duct is defined as,

$$\text{Aspect Ratio (AR)} = \frac{\text{Width}}{\text{Height}} \tag{3-1}$$

Figure 3.1 illustrates the width and height of cross section of a rectangular duct.

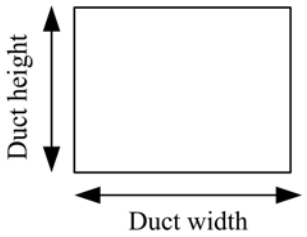

Figure 3.1 Schematic diagram of the duct cross section showing duct width and height

In order to investigate the effect of radiation on the flow and heat transfer in a rectangular duct, two radiation cases - strong and weak radiation, are simulated for each convection heat transfer condition, and for each duct size. Strong and weak radiation cases are represented by two wall surface emissivity values: 0.85 and 0.05 respectively. These emissivity values are applied to the surface of all duct walls.

3.3 Assumptions

The following assumptions are made in the present work:

- The airflow is laminar.
- The flow is modelled to be steady and incompressible.

- The flow has no-slip condition at all the walls of the duct.
- Density, viscosity, specific heat and thermal conductivity of air are a function of temperature only. Other fluid properties are assumed to be constant.
- Conduction heat transfer is neglected.
- Air is assumed to be non-participating as far as radiation is concerned.
- The duct surfaces are diffuse and gray.

3.4 Numerical Formulation

3.4.1 Governing Equations

To solve for flow and heat transfer, three basic governing equations are applied to laminar flow in a rectangular duct. These equations are:

Continuity equation

$$\frac{\partial \rho}{\partial t} + \nabla \cdot (\rho \vec{v}) = 0 \tag{3-2}$$

where $\vec{v} = u + v + w$. Equation (3-2) is regarded as the conservation of mass. The conservation of momentum equation is written as,

Navier-Stokes (momentum conservation) equation

$$\frac{\partial (\rho \vec{v})}{\partial t} + \nabla \cdot (\rho \vec{v} \vec{v}) = -\nabla p + \nabla \cdot (\bar{\bar{\tau}}) + \rho \vec{g} + \vec{F} \tag{3-3}$$

where p is the static pressure, $\bar{\bar{\tau}}$ is the stress tensor, and $\rho \vec{g}$ and $\vec{F}$ are the gravitational body force and external body forces, respectively. For modelling the heat transfer problem, energy equation is also required.

Energy equation

$$\frac{\partial(\rho E)}{\partial t} + \nabla \cdot (\vec{v}(\rho E + p)) = \nabla \cdot (k\nabla T + (\bar{\bar{\tau}} \cdot \vec{v})) \tag{3-4}$$

where $E = h - \frac{p}{\rho} + \frac{|\vec{v}|^2}{2}$, h is the enthalpy.

Because of the steady flow condition, the time-dependant terms on the left hand side of equations (3-2), (3-3) and (3-4), which express the change of fluxes over time, are equal to zero.

In addition to these basic flow and energy equations, a radiation model is required to provide a complete mathematical description of the problem. It is formulated using the radiative transfer equation (RTE).

Radiative Transfer Equation (RTE)

For radiation that concerns absorption and scattering, the radiative transfer equation is written as,

$$\frac{dI(\vec{r},\vec{s})}{ds} + (a + \sigma_s)I(\vec{r},\vec{s}) = an^2\frac{\sigma T^4}{\pi} + \frac{\sigma_s}{4\pi}\int_0^{4\pi} I(\vec{r},\vec{s}')\Phi(\vec{s}\cdot\vec{s}')d\Omega' \tag{3-5}$$

where $\vec{r}$, $\vec{s}$, $\vec{s}'$ are the position vector, direction vector and scattering direction vector, respectively.

The Discrete Ordinate (DO) radiation model is chosen to solve for the radiation problem. This model considers radiative transfer equation (RTE) in the direction $\vec{s}$ as a field equation. Thus the RTE can be written as,

$$\nabla \cdot (I(\vec{r},\vec{s})\vec{s}) + (a + \sigma_s)I(\vec{r},\vec{s}) = an^2\frac{\sigma T^4}{\pi} + \frac{\sigma_s}{4\pi}\int_0^{4\pi} I(\vec{r},\vec{s}')\Phi(\vec{s}\cdot\vec{s}')d\Omega' \tag{3-6}$$

The above equation is for the case when absorption and scattering are considered in the problem. Otherwise, radiative transfer equation which only considers emissivity between surfaces will be utilised. Equations (3-2), (3-3), (3-4)

and radiative transfer equation are discretised for the numerical model. These equations are the governing equations that describe the problem. Based on the assumptions stated earlier, and the discretisation schemes selected later on, the governing equations are applied to each nodal cell in the computation domain. The computation domain comprises numerical cells combined together to represent a chosen geometry. Therefore, the solution of the problem can be obtained by solving a set of equations from all numerical cells in the calculation domain, for the chosen geometry.

3.4.2 Modelling of a Rectangular Duct

Figure 3.2 shows the schematic diagram of a horizontal rectangular duct. The aspect ratios of the duct considered in the study are 0.5, 1 and 2, which refer to the physical cross-sectional sizes (height x width) of 50 × 25, 50 × 50 and 50 × 100 mm, respectively.

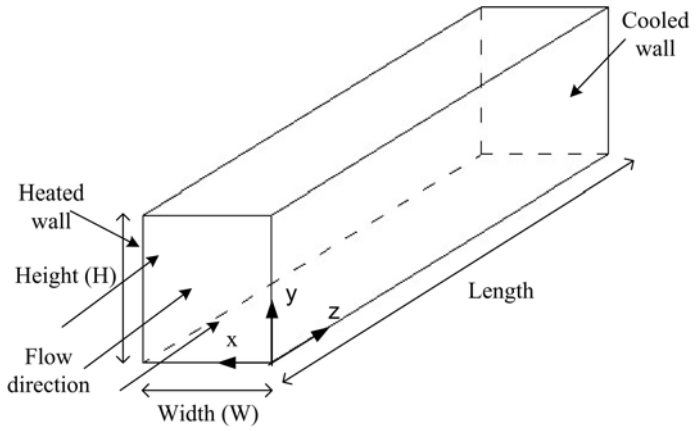

Figure 3.2 Schematic diagram of a horizontal rectangular duct

The duct length has been primarily calculated based on equation (3-7) which is derived from Bejan [31]. For completeness, the relevant equation is given below.

$$\frac{z_{thermal}}{D_h} \cong 0.05\,Re_{D_h}\,Pr \tag{3-7}$$

where $z_{thermal}$ is the length of the duct in which the thermal boundary layers are regarded as fully developed. Table 3-1 shows the calculations.

Table 3-1 Calculations for thermal entrance length based on [31]

Aspect ratio	Cross-sectional duct size (Height x Width), mm	Hydraulic diameter, mm	Re	Pr	Estimated thermal entrance length from Bejan[31], mm
0.5	50x25	33.33	100	0.71	118.32
1	50x50	50	100	0.71	177.50
2	50x100	66.67	100	0.71	236.68

From the above Table, a duct length of 400 mm is chosen for the present study in order to ensure the flow is thermally fully developed for all duct sizes.

All the duct walls are applied with boundary conditions as specified by the heating configurations (uniform and linearly varying temperature; CS1, CS2 and CS3). The results and discussion of these heating configurations are presented in three separate case studies on later chapters.

The CFD package, FLUENT, is used to solve the numerical model. The FLUENT's implicit Segregate 3-D solver is chosen for the present study due to its stability in handling incompressible steady flow problem. Another more sophisticated 3-D solver available in FLUENT called the Coupled solver was used to compare the results from Segregate solver for the preliminary study. This was done to ensure that the selected solver was capable of giving accurate results. The results obtained from both solvers had no significant difference. However, the Coupled solver required more computational resources than Segregate solver. As a result, the Segregate solver is selected for the analysis of all cases considered in the present study.

In order to obtain a fully developed velocity profile in a rectangular duct, the pre-run numerical simulation is carried out with periodic boundary conditions applied to both inlet and outlet. This type of boundary condition will create the fully developed velocity profiles in the steady-state solution. Without duct heating, the airflow is simulated to have steady-state condition where fully developed velocity profiles for all aspect ratios are obtained. These profiles are further validated with analytical solutions for laminar fully developed flow in a rectangular duct provided

by Marco and Han [25]. The results were found to be in very good agreement. Figure 3.3 shows the agreement between the present numerical work with the analytical solution for a typical case at the mid section. The profiles obtained can be readily applied to the present work without implementing additional programming from analytical formulae.

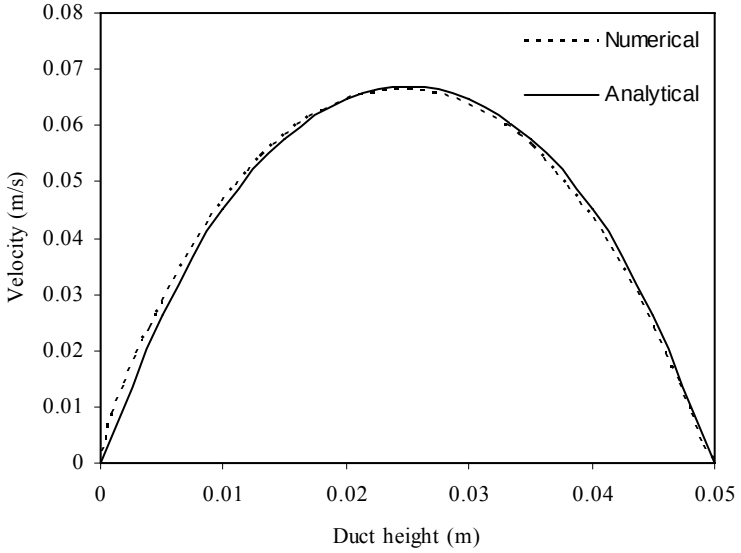

Figure 3.3 Comparison of fully developed velocity profile with Marco and Han [25] (x = 0.025 m , AR = 1)

The Body Force-Weighted scheme is applied for pressure discretisation. The Body Force-Weighted scheme is appropriate to capture the situations that involve the gradient of body forces similar to the current study in which body forces are induced by natural convection heat transfer. The SIMPLE algorithm [30, 33] is applied as a standard scheme for pressure-velocity coupling. Momentum and energy equations are discretised under Second Order Upwind scheme.

The Discrete Ordinate method [32, 34] is chosen to model radiation heat transfer. This model is appropriate to solve problems that involve diffuse gray as well as non-gray properties in radiation heat transfer.

The radiative and total heat fluxes of the heated wall are obtained from the converged results. The local Nusselt number for the wall is defined as

$$Nu_l = \frac{q'' D_h}{k(T_{wall} - T_b)} \tag{3-8}$$

where T_{wall} is the temperature of the wall. Thermal conductivity (k) of air is obtained based on material properties [29] at T_b, where T_b is the bulk mean temperature of the fluid at each cross section along the length of the duct, and is defined as

$$T_b(z) = \frac{1}{U(z)A} \int u(x,y,z)T(x,y,z)dA \tag{3-9}$$

where U(z) is the average fluid velocity at each cross section. The transverse average Nusselt number for each cross section along the heated wall is defined as

$$Nu_{trans,avg,h} = \frac{\int_0^H Nu_l \, dy}{H} \tag{3-10}$$

The convective and radiative Nusselt numbers are defined based on convective and radiative heat flux values respectively.

3.5 Grid Independence Study

The grid independence study was performed to find out appropriate grid sizes for the present work. There are three duct aspect ratios considered in the study. Each of them will be represented in the numerical model with appropriate grid sizes that will provide an acceptable level of accuracy of the results, and require acceptable amount of calculation time.

Three duct aspect ratios - 0.5, 1 and 2, have physical sizes of 50 × 25 × 400, 50 ×50 × 400, and 50 ×100 × 400 mm in Height × Width × Length, respectively. In the meshing scheme, each numerical node represents a specific size of real physical domain. Cross-sectional sizes (width and height) are the main consideration, while duct length is fixed at one millimetre per grid. At first, the grid

independence study considers aspect ratio of 2, due to its largest physical size in this present study and results in having the highest number of grids. The computer used in the study is a Pentium D processor computer. Considering the available computer resources, three grid sizes were selected for aspect ratio of 2: 50 × 25 × 400, 67 × 34 × 400 and 67 × 50 × 400, which follow the meshing dimensions of 2 mm per grid, 1.5 mm per grid, and less than 1.5 mm per grid, respectively.

Three grid sizes were tested in the heating configuration CS1 in which airflow and cooled wall have the same temperature at 300 K, while the temperature difference between heated and cooled walls is kept constant at 50 K. An average Nusselt number of the entire heated wall is calculated. The results are presented in Table 3-2.

Table 3-2 Grid independence study for aspect ratio 2

Grid size	No. of Grids	Average Nu at entire heated wall	% change	Computational time (hr:min)
50×25×400	500000	13.19	3.48	2:43
67×34×400	911200	12.75	0.02	4:05
67×50×400	1340000	12.75	0	5:46

The results show that the grid size 67 × 34 × 400 provides a small change in Nusselt number compared with the grid size 67 × 50 × 400 while having benefits of significantly less computational time. Therefore, for aspect ratio 2, a grid size of 67 × 34 × 400 is adopted.

For the aspect ratios of 0.5 and 1, finer meshing can be applied to acquire more accurate results. Grid sizes of 25 × 25 × 400, 50 × 50 × 400, and 60 × 60 × 400 which refer to 2 mm per grid, 1 mm per grid, and less than 1 mm per grid meshing concepts respectively, is considered. The results are shown in Table 3-3.

Table 3-3 Grid independence study for duct aspect ratio 1

Grid size	No. of Grids	Average Nu at entire heated wall	% change	Computational time (hr:min)
25×25×400	250000	9.01	12.5	2:13
50×50×400	1000000	10.28	0.1	4:10
60×60×400	1440000	10.29	0	4:36

As seen from the Table 3-3, the grid size 50 × 50 × 400 is found to be suitable for the current study due to an acceptable deviation of less than 1%, and having a reasonable computational time.

The aspect ratio of 0.5 is applied with the same meshing concept as aspect ratio 1, since finer grids do not provide any significant improvement in the result while consuming large amount of computer resources. Thus, aspect ratio of 0.5 is provided with a grid size of 25 × 50 × 400 (one millimetre per one grid).

In summary, grid sizes of 25 × 50 × 400, 50 × 50 × 400, and 67 × 34 × 400 have been chosen for aspect ratios 0.5, 1 and 2 respectively.

3.6 Solution Procedure

Starting with the assumed initial values, the governing equations are solved using the set of discretised equations for the first iteration. Iteration was continued until convergence criteria were satisfied. For convergence criteria, firstly, the flux variables are monitored. Convergence was obtained when the residual mass flux values become close to zero. In the present study, all simulation cases are satisfied this criterion with the mass flux residual less than 10^{-10} Kg/s. The net residual of radiation and total heat transfer rate were also maintained to be less than 1% of the total heat transferred across the heated wall. Secondly, the scaled residuals of energy equation and radiation transfer equation were less than 10^{-6}. These criteria were found to provide satisfactory results.

3.7 Model Validation

To validate the formulated model, the results from the present work has been compared with the experimental work of Gau et al. [14]. Figure 3.4 shows the variation of normalized transverse average Nusselt number along the length of the duct for the numerical model considered for comparison with correlation data obtained from the experimental study of Gau et al. [14] for the case of Gr/Re^2 = 1,000 and Re = 500. According to their study, the normalized transverse average Nussult number is defined as the following:

$$Nu_{trans,avg,norm} = \frac{Nu_{trans,avg,h}}{Re^{0.4}} \tag{3-11}$$

The comparison is shown in Figure 3.4 given below.

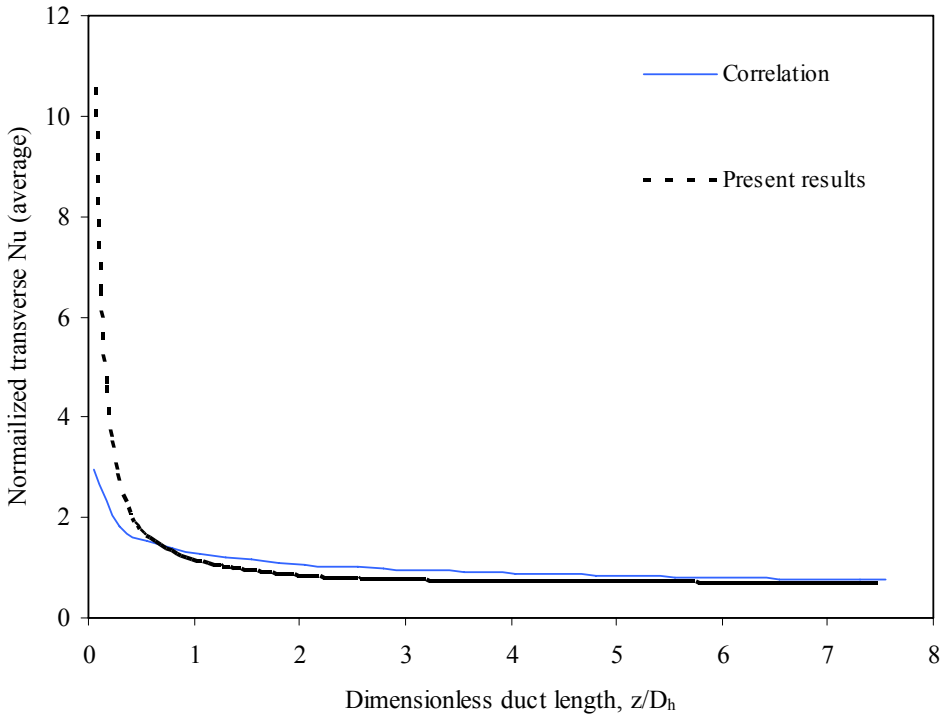

Figure 3.4 Comparison of present work with [14]
(Gr/Re^2 = 1000 and Re = 500)

The present numerical model agrees well with the correlated data. From the experimental data presented in Gau at el. [14], the predicted values also agree well with the experimental data at the location near the entrance region.

Another validation is made from the experimental data of Maughan and Incropera [3] to investigate the validation of the formulated model under the condition of bottom wall heating. Figure 3.5 shows the result of the comparison.

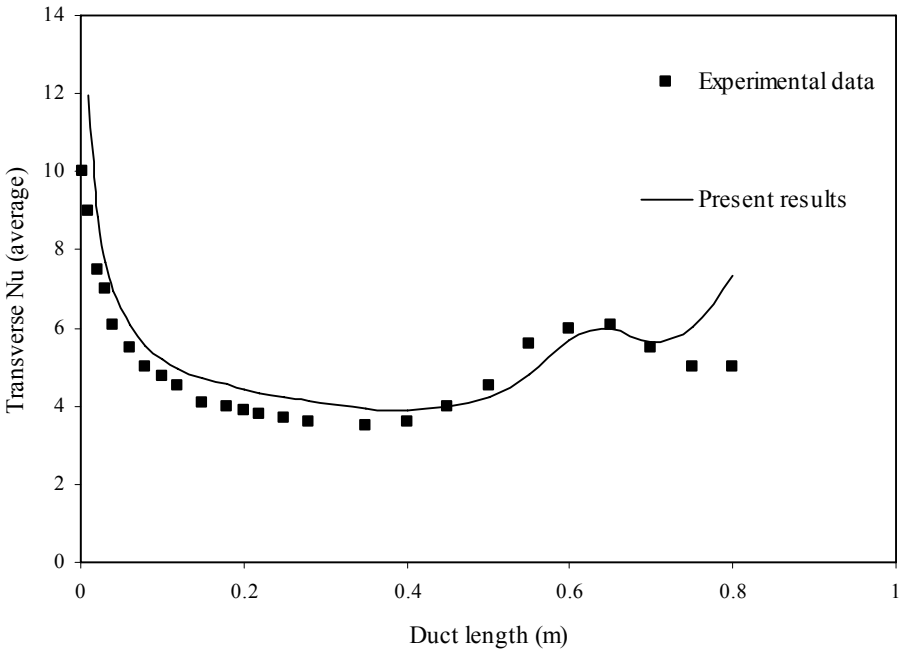

Figure 3.5 Comparison of numerical results with experimental data from [3] ($Gr = 2x10^5$ and $Re = 250$)

From Figure 3.5, it can be seen that the onset of instability occurs approximately 0.6 m after the duct inlet. Although there are discrepancies between experimental results and present numerical calculations near the outlet, the results of the present model generally has a good agreement with the experimental data. The discrepancies are attributed to the fact that the flow in [3] is no longer laminar after the onset of instability. In the present numerical model, laminar flow is assumed throughout the length of the duct.

The previous model validation studies discussed above have not considered radiation in the analysis. To validate a case with radiation, the numerical results from Colomer et. al. [24], which used Discrete Ordinate model with 3 × 2 discretisation scheme on their work, was considered. The discretisation scheme on the Discrete Ordinate model indicates the refinement of the calculation of radiation heat transfer. The higher the number, the more refinement and more calculation time

required. Two discretisation schemes of Discrete Ordinate model, and one surface to surface radiation model, have been verified against numerical data available in literature. The Discrete Ordinate radiation model is suitable for most applications. However, it comes with a premium for computational time. Surface to Surface model is also suitable for flow in an enclosure, but this model requires preliminary calculation for the view factor. Table 3-4 compares radiation heat flux (dimensionless) values from Discrete Ordinate (DO) and Surface to surface (S2S) radiation models of the present work with [24].

Table 3-4 Comparison of different radiation models with data from [24]. (Ra =105, Pl = 0.043, $T_c/(T_h-T_c) = 15$)

Number	Radiation model, number of discretisation	Emissivity for all walls	Dimensionless Average Radiation Heat Flux	Computational time (hr:min)
Reference case[24]	DO, 3×2	1	3.385	n/a
1	DO, 2×2	1	3.346	1:18
2	DO, 3×3	1	3.371	2:11
3	S2S, 2 clusters per face	1	3.427	2:36

It can be seen that the total calculation time required for Surface to Surface model is higher than Discrete Ordinate model. As a result, the Discrete Ordinate model has been chosen for the present study as it provides more accuracy over Surface to Surface model.

A 2 × 2 discretisation is chosen because it provides good prediction with approximately 1% discrepancy, and uses less computation time compared with a 3 × 3 discretisation.

It must be stated that the present study involves the heating configurations where heated wall temperatures have been specified. Therefore, the mechanism of convection and radiation heat transfer can be separately calculated. The temperature

values on the internal surface walls of the duct can be updated by combining both convection and radiation heat transfer effects. The multimode heat transfer effects of cooled and heated walls of the present study can be regarded as uncoupled heat transfer modes [32]. Therefore, the Nu_{total} which is calculable from numerical approach is written as follows.

$$Nu_{total} = Nu_{con} + Nu_{rad} \tag{3-12}$$

3.8 Simulation Parameters

As stated in the definition of the problem, the study considers a range of Grashof numbers from 2,000 to 1,000,000 in order to investigate the development of flow from domination by forced convection, to domination by natural convection heat transfer. Reynolds number was fixed at 100. Both Grashof and Reynolds numbers are evaluated based on fluid properties at the inlet. A set of aspect ratios - 0.5, 1 and 2, are considered in this study. Two emissivity values: 0.05 and 0.85 are used to analyse the effect of weak or no radiation ($\varepsilon = 0.05$) and strong ($\varepsilon = 0.85$) radiation heat transfer.

Appendix 1 provides the complete range of parameters for the simulation considered in this work.

3.9 Closure

The formulation of the numerical model was presented in this chapter. This model was also validated with relevant work available in the literature. The results from the present numerical model agreed well with the published work.

In the next chapter, the numerical model for the duct which is heated by a vertical wall with uniform temperature (heating configuration CS1) is considered. The numerical results obtained will be presented and discussed.

CHAPTER 4
CASE STUDY CS1 - UNIFORM WALL TEMPERATURE

4.1 Introduction

The numerical model formulated from the previous chapter is applied to the first case study CS1 - the uniform temperature heating. In this case, the rectangular duct is heated differentially on vertical walls. These vertical walls are maintained at isothermal temperatures while the top and bottom walls are insulated.

In this chapter, results from the numerical work for this case study will be presented and discussed. The chapter begins with the problem statement where the heating configuration and boundary conditions are described. This is followed by results and discussion.

4.2 Problem Statement

In the present study, the heating configuration shown in Figure 4.1 is specified as configuration CS1.

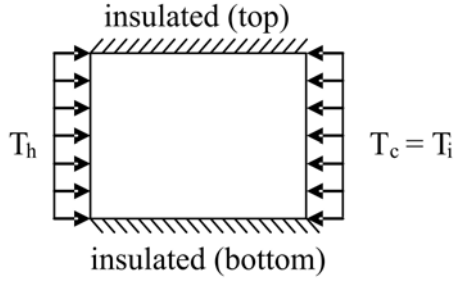

Figure 4.1 Schematic diagram of the heating configuration CS1

The formulated numerical model and its assumptions from Chapter 3 are applied to investigate the heat transfer characteristics in a duct with one wall isothermally heated. The heated wall temperature (T_h) is the main parameter that controls the values of Grashof number. The opposite vertical wall is maintained at a constant temperature. This cooled wall temperature (T_c) has the same temperature as the inlet air temperature. For all cases, the cooled wall temperature and the inlet air temperature are maintained at 300 K.

In the present study, the Grashof number is varied from 2,000 to 1,000,000 in suitable steps to investigate the heat transfer characteristics from forced to natural convection flow. The region of mixed convection is considered in this range. The Reynolds number is fixed at 100 to ensure laminar flow at the inlet, and also to allow only Grashof number to function as the influencing parameter on the convection flow. This would give the buoyancy parameter, Gr/Re^2, values ranging from 0.2 to 100. Grashof and Reynolds numbers are calculated based on fluid properties at the inlet. A low value of Gr/Re^2 (0.2) denotes domination of forced convection, whereas a high value of Gr/Re^2 (100) indicates strong natural convection inside the duct.

Surface radiation from the internal walls is also included in the study. It is represented through wall surface emissivity, which has two values: 0.05 and 0.85, to represent for weak and strong radiation effects, respectively. The rectangular duct is given three values for aspect ratios in this study: 0.5, 1 and 2. The higher value of aspect ratios indicates larger distance between the heated and cooled vertical walls.

All simulation cases are satisfied with the convergence criteria outlined in Chapter 3. The transverse average convective and radiative Nusselt numbers are calculated using Equation (3-8) and (3-10), which uses convective and radiative heat transfer coefficients obtained from the simulation respectively. Equation (3-9) is used to calculate T_b. The results are presented in the next section.

4.3 Results and Discussion

4.3.1 Combined Forced and Natural Convection Heat Transfer

In this section, the results presented have minimized effect of radiation heat transfer. This will allow examination of the heat transfer characteristics due to mixed convection heat transfer only. Figures 4.2 to 4.4 show the variation of transverse average convective Nusselt number (Nu_{con}) along the heated wall at different distances from the inlet with respect to Grashof numbers for $\varepsilon = 0.05$ (low emissivity) and AR = 0.5, 1 and 2, respectively.

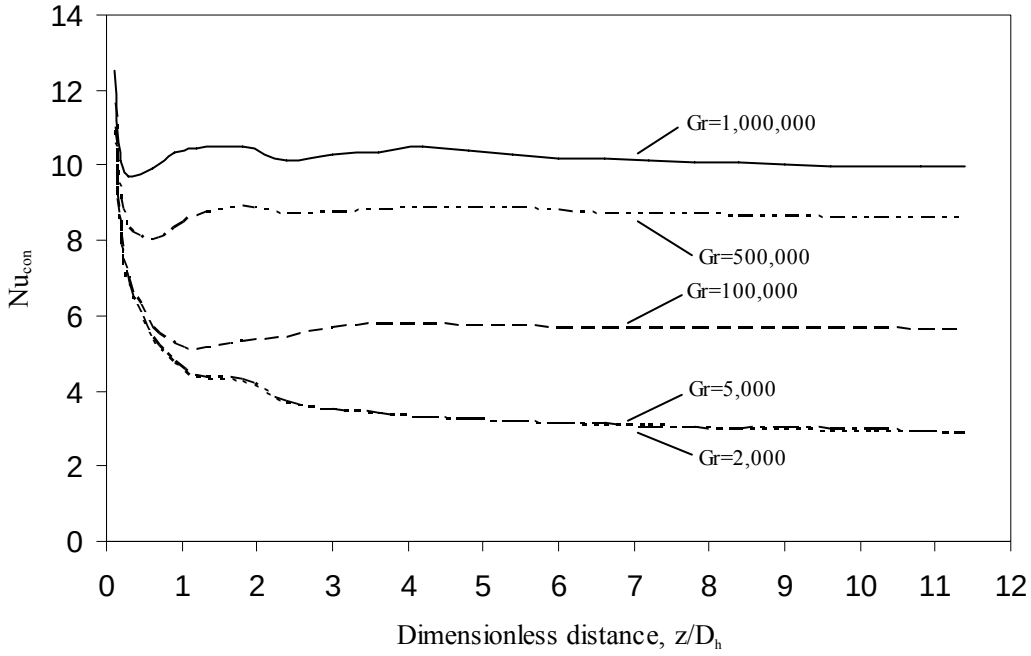

Figure 4.2 Effect of Grashof number on the average convective Nusselt number at heated wall (AR = 0.5, ε = 0.05)

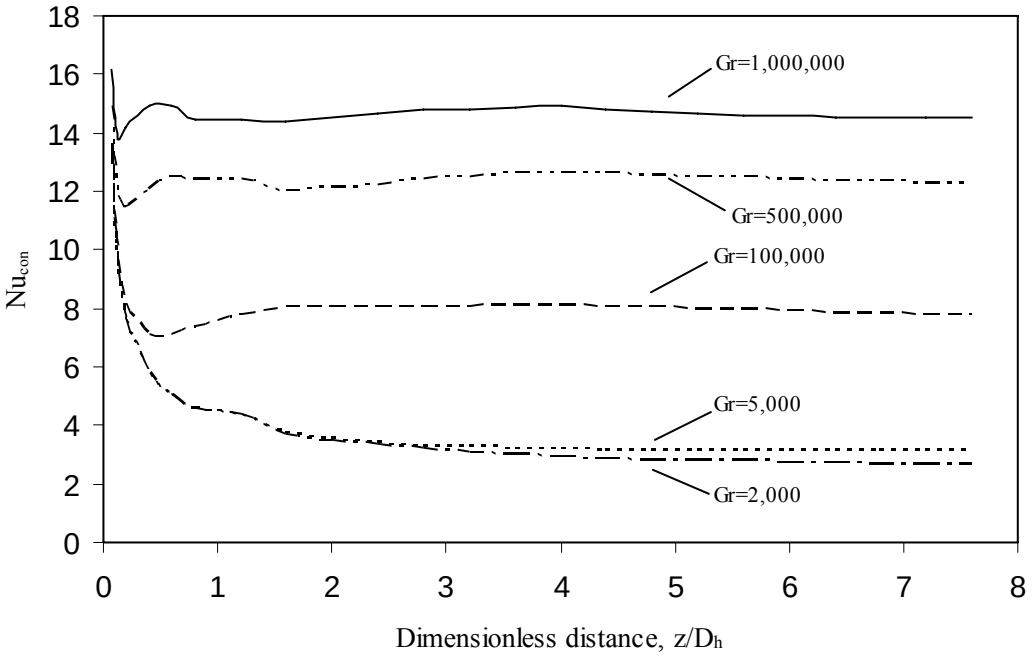

Figure 4.3 Effect of Grashof number on the average convective Nusselt number at heated wall (AR = 1, ε = 0.05)

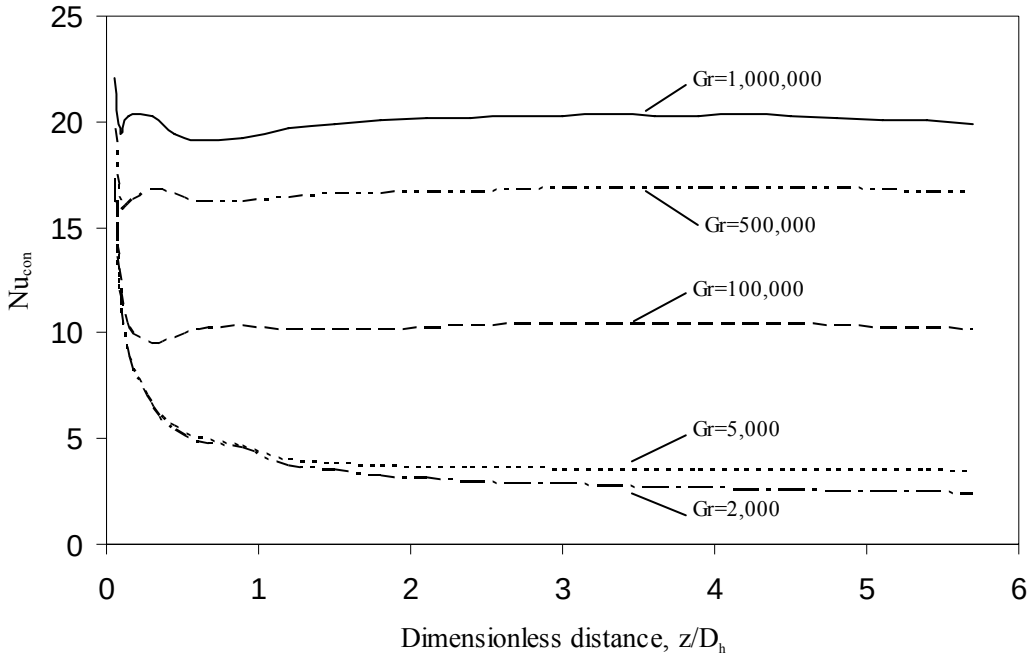

Figure 4.4 Effect of Grashof number on the average convective Nusselt number at heated wall (AR = 2, $\varepsilon = 0.05$)

For each aspect ratio, the transverse average convective Nusselt number along the heated wall increases when Grashof number increases. The heat transfer patterns follow the pattern of forced convection flow for the cases of Gr = 2,000 and 5,000, in which the Nusselt number rapidly declines near the region where the flow enters the duct inlet, and then finally become thermally fully developed when the flow has travelled approximately 2 - 4 times the hydraulic diameter. The effect of natural convection heat transfer is obviously seen as an augmentation of convective Nusselt number for cases where Gr = 100,000 and above. The enhancement of Nusselt number can be described due to the natural convection effect inducing circulation that allows flow to circulate and transfer the energy from heated wall to cooled wall. The region of mixed convection where the flow is influenced by both forced and natural convection effects has a potential to enhance heat transfer. After the entrance region, which is about 2 - 4 times the hydraulic diameter, the graphs of transverse average convective Nusselt number show constant value along the duct length. Moreover, no fluctuation is detected from the graph patterns.

To illustrate the characteristics of the flow, a set of figures that show the temperature and velocity at a location where $z/D_h = 1$ for all aspect ratios, and for

some selected cases of Grashof numbers (2,000, 100,000 and 1,000,000) is presented below. A series of figures (Figures 4.5 to 4.13) that provide interesting insights is given next. The flow cross section shown is at a location when the flow is still under the thermally developing region.

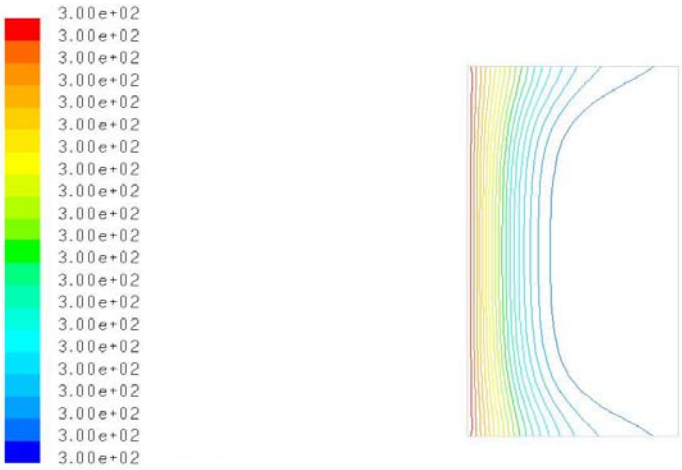

(i)

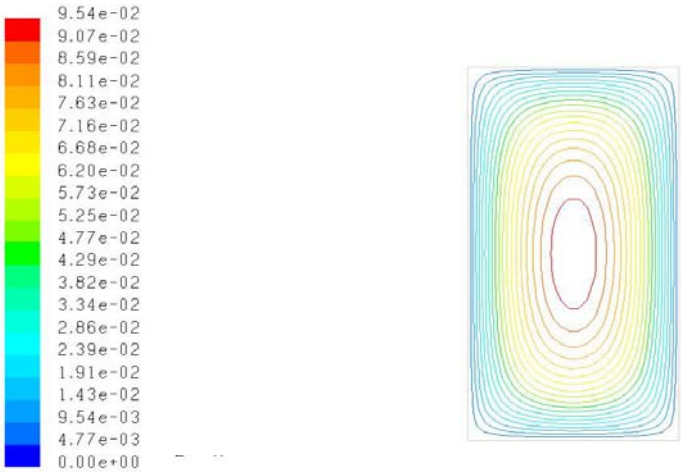

(ii)

Figure 4.5 (i) Temperature (K) and (ii) velocity (m/s) contours for Gr = 2,000, AR = 0.5 and ε = 0.05. Note: Temperature contours have colour bar close to 300 K due to low Gr

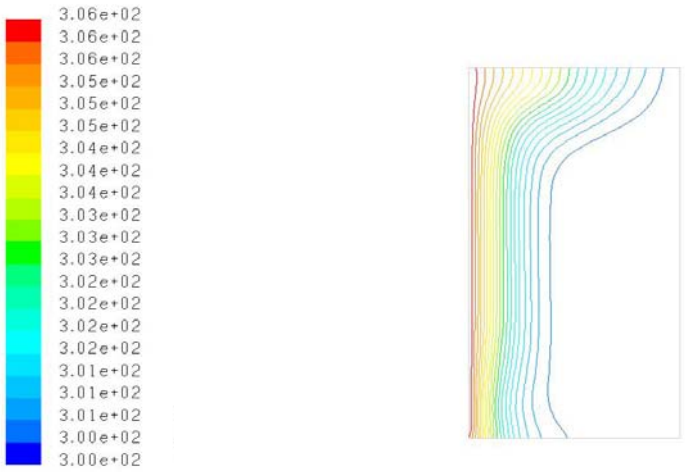

(i)

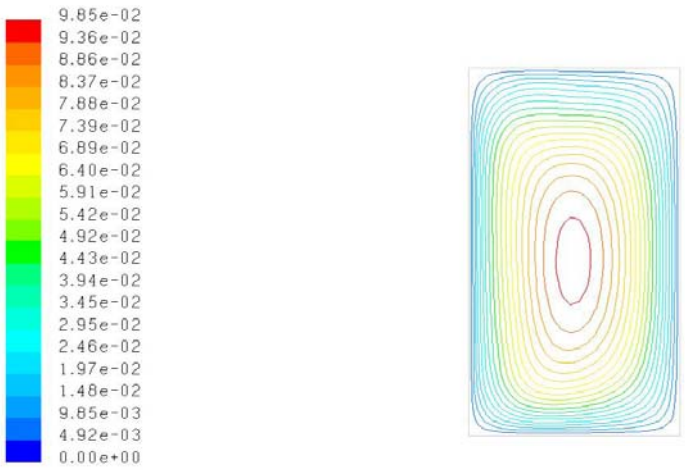

(ii)

Figure 4.6 (i) Temperature (K) and (ii) velocity (m/s) contours for Gr = 100,000, AR = 0.5 and $\varepsilon = 0.05$

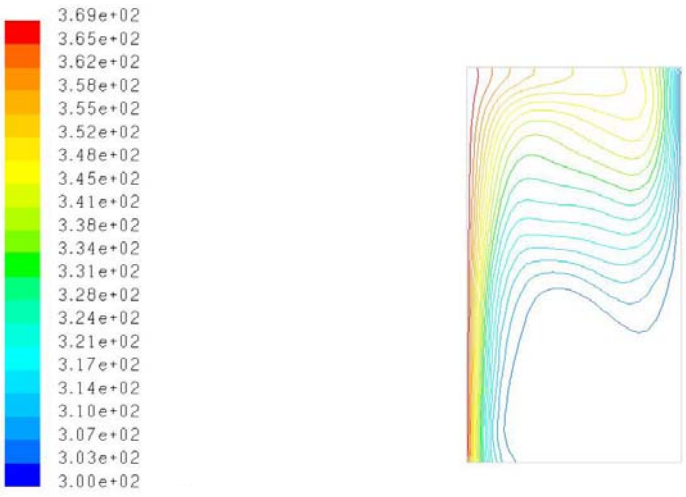

(i)

(i)

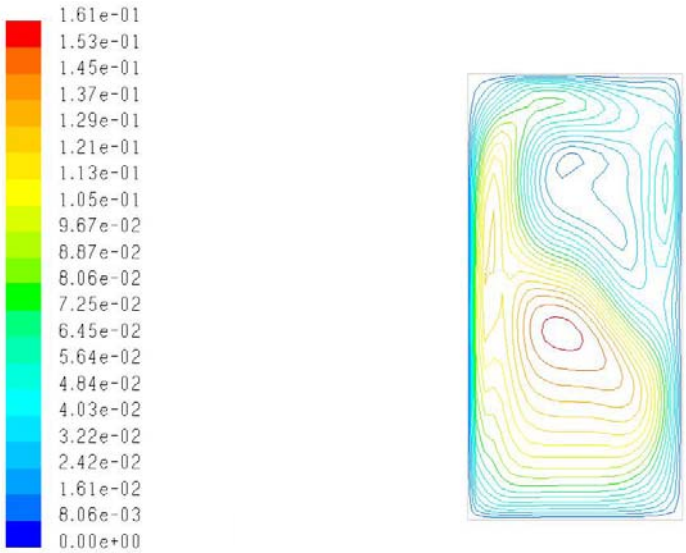

(ii)

Figure 4.7 (i) Temperature (K) and (ii) velocity (m/s) contours for Gr = 1,000,000, AR = 0.5 and $\varepsilon = 0.05$

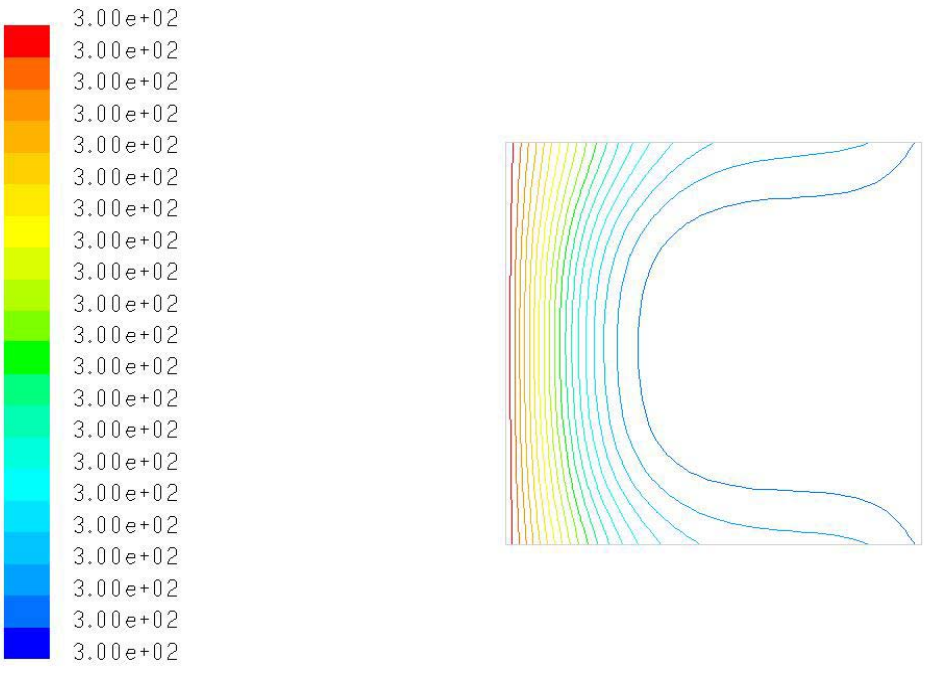

(i)

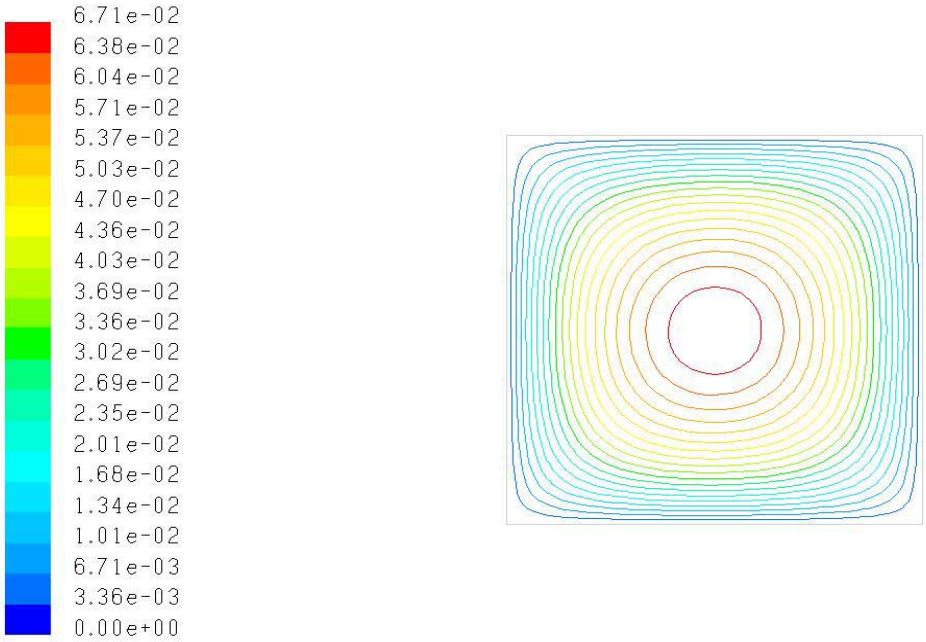

(ii)

Figure 4.8 (i) Temperature (K) and (ii) velocity (m/s) contours for Gr = 2,000, AR = 1 and ε = 0.05

Note: Temperature contours have colour bar close to 300 K due to low Gr

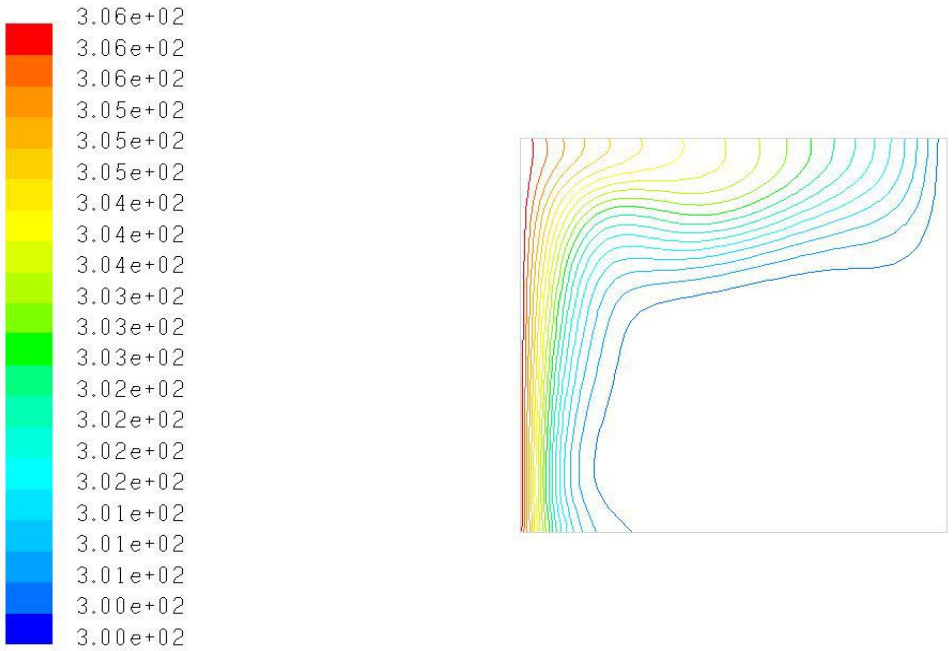

(i)

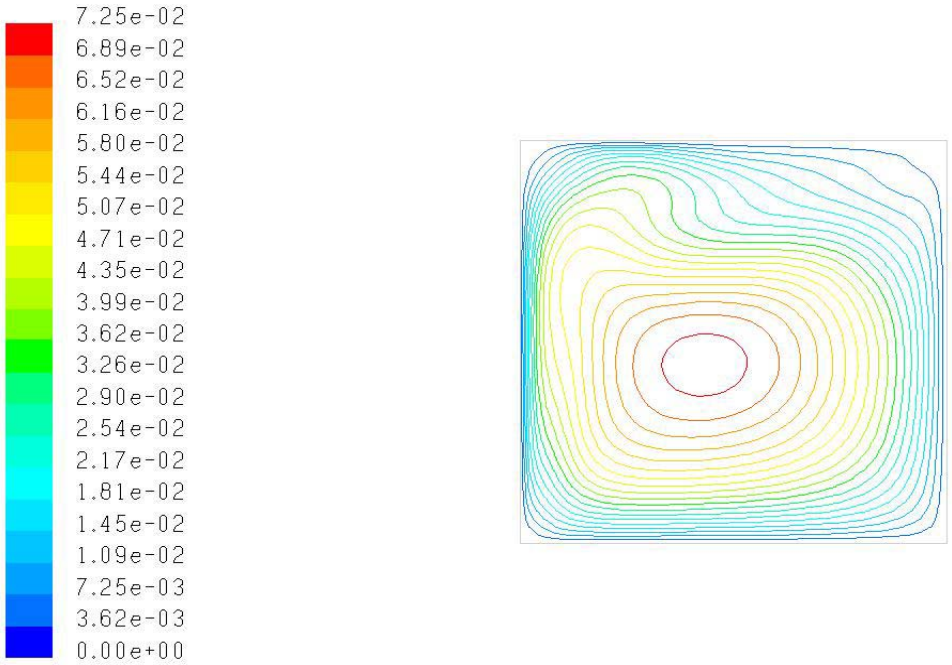

(ii)

Figure 4.9 (i) Temperature (K) and (ii) velocity (m/s) contours for Gr = 100,000, AR = 1 and ε = 0.05

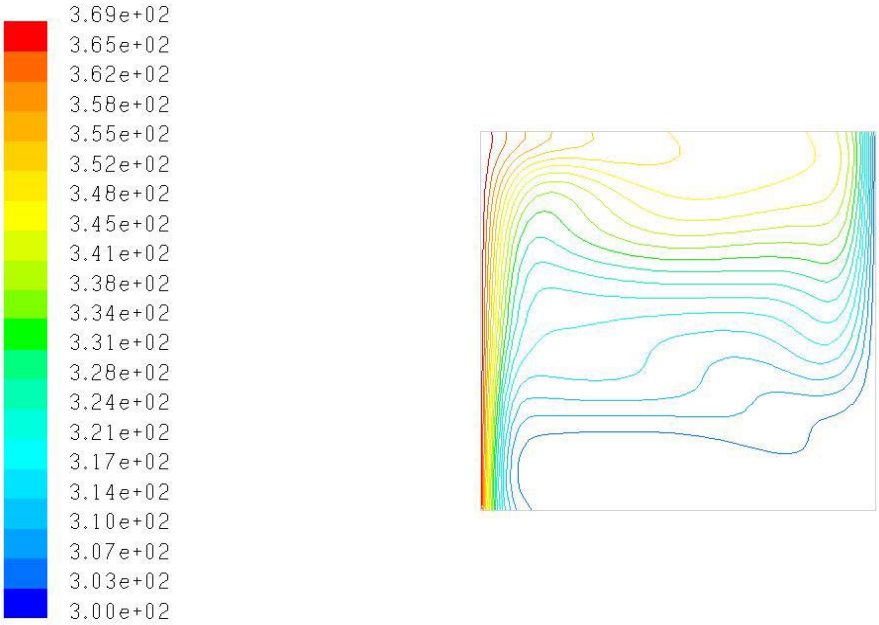

(i)

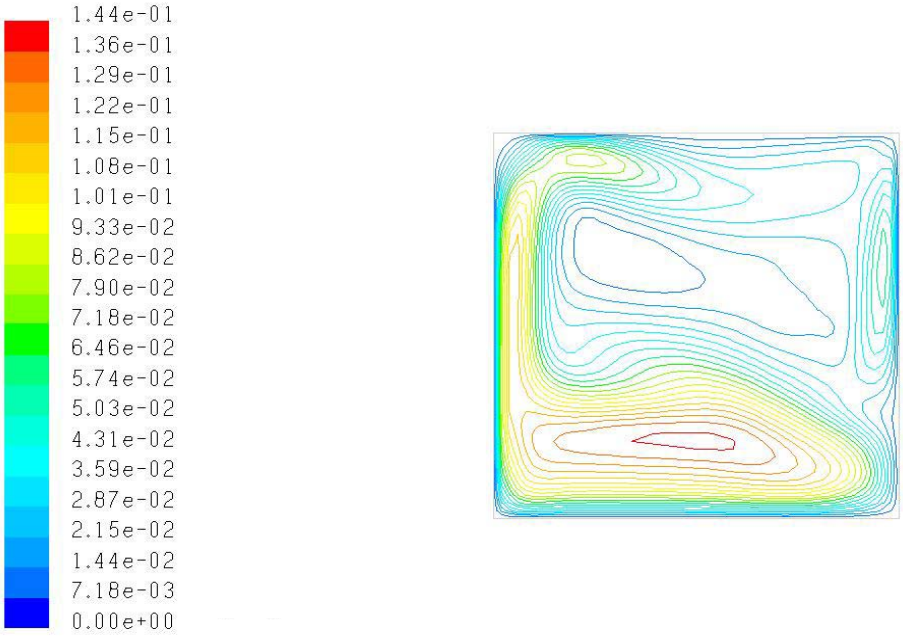

(ii)

Figure 4.10 (i) Temperature (K) and (ii) velocity (m/s) contours for Gr = 1,000,000, AR = 1 and $\varepsilon = 0.05$

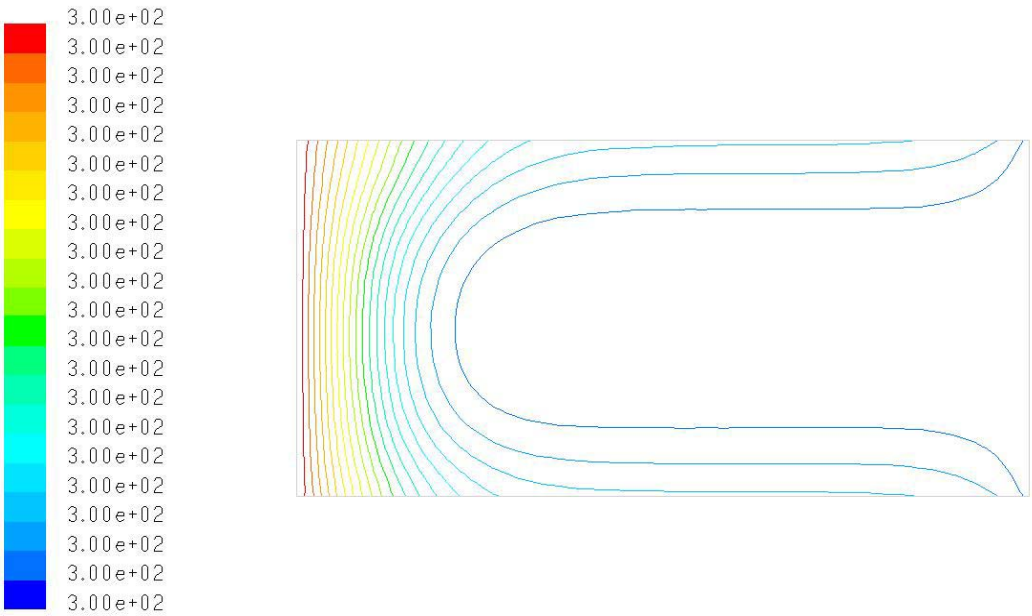

(i)

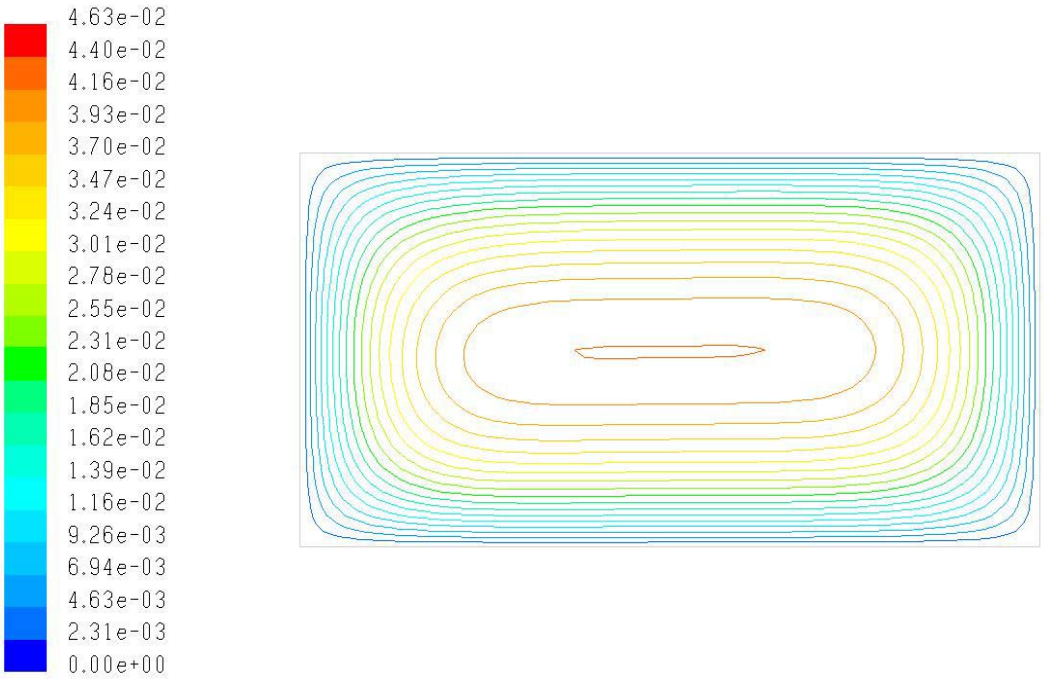

(ii)

Figure 4.11 (i) Temperature (K) and (ii) velocity (m/s) contours for Gr = 2,000, AR = 2 and ε = 0.05

Note: Temperature contours have colour bar close to 300 K due to low Gr

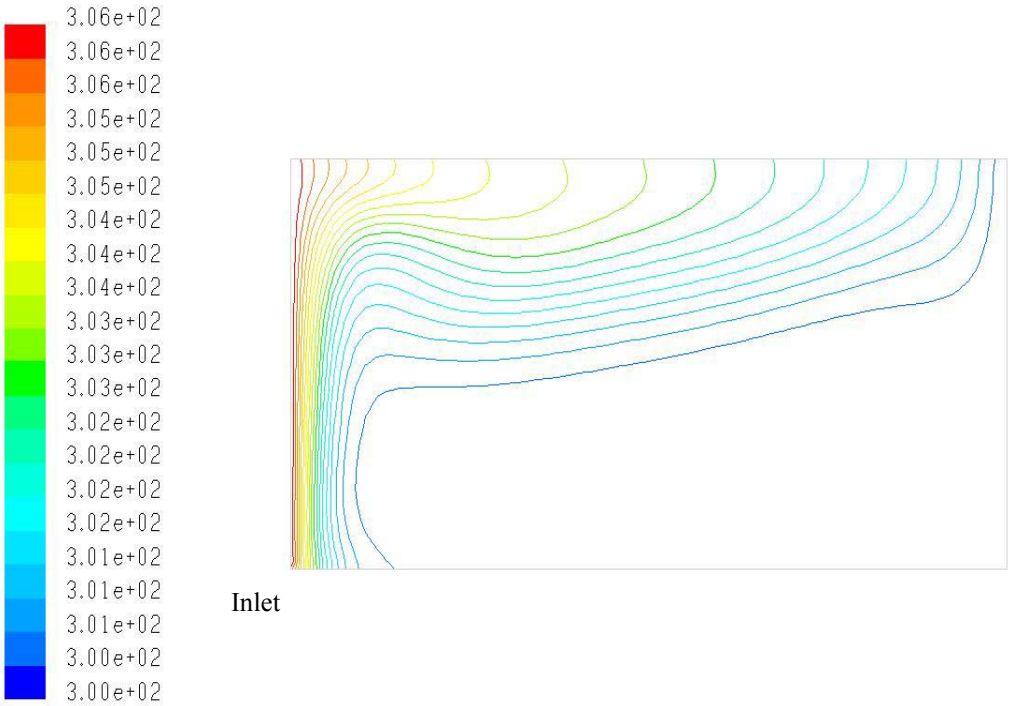

(i)

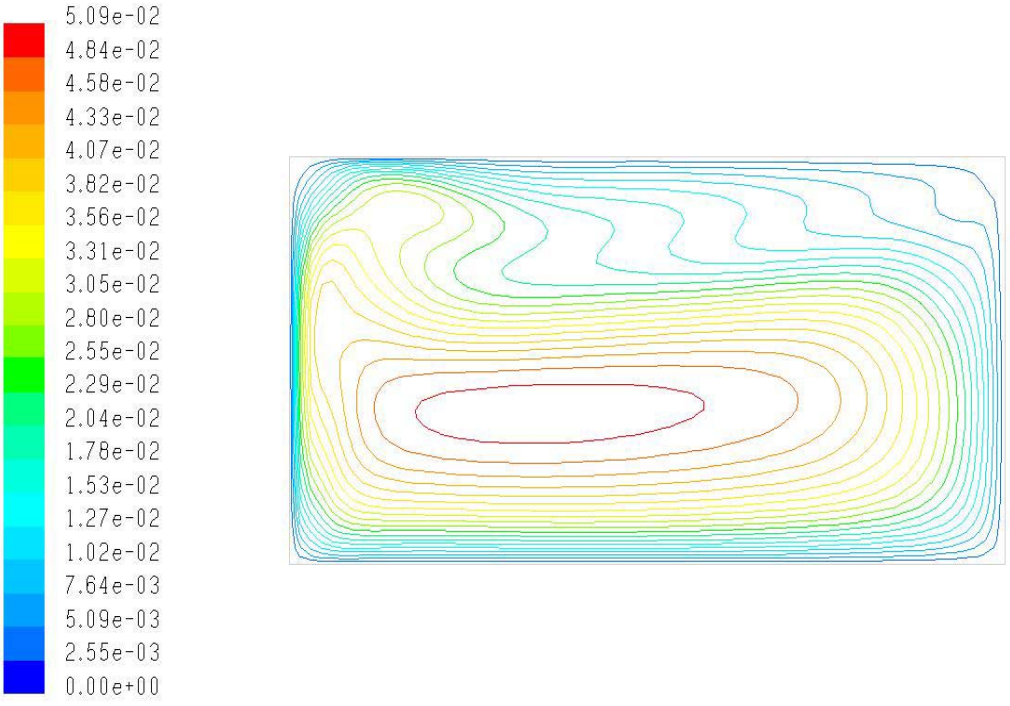

(ii)

Figure 4.12 (i) Temperature (K) and (ii) velocity (m/s) contours for Gr = 100,000, AR = 2 and $\varepsilon = 0.05$

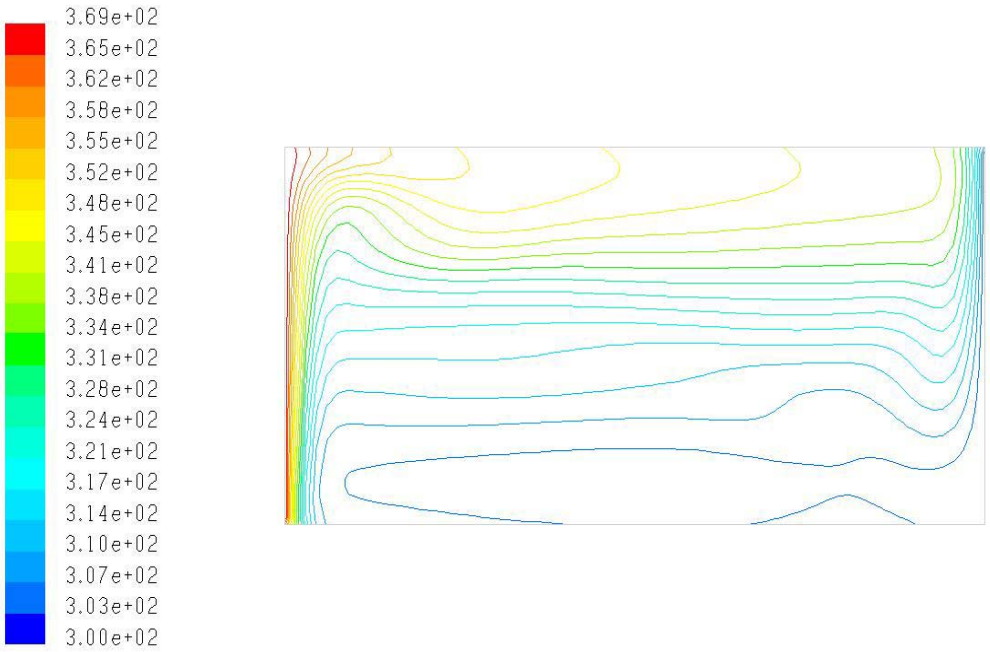

(i)

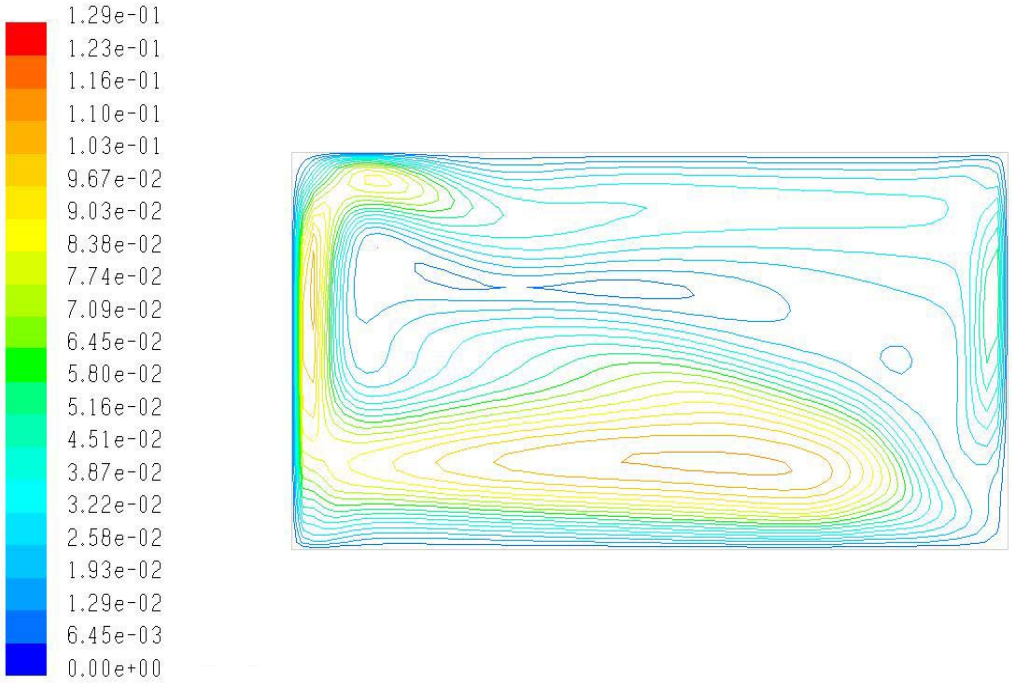

(ii)

Figure 4.13 (i) Temperature (K) and (ii) velocity (m/s) contours for Gr = 1,000,000, AR = 2 and $\varepsilon = 0.05$

The careful examination of these figures show that the flow where Gr = 2,000 has approximately the same flow field as the inlet. The heated wall temperature for this Grashof number is not significantly different from the cooled wall temperature. Therefore, the temperature differential between the heated and cooled walls is not strong enough to cause significant natural convection within the duct. The heat transfer mechanism is therefore dominated by only forced convection heat transfer. Natural convection heat transfer has no influence under this condition.

When the flow is under the condition where Gr = 100,000, the change in velocity contours is seen. Thermal boundary layers follow natural convection patterns, and can be observed from the temperature contours. Fluid with higher temperature moves upward due to the density gradient caused by natural convection effect. The cold fluid accumulates around the bottom part of the duct.

When the flow condition reaches Gr = 1,000,000, secondary flow induced by natural convection can be seen from velocity contours, where the region of high fluid velocity shifts from the middle part of the duct to the lower part. Then it circulates upwards along the heated wall while carrying the cooler fluid. This natural convection mechanism promotes heat transfer from heated wall to cooled wall.

Figure 4.14 shows the complete path lines of the fluid flow when it enters the duct with Gr = 1,000,000 , AR = 1 and $\varepsilon = 0.05$. The path lines show the circulation of the fluid, while being heated and cooled by the respective vertical side walls.

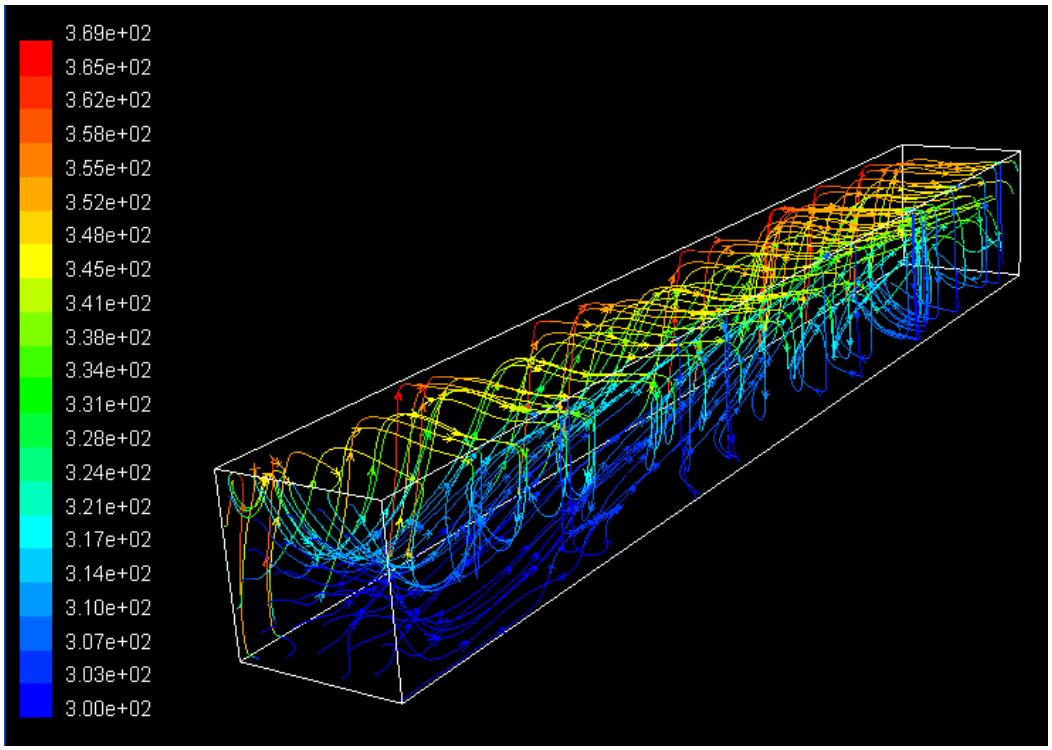

Figure 4.14 Fluid flow path lines showing the flow paths and temperature (K) along the duct (AR = 1, ε = 0.05)

From Figure 4.14, when the flow is under the effects of both forced and natural convection heat transfer, two different temperature fluid zones caused by heated and cooled walls form a circulation pattern, which is regarded as secondary flow. Buoyancy effect induced by natural convection at the heated wall makes warm fluid moving upward to the upper part of the duct, and being circulated to the cooled wall on the opposite side. The cold fluid near the cooled wall shifts to the bottom part of the duct and moves towards the heated wall. The fluid velocity at the upper part of the duct tends to be lower than the lower part. The slow velocity fluid zone at the upper part makes the fluid at the lower part to be accelerated in order to satisfy continuity conditions on any of the cross section in the duct. This can be seen from Figure 4.14, when part of the fluid moves downward to the lower part just after entering the duct and increasing its speed due to heat accumulation at the top part. Two separated fluid zones are then obviously seen. The warm and slow fluid at the upper part, and the cool and fast fluid at the bottom. A circulation pattern is thus being developed. The heat transfer between the heated and cooled wall is enhanced by this mechanism. The flow then becomes thermally fully developed.

4.3.2 Radiation Heat Transfer

While radiation has no direct heat exchange effect to the air which is a non-participating medium, the different temperature contours of the top and bottom walls between the cases of weak radiation ($\varepsilon = 0.05$) and strong radiation ($\varepsilon = 0.85$) from Figure 4.15 to 4.16 indicate that the heat transfer from these two walls is modified due to the effect of radiation heat transfer. Air that flows over these walls gets additional heating from top and bottom walls by means of convection heat transfer. The amount of heat that is transferred from top and bottom walls to the air depends on the radiative energy from heated wall. The rectangular duct with a higher wall temperature contributes significantly to radiation heat transfer. Figures 4.15 and 4.16 show temperature distributions along the duct for the case of AR = 1, Gr = 1,000,000, $\varepsilon = 0.05$ and $\varepsilon = 0.85$ for bottom and top walls, respectively. In the case of high Grashof number (Gr =1,000,000), radiation from heated wall has caused top and bottom walls ,where the combination of radiation and convection effects take place, to heat the fluid and thus resulting in changes of the flow and heat transfer characteristics.

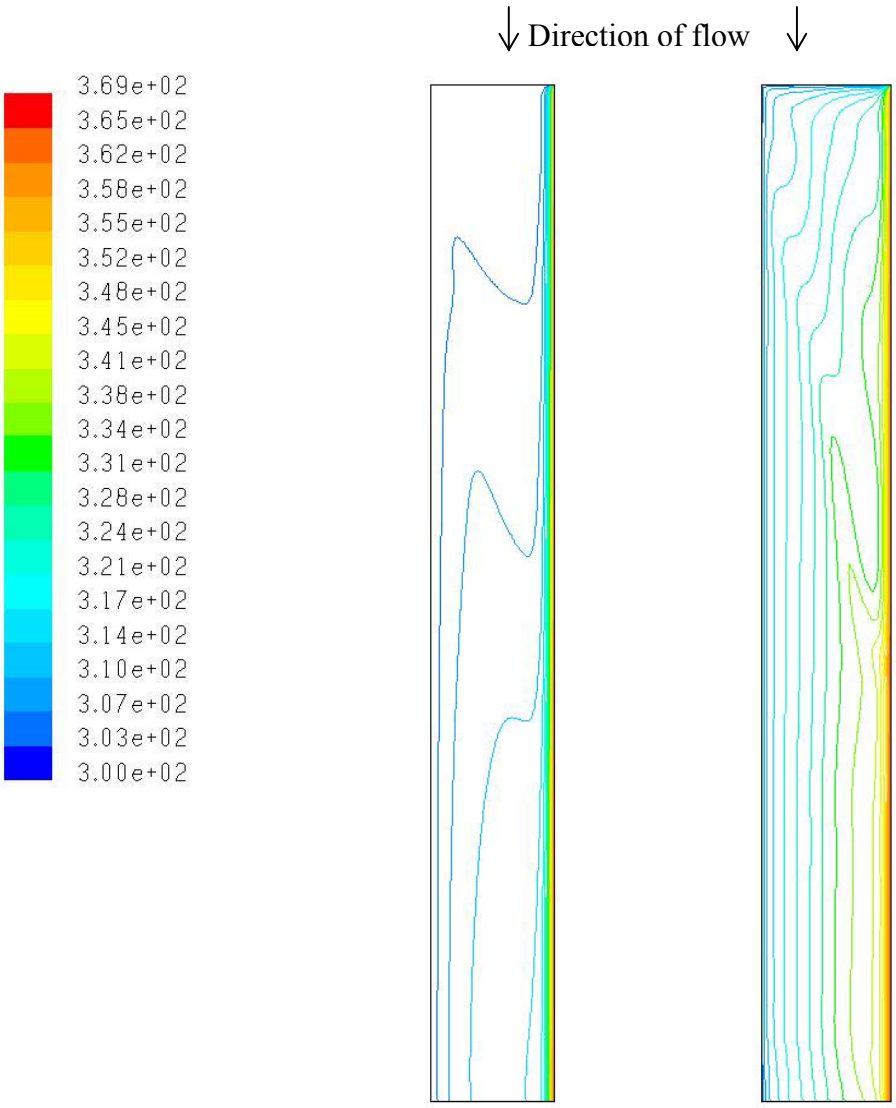

Figure 4.15 Temperature (K) contour of bottom wall for duct surfaces have (i) ε = 0.05, (ii) ε = 0.85 (AR = 1, Gr = 1,000,000)

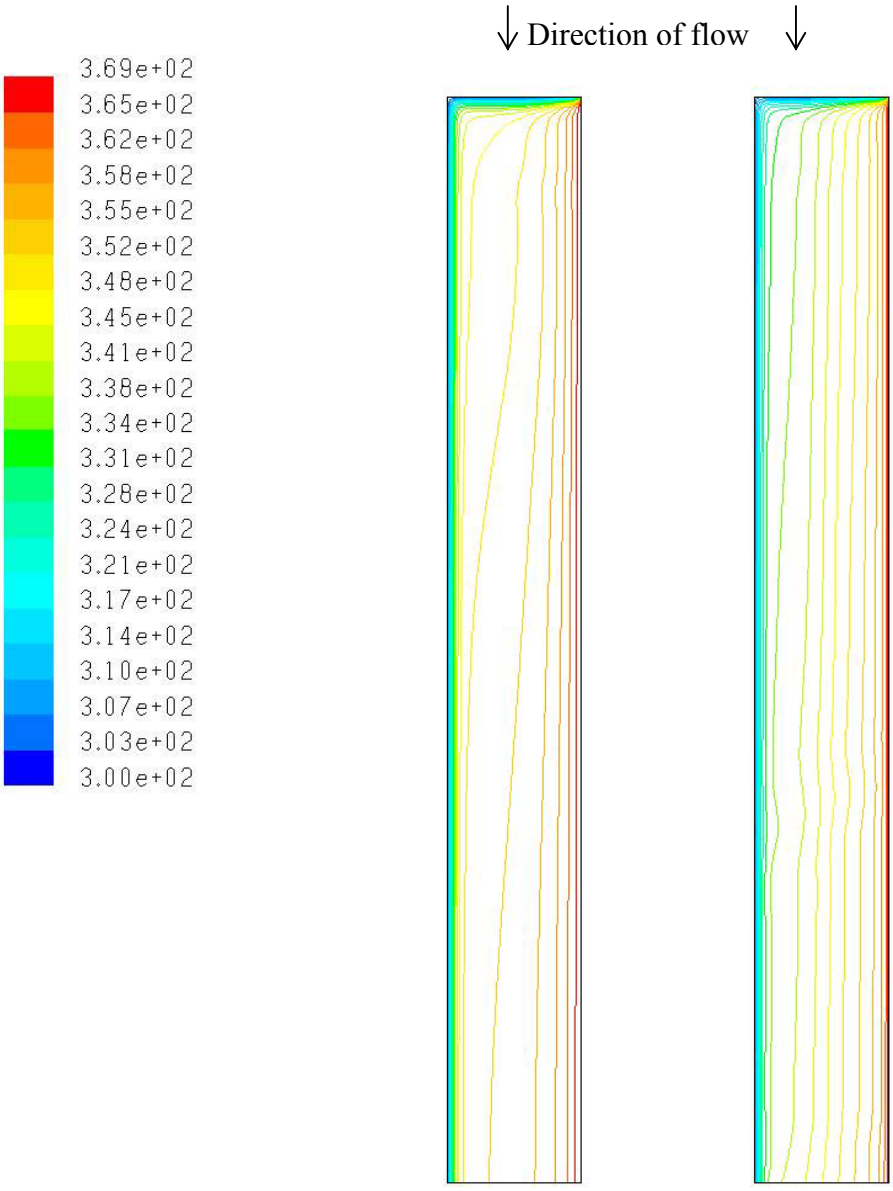

Figure 4.16 Temperature (K) contour of top wall for duct surfaces have (i) ε = 0.05 (ii) ε = 0.85 (AR = 1, Gr = 1,000,000)

Radiation heat transfer not only provides additional heat to the air *via* top and bottom walls, but also affects the thermal boundary layers. This causes the change in heat transfer characteristics of the flow.

Figures 4.17 to 4.19 show the heat transfer characteristics from heated wall for the aspect ratio of 0.5, 1 and 2, respectively. When the effect of radiation is strong (ε = 0.85), the convective Nusselt number is different from the case of ε = 0.05 (Figures 4.2 - 4.4).

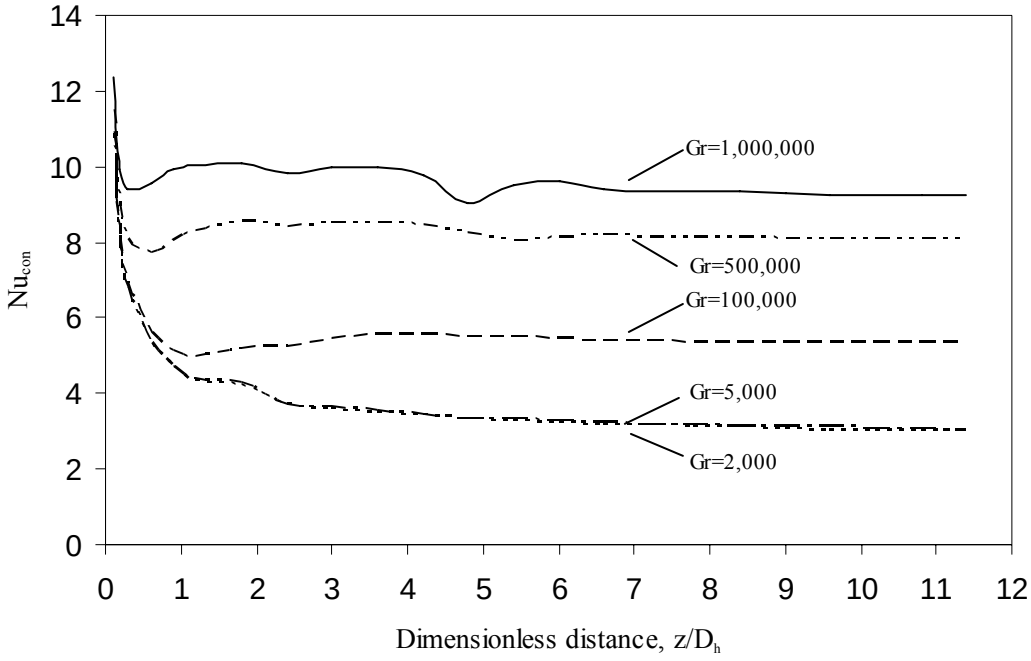

Figure 4.17 Effect of Grashof number on the average convective Nusselt number at heated wall (AR = 0.5, ε = 0.85)

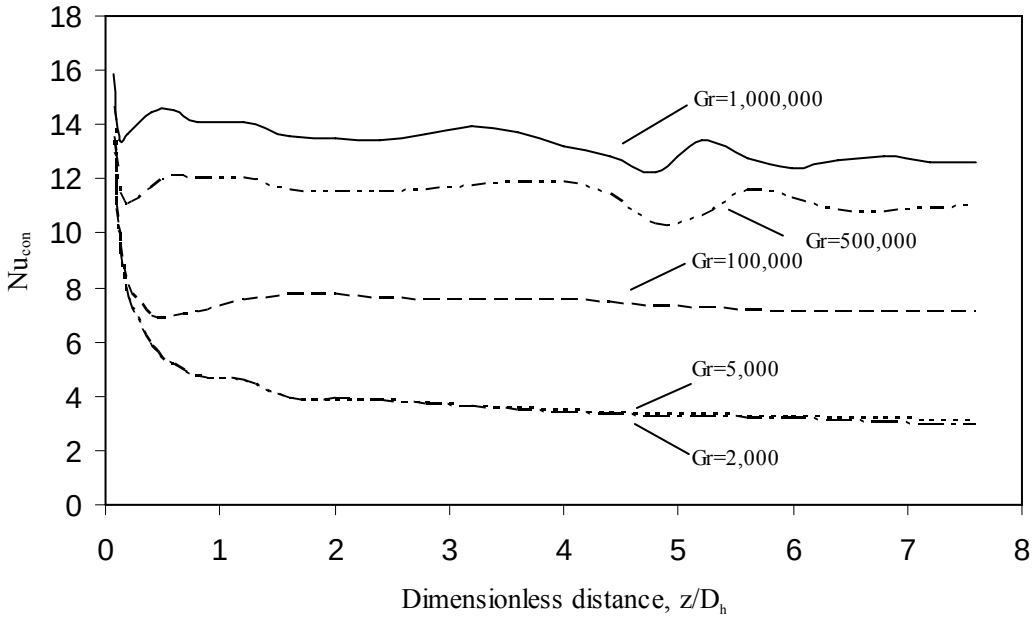

Figure 4.18 Effect of Grashof number on the average convective Nusselt number at heated wall (AR = 1, ε = 0.85)

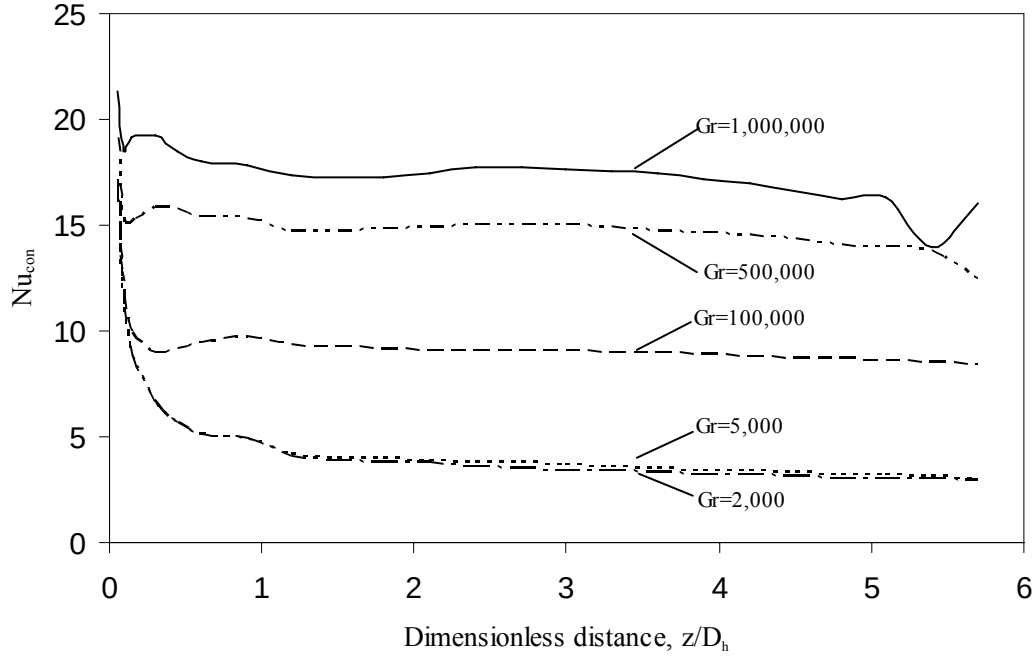

Figure 4.19 Effect of Grashof number on the average convective Nusselt number at heated wall (AR = 2, ε = 0.85)

In most cases, patterns of convective Nusselt number are similar to the case of $\varepsilon = 0.05$. Radiation has no apparent effect on the convective Nusselt number for the case of Gr = 2,000, 5,000 and 100,000. However, in the cases of Gr = 500,000 and above, there are fluctuations on the graph at downstream of the duct. These disturbances can be described as the fluid being influenced by the effect of bottom wall heating. As reported by Maughan and Incropera [3], the onset of instability is detected when the flow is heated from the bottom wall. Buoyancy forces induced by heat from the bottom wall have influenced the instability of the flow, and thus cause the fluctuation in the transverse average Nusselt numbers.

From the results, it is clear that radiation heat transfer affects the heat transfer characteristics of the flow in rectangular duct by inducing the bottom-heated behaviour. However, it will affect only when the duct is under certain heating conditions, and in the present study it starts to occur when Gr = 500,000.

Consider radiative Nusselt number as shown in Figures 4.20 to 4.22. These figures show the change in the heated wall transverse average radiative Nusselt (Nu_{rad}) number along the duct length at different distances from inlet, for aspect ratio of 0.5, 1 and 2, respectively. Although the Nusselt number values tend to increase along the length of the duct, the values of radiation heat flux are almost the same. This indicates that radiation effect is independent from the flow. The reason for radiative Nusselt number increase is due to increment of bulk mean fluid temperature, T_b, which has the direct effect on the values of Nusselt number as defined by equation (3-8). High Grashof number value represents the conditions where the temperature difference between two vertical walls is high. Radiative energy is stronger if the temperature difference is higher. As a result, higher Grashof number value results in higher radiative Nusselt number values.

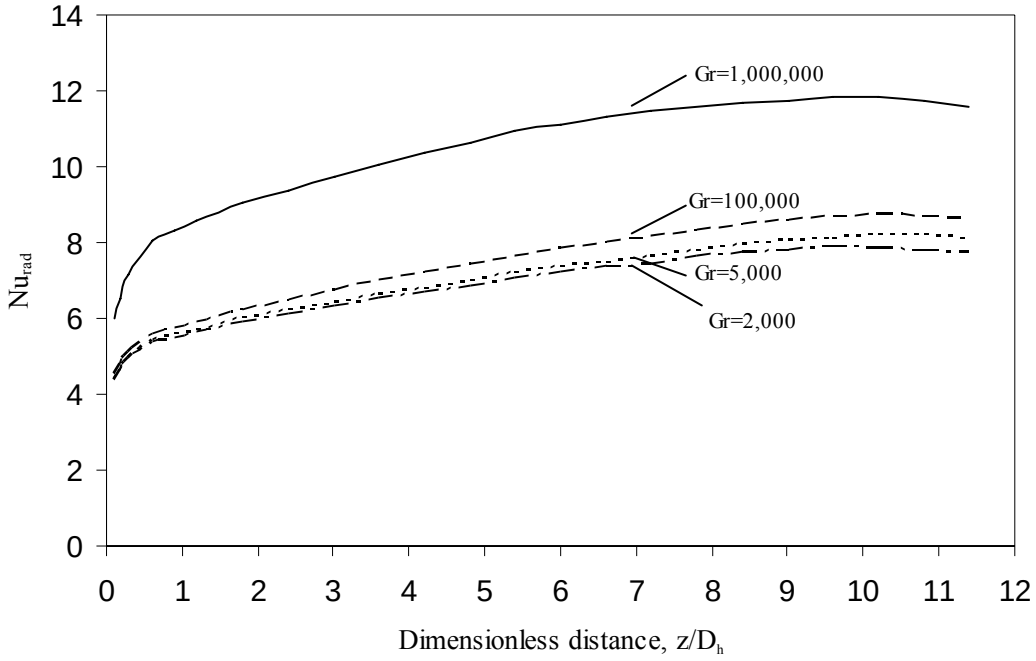

Figure 4.20 Variation of average radiative Nusselt number at heated wall for different Grashof number (AR =0.5, ε = 0.85)

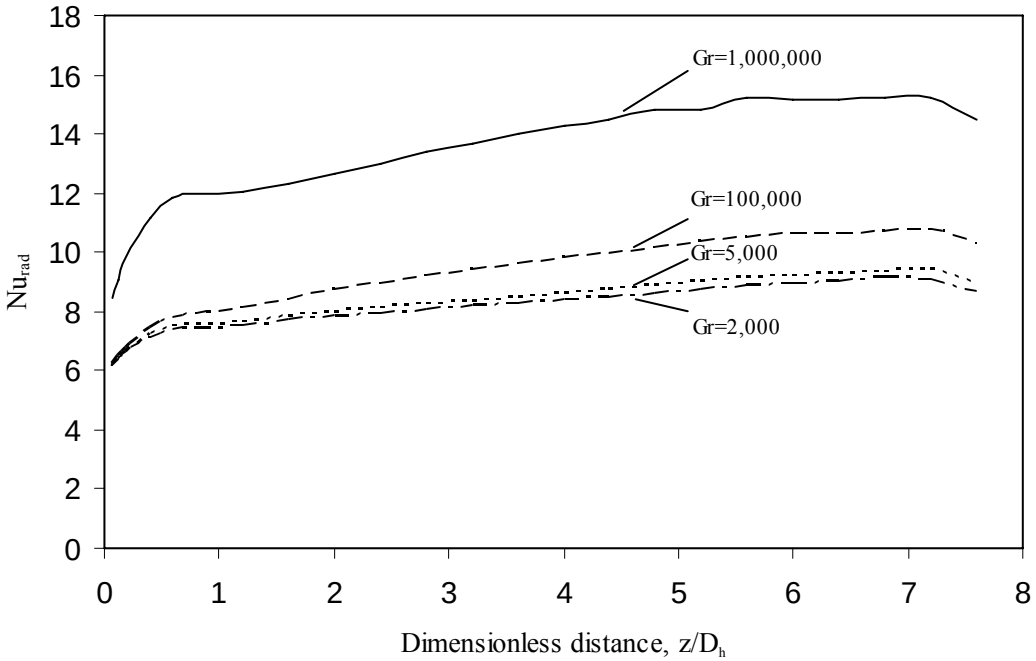

Figure 4.21 Variation of average radiative Nusselt number at heated wall for different Grashof number (AR =1, ε = 0.85)

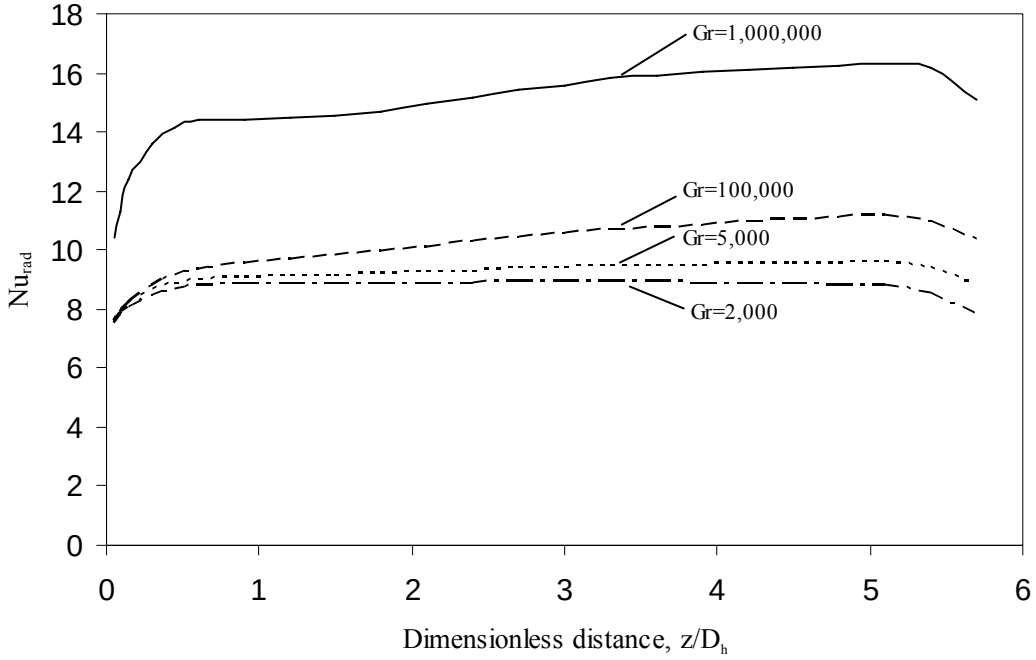

Figure 4.22 Variation of average radiative Nusselt number at heated wall for different Grashof number (AR =2, ε = 0.85)

Figure 4.23 (i) and (ii) show the ratios of convective and radiative Nusselt numbers to the total Nusselt number for a duct of AR= 1. Due to the present problem having the specified temperature at the boundary, the problem is regarded as an uncoupled problem. Hence, the relationship between total, convective and radiative Nusselt values can be defined [32] as:

$$Nu_{total} = Nu_{con} + Nu_{rad} \tag{4-1}$$

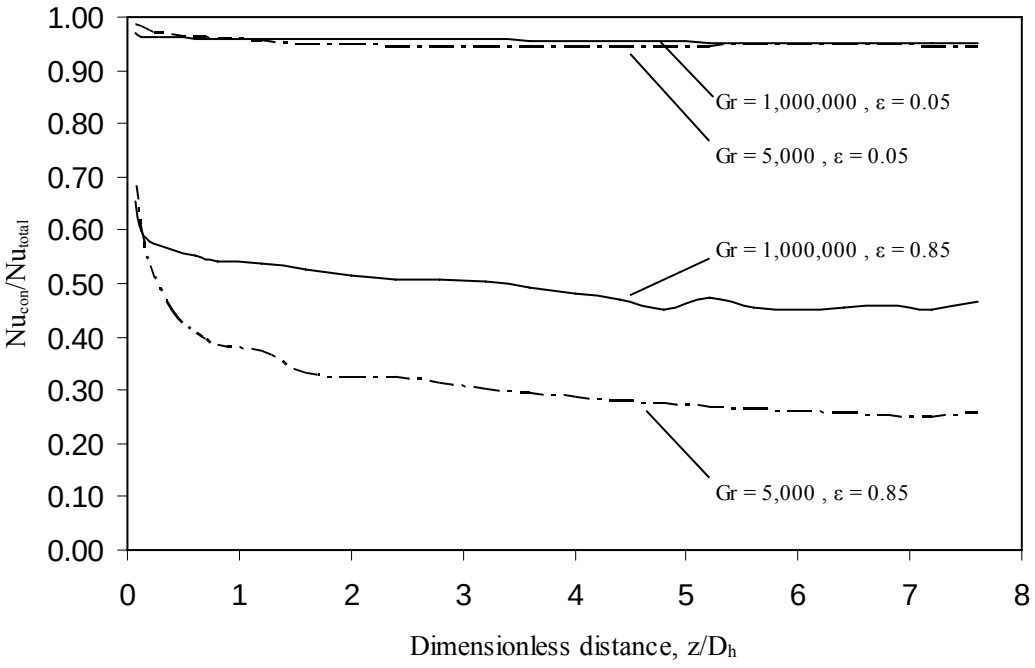

(i)

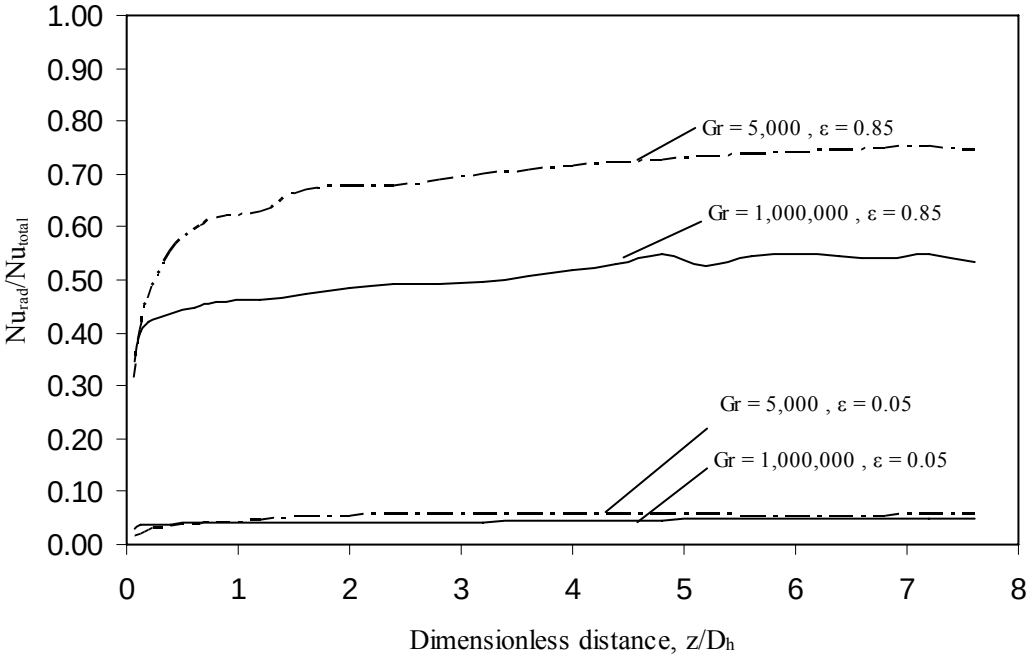

(ii)

Figure 4.23 Ratio of (i) convective to total Nusselt number and (ii) radiative to total Nusselt number (AR = 1)

From the above figures, it can be seen that the ratios of convective to total Nusselt number are close to one, and ratios of radiative to total Nusselt number are close to zero for any Grashof number when the surface emissivtiy is equal to 0.05. On the other hand, for a surface emissivity of 0.85, the ratios vary depending on the Grashof number. In the figures, Gr = 5,000 and Gr = 1,000,000 represent the mixed convection flow in the condition of strong forced convection and strong natural convection, respectively. Higher Grashof number flows dominated by natural convection have a higher value of convective part than radiative part irrespective of aspect ratio or wall emissivity. This would suggest that natural convection heat transfer is the main heat transfer mechanism in the conditions of high Grashof number. For low Grashof number cases, the contribution from radiation heat transfer is found to be higher.

The figures shown above are derived from the duct with aspect ratio of 1. For aspect ratio of 0.5 and 2, in general, they follow the same trends as aspect ratio of 1. The convective and radiative part contributions to the total Nusselt number are comparable to each other for the case of AR = 1. This means that the influence of convection and radiation heat transfer is unaffected by the aspect ratio of the duct when all other parameters being the same.

4.3.3 Duct Aspect Ratio

Considering only the cases where radiation effect is minimized ($\varepsilon = 0.05$), from the previously presented Figures 4.2 to 4.4, it was found that the aspect ratio of 0.5 has lower overall convective Nusselt (Nu_{con}) numbers when compared with aspect ratio of 1, while aspect ratio of 2 has the highest. Figure 4.24 shows the transverse average convective Nusselt number patterns for each aspect ratio compared for the case of Gr = 1,000,000. The patterns of heat enhancement due to mixed convection flow are the same for all aspect ratios. The aspect ratio of 0.5 provides thermally fully developed flow with a shorter entrance length when compared with aspect ratio of 1 and 2. The aspect ratio of 2, however, has the highest heat transfer rates.

In the present study, the height of the duct is fixed. As a result, higher aspect ratio indicates larger distance between two vertical side walls. The higher aspect ratio benefits from having more volume of air in the duct. If air is the fluid used to cool the heated duct, more air enters to the duct thereby allowing more heat transfer. Alternatively in terms of bulk mean fluid temperature, higher aspect ratio has more volume and thus results in lower bulk mean fluid temperature, which increases the heat transfer rates.

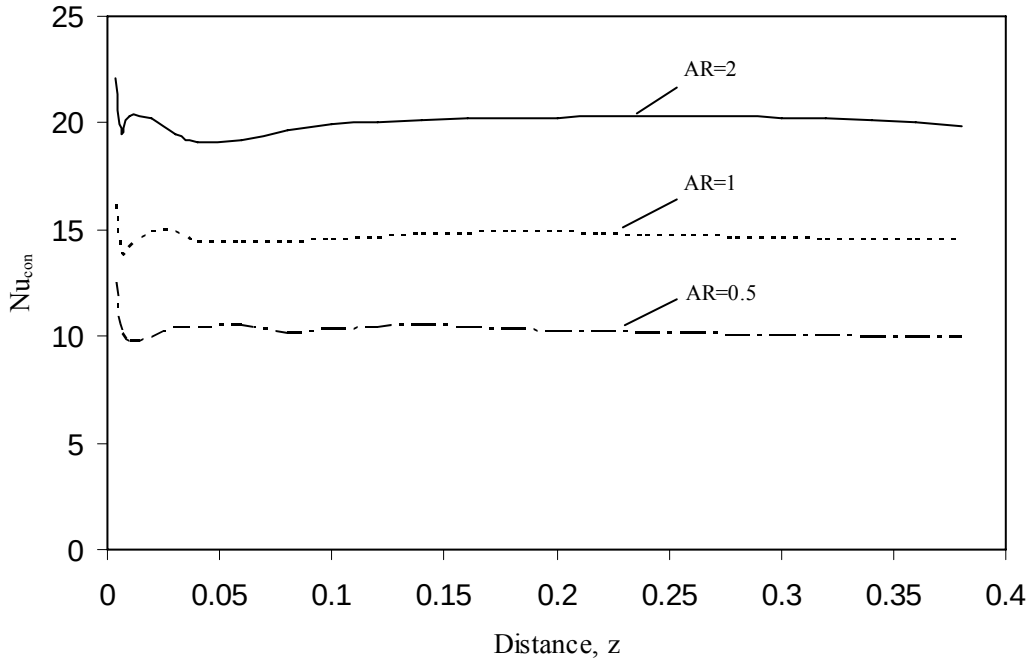

Figure 4.24 Effect of duct aspect ratio on average convective Nusselt number at heated wall (Gr = 1,000,000 , ε = 0.05)

When considering the heat transfer conditions where strong radiation effect (ε = 0.85) is imposed, higher aspect ratio generally has higher overall convective Nusselt (Nu_{con}) number values than lower aspect ratio. However, results from section 4.3.2 indicate that strong radiation (ε = 0.85) could generate the effect of bottom wall heating. When considering the effect of aspect ratio in the case of strong radiation, it is found that increasing aspect ratio delays the occurrence of the onset of instability. Figure 4.25 compares the variation of transverse average convective Nusselt number along the heated wall for each aspect ratio when Gr = 1,000,000 and ε = 0.85. The onset of instability detected in aspect ratio of 2 is near the outlet of the duct while for aspect ratio of 0.5, it is detected at approximately the

middle of the length of duct. On the other hand, with the same Grashof number, lower aspect ratio tends to lessen the amplitudes of fluctuations on the convective Nusselt number. This effect can be described due to the fact that a lower aspect ratio duct has less bottom wall area, and therefore has less influence in bottom wall heating.

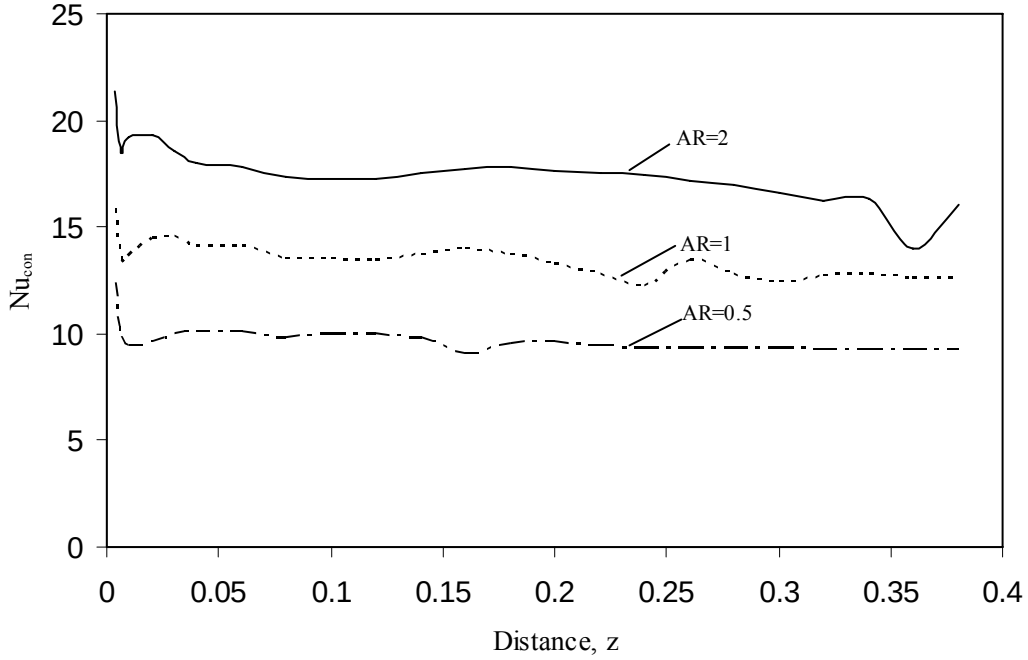

Figure 4.25 Effect of duct aspect ratio on heated wall average convective Nusselt number (Gr = 1,000,000 , ε = 0.85)

When considering the cases of strong radiation, the radiative Nusselt (Nu_{rad}) numbers from each aspect ratio need to be discussed. In general, higher aspect ratio has higher values of radiative Nusselt number irrespective of the wall surface emissivity. Figure 4.26 shows radiative Nusselt number variations for Gr =1,000,000 and ε = 0.85 on each aspect ratio. Higher aspect ratio benefits from having lower bulk mean fluid temperature, thereby causing the radiative Nusselt number to be higher.

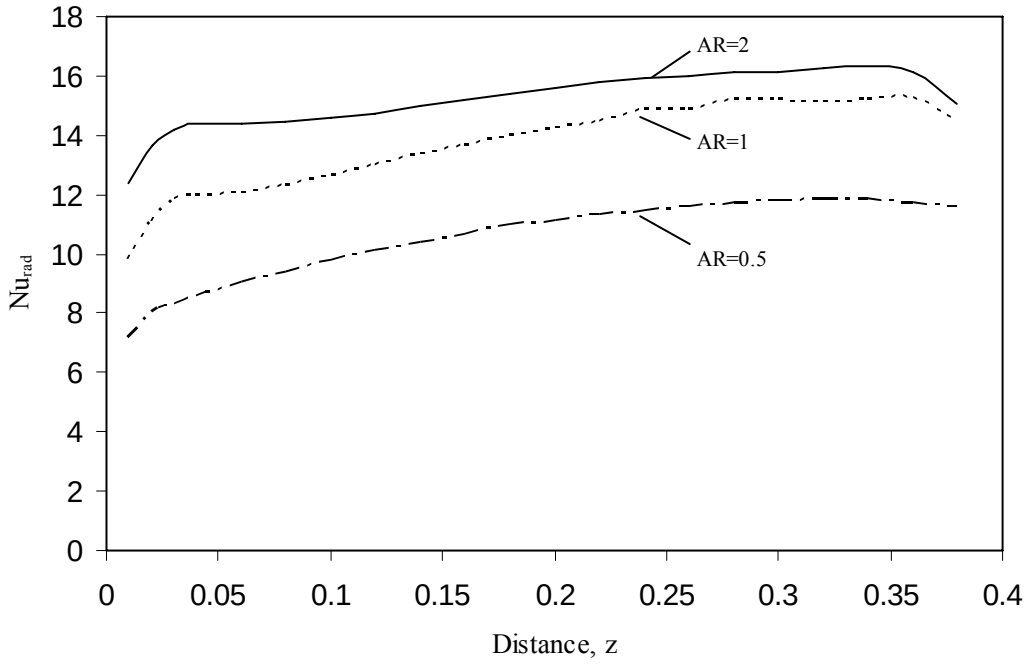

Figure 4.26 Effect of duct aspect ratio on heated wall average radiative Nusselt number (Gr = 1,000,000 , ε = 0.85)

For each aspect ratio, the radiative Nusselt number slightly increases along the length of the duct. The radiative heat flux is maintained to be approximately a constant value for the most part of the duct, except the inlet and outlet where some of the radiative energy is lost to the surroundings. This behaviour is represented in the rapid increase of Nusselt number around the inlet and rapid decline around the outlet regions of Figure 4.26.

4.3.4 Variation of Bulk Mean Fluid Temperature

In the present study, the bulk mean fluid temperature is a significant parameter in order to calculate the values of Nusselt number. Generally, for any case, the bulk mean fluid temperature increases as the fluid flows through a heated duct. Figures 4.27 to 4.29 show the variation of bulk mean fluid temperature as a function of duct length for ε = 0.05, 0.85, for a range of Grashof numbers - 2,000, 100,000 and 1,000,000, respectively, in order to represent the flow condition from being dominated by forced convection, to dominated by natural convection flow.

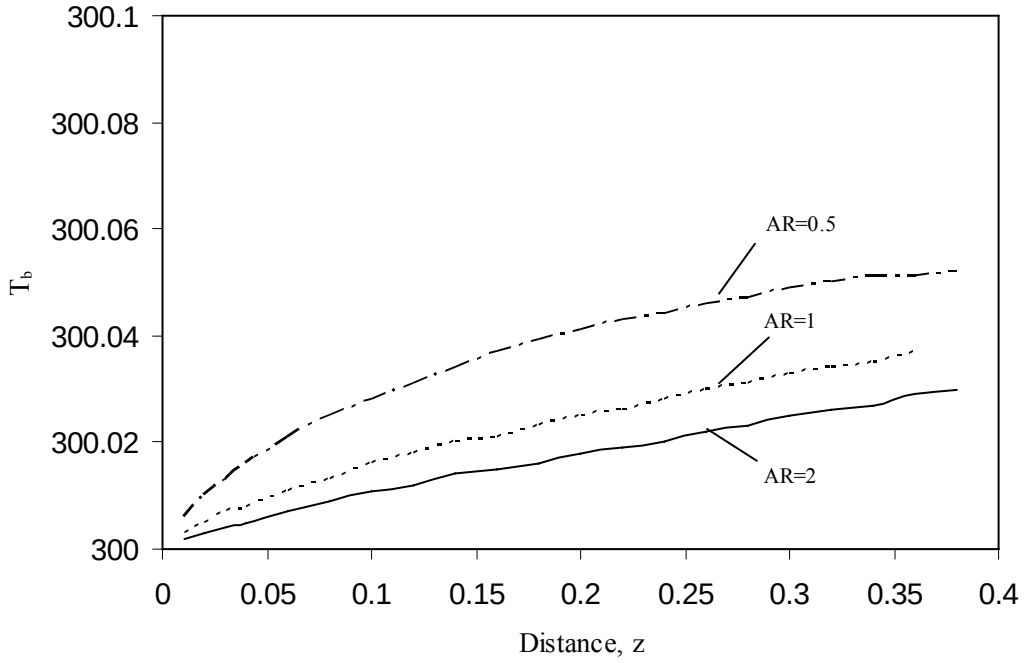

(i)

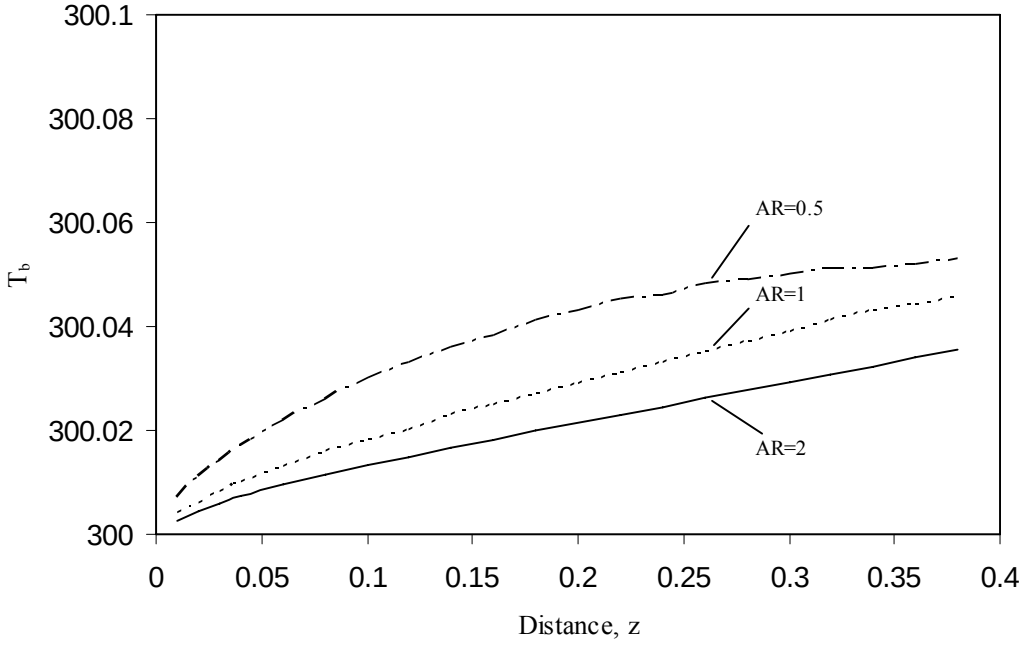

(ii)

Figure 4.27 Variation of bulk mean fluid temperature (K) for different AR and Gr = 2,000 (i) $\varepsilon = 0.05$, (ii) $\varepsilon = 0.85$

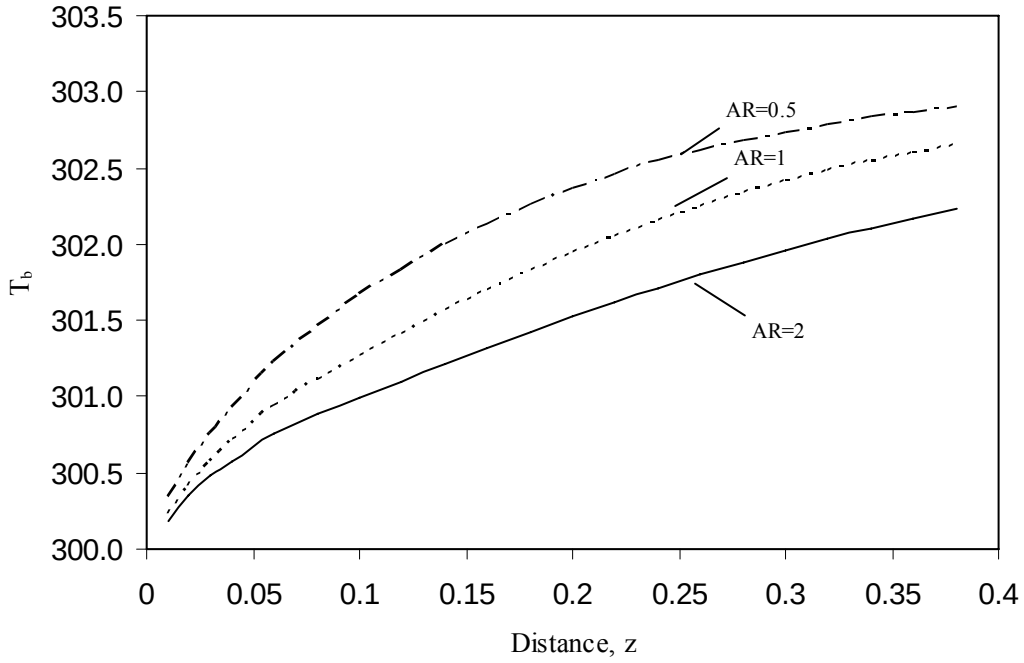

(i)

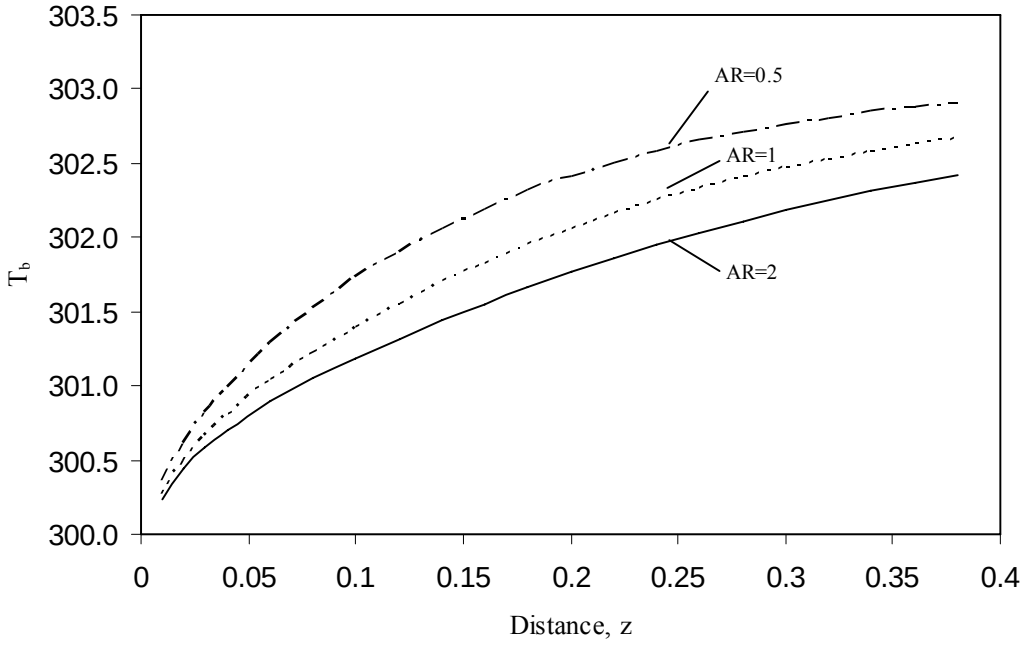

(ii)

Figure 4.28 Variation of bulk mean fluid temperature (K) for different AR and Gr = 100,000 (i) $\varepsilon = 0.05$, (ii) $\varepsilon = 0.85$

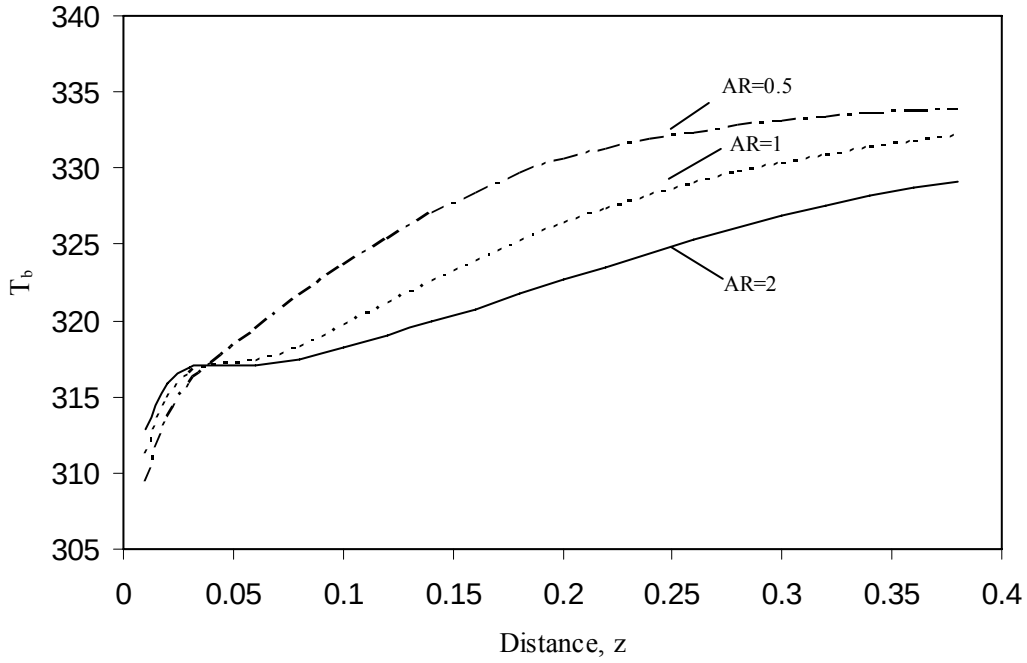

(i)

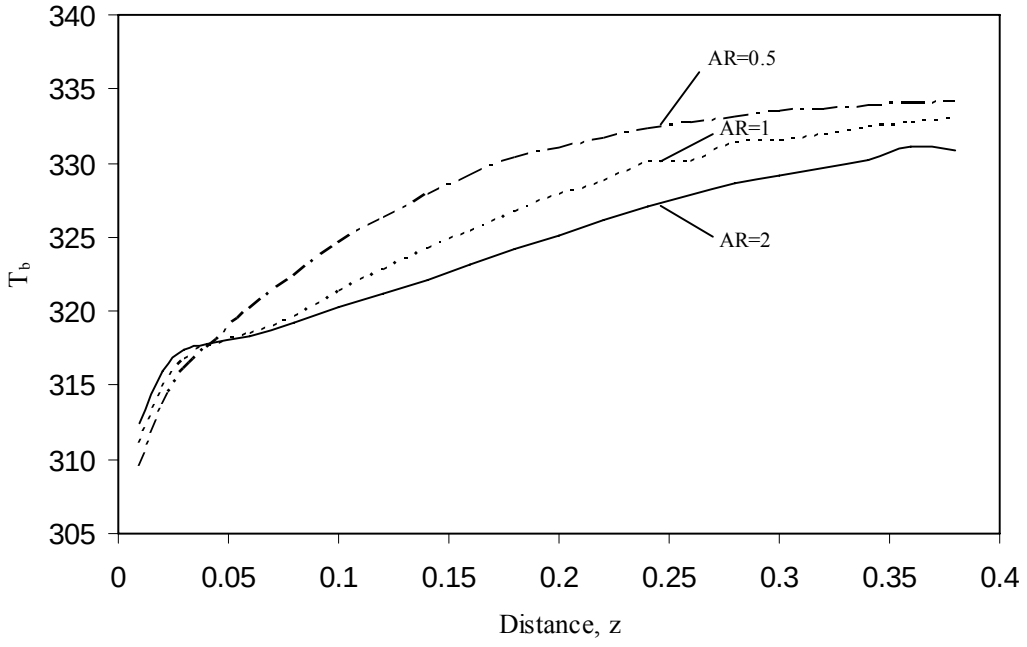

(ii)

Figure 4.29 Variation of bulk mean fluid temperature (K) for different AR and Gr = 1,000,000 (i) $\varepsilon = 0.05$, (ii) $\varepsilon = 0.85$

From the above figures, Figure 4.29 (i) and (ii) have different patterns compared to the others. For both emissivity cases, first the bulk mean fluid temperature patterns show decrease in the rate of change around the mixing length approximately 0.05 m from the entrance. Then the temperature patterns increase where the flow becomes thermally fully developed. The minor disturbances in AR = 1 and 2 in Figure 4.29 (ii) represent the fluid temperature variations caused by the bottom wall heating effect.

4.4 Closure

The results of a rectangular duct maintain at a uniform temperature on one vertical wall, and cooled by uniform temperature on the opposite wall, were presented in this chapter. The effects of mixed convection, radiation heat transfer, and aspect ratio have also been thoroughly discussed. These effects were found to influence the heat transfer characteristics. The heat transfer enhancement caused by natural convection, and the effect of bottom wall heating in strong radiative conditions are significant findings found in the study of uniform heating configuration. This completes the discussion of results for the case study CS1.

The results obtained from this chapter will be used later to compare with the linearly varying wall temperature heating in order to better understand each heating configuration. In the next chapter, the results obtained from heating configuration CS2 will be presented and discussed.

CHAPTER 5
CASE STUDY CS2 - LINEARLY VARYING WALL TEMPERATURE

5.1 Introduction

Variable temperature heating is found in several applications where the temperature on the heated wall is not uniform. Linearly varying temperature is a simplified model of the variable temperature heating. It will be extensively studied in this chapter and chapter 6.

Two important linearly varying temperature profiles are considered in the present work. The varying temperature profile is applied to only one vertical wall of the duct. The first profile is modelled such that it has the highest temperature (T_h) at the bottom of the vertical wall, and linearly decreases to the lowest temperature (T_c) at the top (configuration CS2). The second profile being studied is the case that has the highest temperature at the top, and linearly decreases to the lowest temperature at bottom of the vertical wall (configuration CS3). The difference in heating orientation leads to the difference in heating mechanisms, and thus results in different heat transfer characteristics.

Figure 5.1 illustrates the schematic diagram for the heating configuration CS2. The results of configuration CS2 will be presented and discussed in this chapter, while configuration CS3 will be presented in the next chapter.

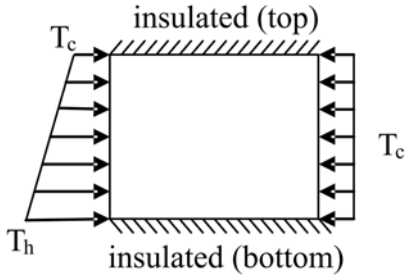

Figure 5.1 Heating configuration CS2

5.2 Problem Statement

In order to specify the buoyancy parameter in the case of uniform temperature (heating configuration CS1), the Grashof number was calculated directly from the specified values of T_h and T_c. However, for the case of temperature variation as given by CS2, neither the temperature nor the heat flux is uniform. The review of literature that involves non-uniform temperature or heat flux heating such as [21 - 23, 26] has shown that the Grashof number is defined based on the temperature difference ($T_h - T_c$) or the average heat flux. This definition of Grashof number does not fully describe the physical meaning in a non-uniform heating situation. However, this definition has been followed in the present study due to the fact that it provides a common base for comparison between uniform and non-uniform cases.

Therefore, the results for non-uniform heating cases are based on the Grashof number defined by:

$$Gr = \frac{g\beta(T_h - T_c)H^3}{\nu^2} \tag{5-1}$$

where T_h and T_c are the highest and lowest temperatures respectively. Both are equal to hot and cold temperature on the heated and cooled walls respectively in the case of uniform temperature heating. This implies that both uniform and variable temperature cases will have the same Grashof number as long as they have the same values of T_h and T_c. However, to simplify the calculation of local Nusselt number used in representing the heat transfer characteristics, equation (3-8) is changed in the case of variable wall temperature to:

$$Nu_l = \frac{q_l'' D_h}{k(T_{wall,avg} - T_b)} \tag{5-2}$$

where $T_{wall,avg}$ replaces T_{wall} in equation (3-8). $T_{wall,avg}$ can be obtained from averaging between T_h and T_c. This definition will simplify the calculation of local Nusselt number, but yet provide a meaningful result.

The simulation parameters in the case of variable wall temperature heating are the same as in the case of uniform wall temperature considered earlier in Chapter 4. The Grashof number ranges from 2,000 to 1,000,000, and the wall emissivity has two values: 0.05, 0.85. The aspect ratio is varied as 0.5, 1 and 2.

5.3 Results and Discussion

5.3.1 Combined Forced and Natural Convection Heat Transfer

Figures 5.2 to 5.4 show transverse average convective Nusselt number at the heated wall with the variation of Grashof numbers, for aspect ratio of 0.5, 1 and 2 respectively. The emissivity value is maintained at 0.05. Hence, radiation effect has no significant influence on the overall heat transfer.

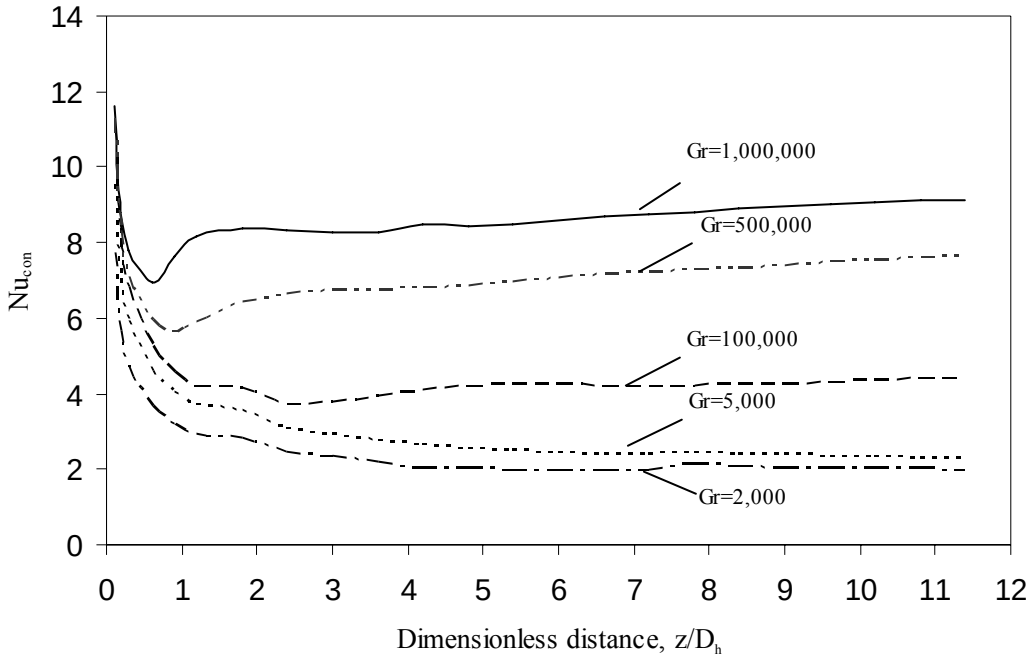

Figure 5.2 Effect of Grashof number on the average convective Nusselt number at heated wall (AR = 0.5, ε = 0.05)

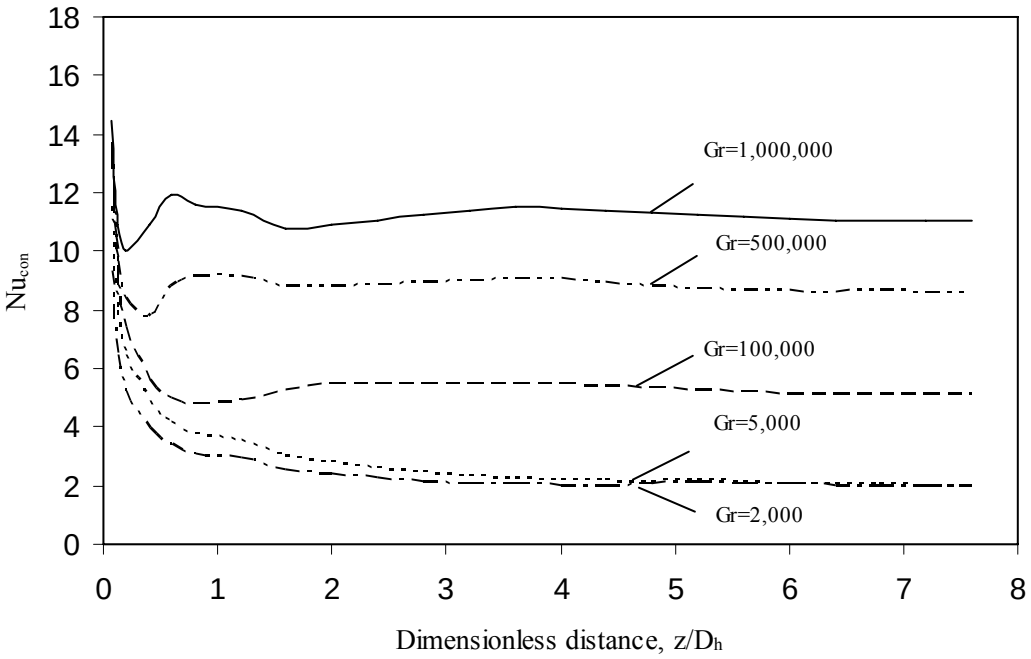

Figure 5.3 Effect of Grashof number on the average convective Nusselt number at heated wall (AR = 1, ε = 0.05)

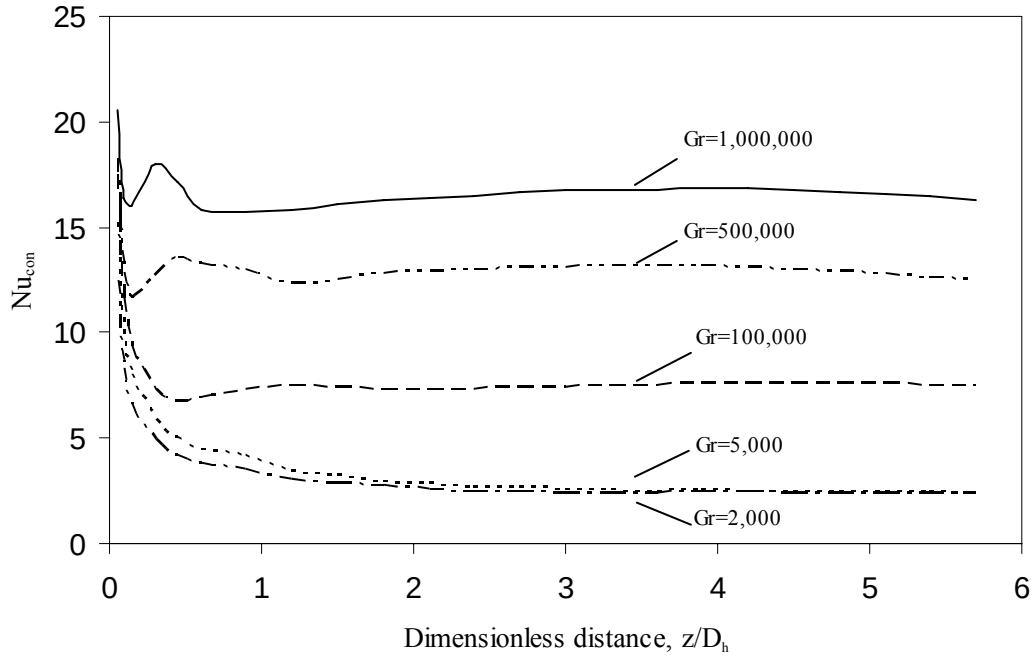

Figure 5.4 Effect of Grashof number on the average convective Nusselt number at heated wall (AR = 2, ε = 0.05)

It can be seen from the graphs that the Nusselt number decreases along the duct length and eventually reaches the thermally fully developed state. For low Grashof numbers, the pattern is similar to the forced convection cases for uniform wall heating.

The enhancement of heat transfer is seen at Grashof number equal to 100,000 and above. The graph patterns indicate an increment of Nusselt numbers because of augmentation due to natural convection. The entrance length where the flow is thermally developing for these high Grashof numbers is approximately 1-3 times the hydraulic diameter of the duct.

For heating configuration CS2, when air enters the duct with Grashof number high enough to induce the effect of natural convection (as in the present work, Gr = 100,000 and above), the heated wall increases the air temperature non-uniformly near its vicinity. It gives higher heat transfer rates at the bottom than the top part of the duct. Thermal boundary layer starts developing rapidly near the bottom part of the heated wall. Warm air rises and accumulates at the top part of the duct due to buoyancy effect. With the same behaviour as in the cases of uniform wall temperature, the accumulated warm air at the top moves slowly, and hence reduces the speed of the flow around this area. As a result, air near the top has lower velocity than the bottom. As air moves along the length of the duct, warm air accumulating at the top part of the duct causes the cool air at the bottom part to flow at a higher velocity, in order to satisfy continuity conditions. The onset of secondary circulation is also developing, together with the presence of high fluid velocity at the bottom areas. This effect causes cool and high velocity fluid moving toward the heated wall and eventually enhances heat transfer.

The heating configuration CS2 where the highest temperature (T_h) is at the bottom heats up and accelerates the air at a higher rate than the top part of the duct. However, once the air rises to the top part, the heated wall has a lower heating temperature. This effect causes flow separation around the top corner of the heated wall. This can be seen from the velocity contour plot. Figures 5.5 to 5.7 illustrates the temperature and velocity contours of the air for certain cases. At the top left corner of Figure 5.7, there is a circulation zone of the cool air caused by heated wall

where temperature around this location approaches the lowest temperature (T_c). This effect makes the top part of the heated wall remove heat from the air instead of heating it. As a result, it reduces the overall heat transfer rate, and lessens the heat transfer enhancement promoted by natural convection heat transfer.

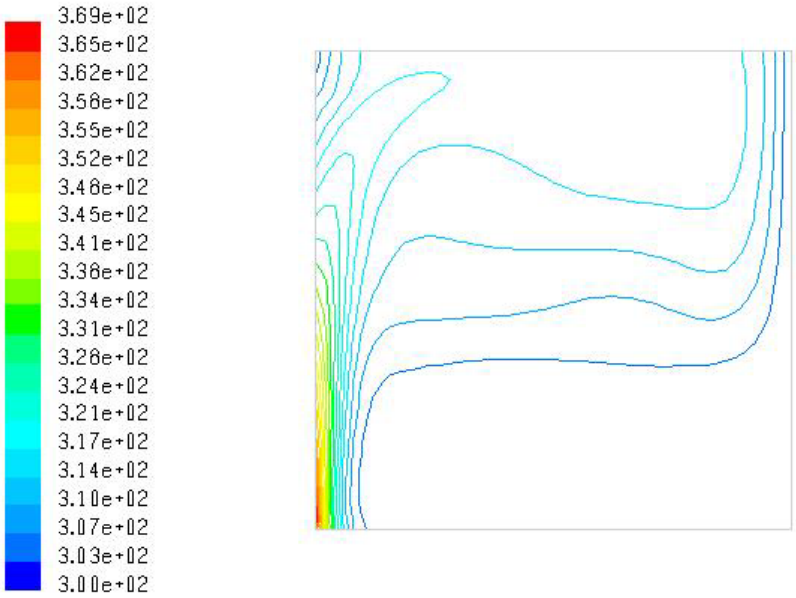

Figure 5.5 Cross sectional temperature (K) contour of air in the rectangular duct at a distance of 1 hydraulic diameter from inlet
(AR = 1, Gr = 1,000,000, ε = 0.05)

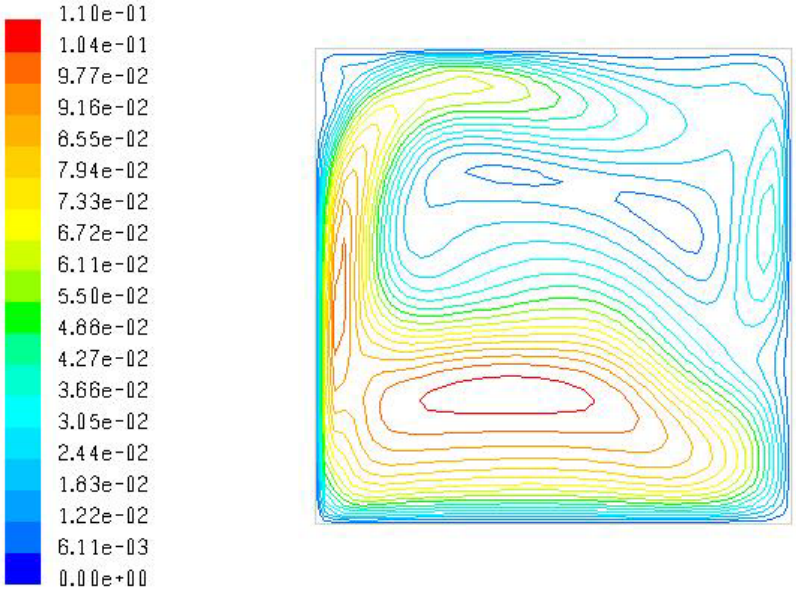

Figure 5.6 Cross sectional velocity (m/s) contour of air in the rectangular duct at a distance of 1 hydraulic diameter from inlet (AR = 1, Gr = 1,000,000, ε = 0.05)

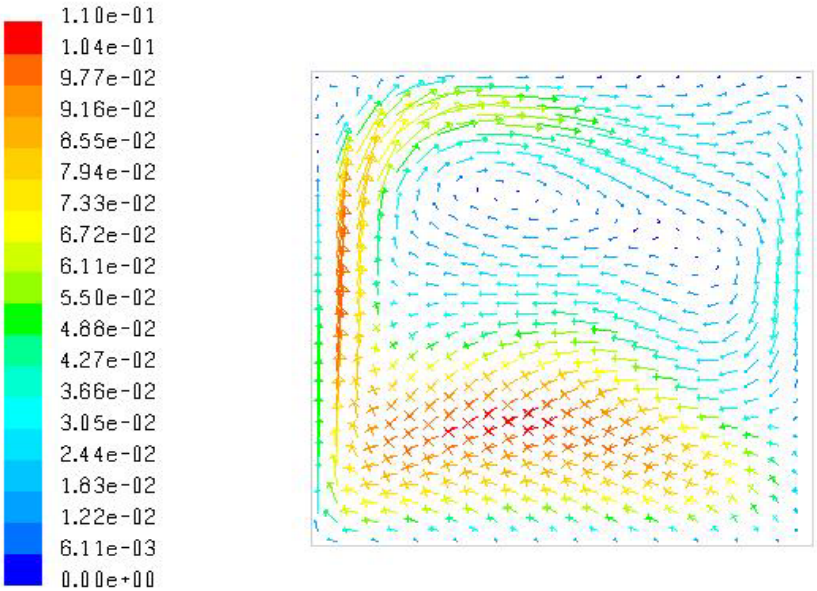

Figure 5.7 Cross sectional velocity (m/s) vector of air in the rectangular duct at a distance of 1 hydraulic diameter from inlet. The vectors show flow separation at the top left corner. (AR = 1, Gr = 1,000,000, ε = 0.05).

5.3.2 Radiation Heat Transfer

When the flow through the heated duct with walls having high surface emissivity (ε = 085), Figures 5.8 to 5.10 show the variation of transverse average convective Nusselt number as a function of Grashof number for the case of high emissive walls (ε = 0.85) for aspect ratio of 0.5, 1 and 2, respectively.

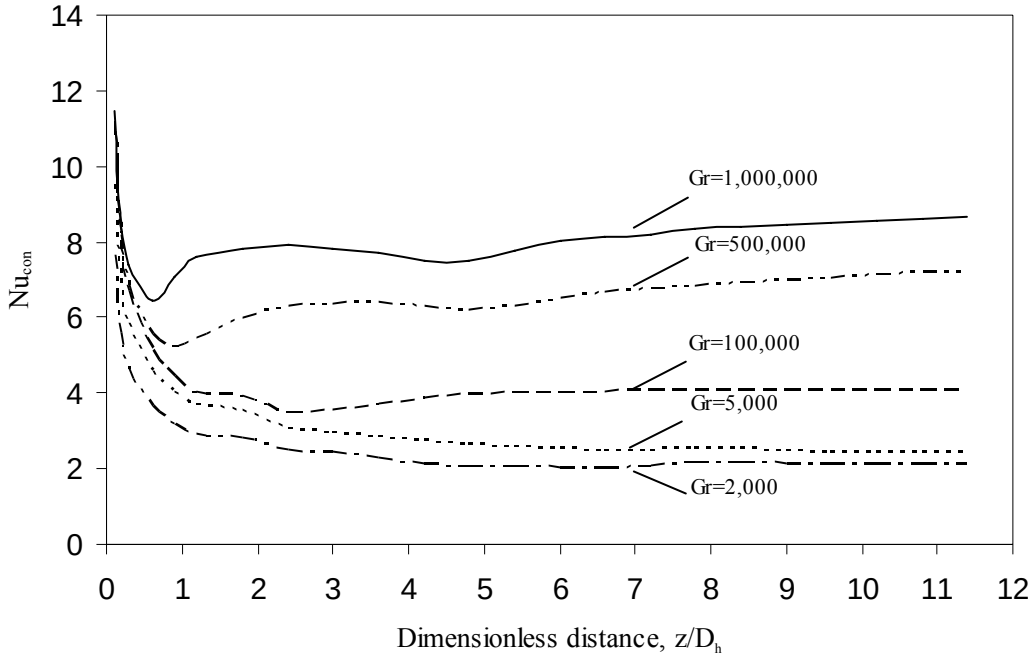

Figure 5.8 Effect of Grashof number on the average convective Nusselt number at heated wall (AR = 0.5, ε = 0.85)

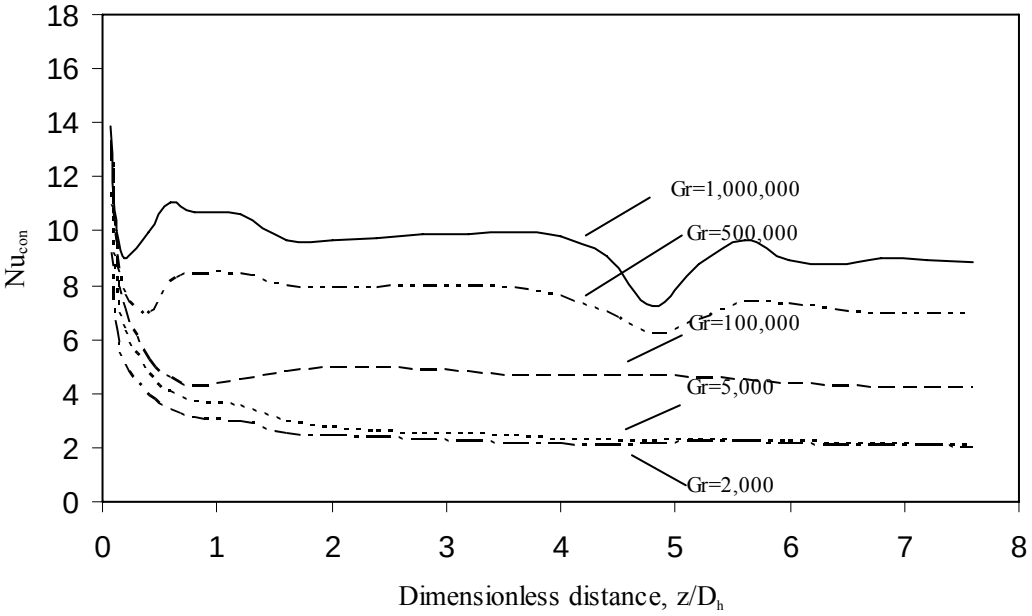

Figure 5.9 Effect of Grashof number on the average convective Nusselt number at heated wall (AR = 1, ε = 0.85)

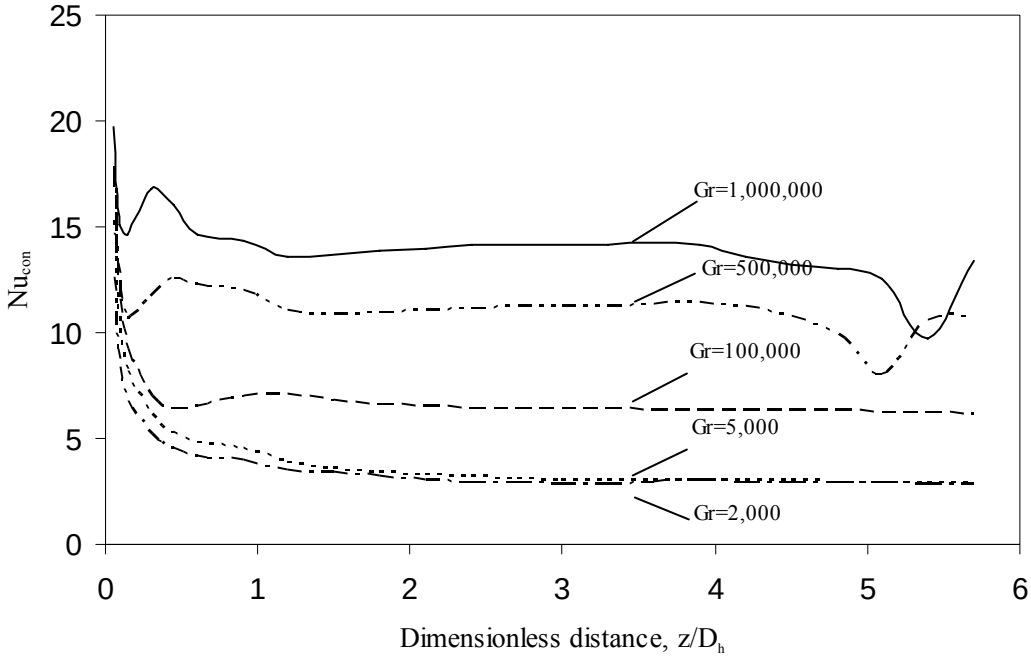

Figure 5.10 Effect of Grashof number on the average convective Nusselt number at heated wall number (AR = 2, ε = 0.85)

It can be seen that the patterns of Nusselt number for different Grashof numbers are comparable to the case of low surface emissivity (ε = 0.05) shown earlier in Figures 5.2 to 5.4. The Nusselt number values for both emissivity cases, 0.05 and 0.85, are of the same order. It is obvious that surface radiation heat transfer has no direct interaction with the convective flow. However, when the temperature difference between hot and cold walls is large, which is the case of high Grashof number, the fluctuations on the Nusselt number values can be seen for all aspect ratios. This effect is also detected in the case of uniform wall temperature. This is because the top and bottom walls are heated by radiation heat transfer from the heated wall. As in the literature of bottom wall heating, instability of heat transfer can be detected downstream from the inlet. Since in this case, the bottom wall is also transferring the energy obtained from heated wall by means of convection heat transfer to the flow, flow instability is expected downstream of the duct.

Figure 5.11 shows the graph of transverse average radiative Nusselt number for different Grashof numbers at heated wall for AR = 1. Generally, increasing Grashof number also increases the values of radiative Nusselt number. The pattern

of the graphs shown follows the same pattern as in the case of uniform temperature where radiative Nusselt number rapidly increases at the initial part of the duct. The graph then slightly increases along the length of the duct until it drops near the outlet. The increment of radiative Nusselt number is contributed by values of bulk mean fluid temperature (T_b) which is used to calculate Nusselt number in equation (5-2). The values of radiative heat flux are slightly changed along the duct except only at the inlet and outlet. This agrees with the expectation that surface radiation is independent to the flow, and remains almost constant throughout the length of the duct except in the area near the inlet and outlet, where radiative energy is lost to the surroundings.

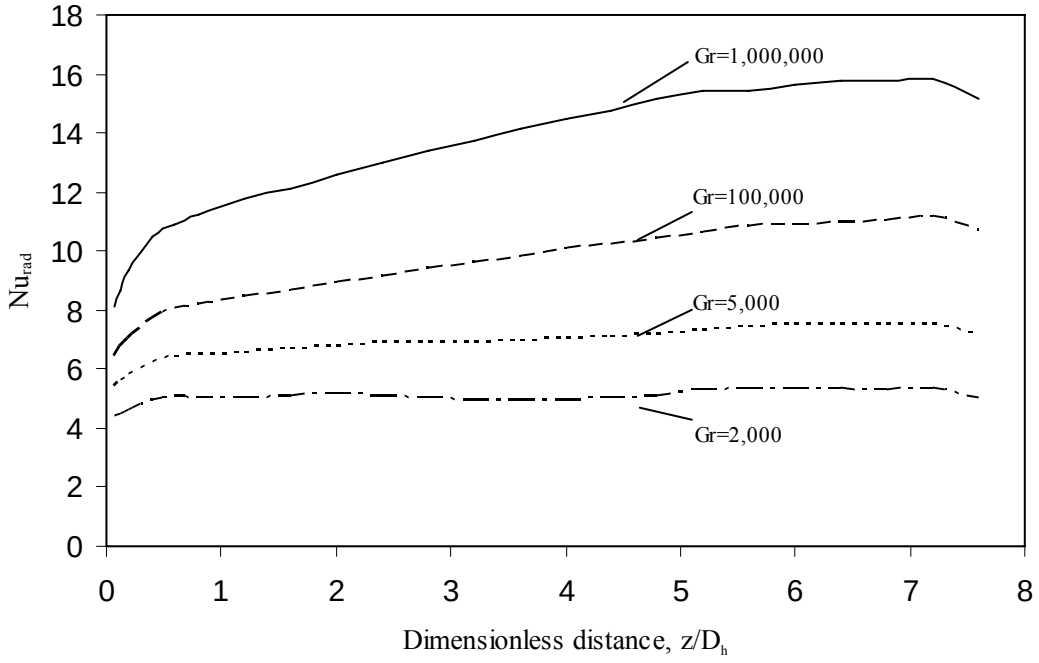

Figure 5.11 Effect of Grashof number on the average radiative Nusselt number at heated wall (AR = 1, ε = 0.85)

To give a clear picture of the interaction between convection and radiation heat transfer, Figure 5.12 (i) and (ii) show the ratio of convective and radiative Nusselt number to the total Nusselt number respectively.

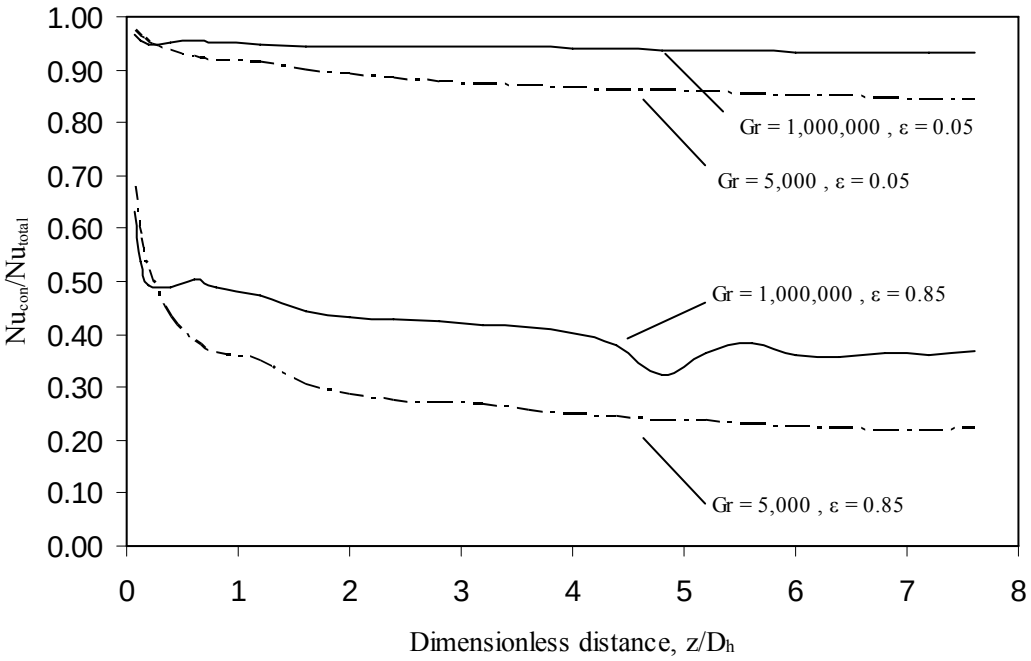

(i)

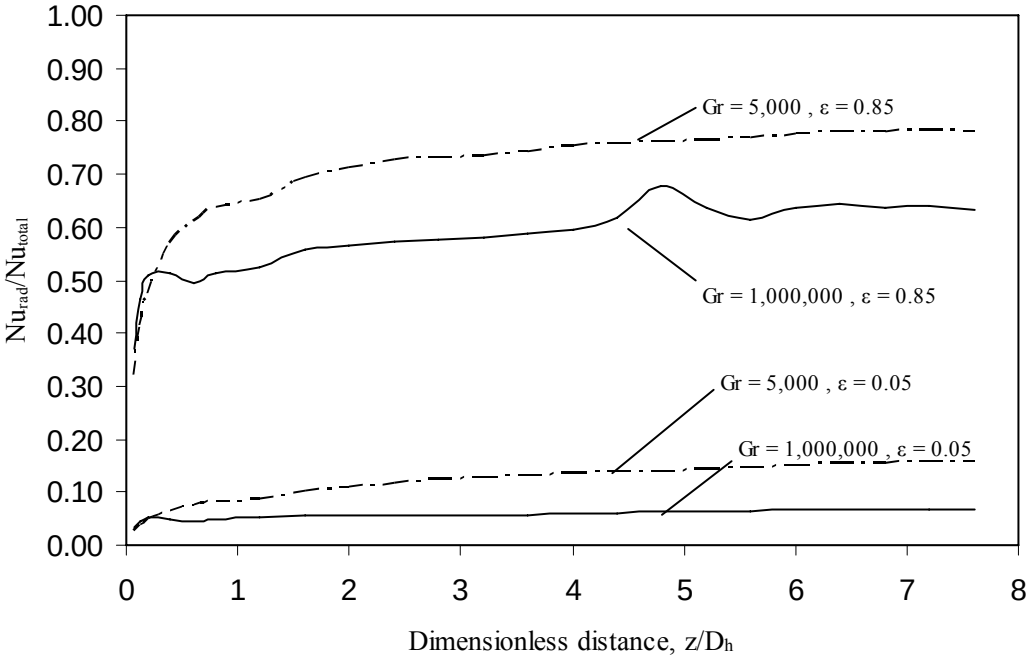

(ii)

Figure 5.12 Ratio of (i) convective to total Nusselt number and (ii) radiative to total Nusselt number (AR = 1)

The patterns in Figure 5.12 follow the same trend as in the previous chapter (Figure 4.23). However, the percentage of radiation is higher than convection for both strong forced convection and strong natural convection. The fluctuations of the graph as seen in the case of high emissivity indicate the onset of thermal instability of the flow. Radiation heat transfer appears to influence this type of heating configuration (CS2) more than the previous one (CS1).

5.3.3 Duct Aspect Ratio

Figures 5.13 and 5.14 show the graphs of transverse average convective Nusselt number (Nu_{con}) at heated wall for the aspect ratios considered in this study. Figure 5.13 is for the case of weak radiation effect ($\varepsilon = 0.05$), while Figure 5.14 shows the results for the case of strong surface radiation ($\varepsilon = 0.85$). Both figures present the flow conditions when Grashof number is equal to 1,000,000, which provides the most meaningful results.

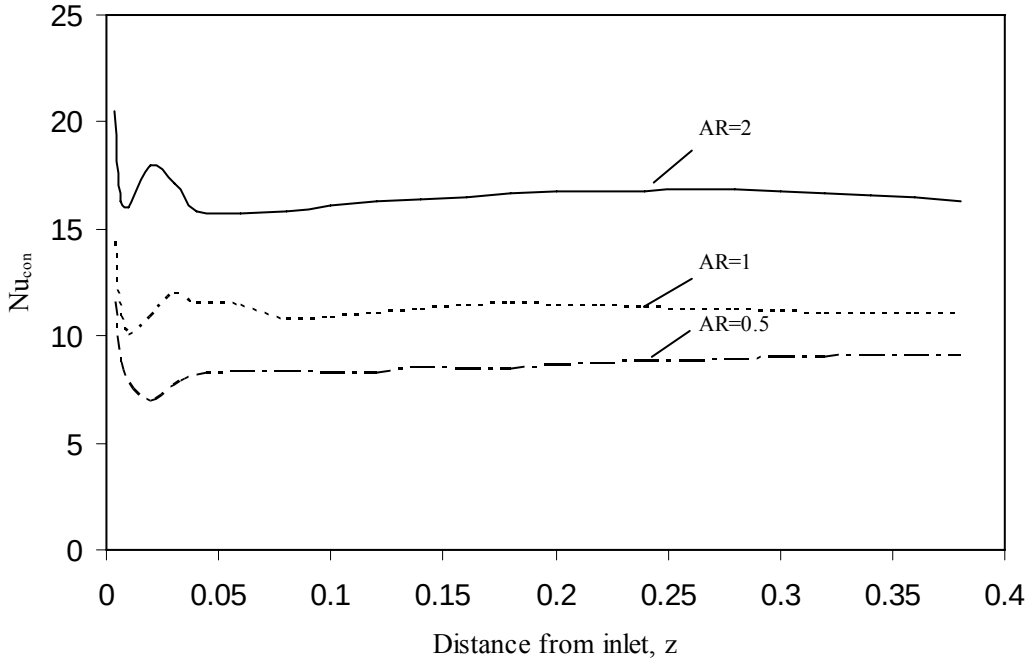

Figure 5.13 Effect of aspect ratio on the average convective Nusselt number at heated wall (Gr = 1,000,000, $\varepsilon = 0.05$)

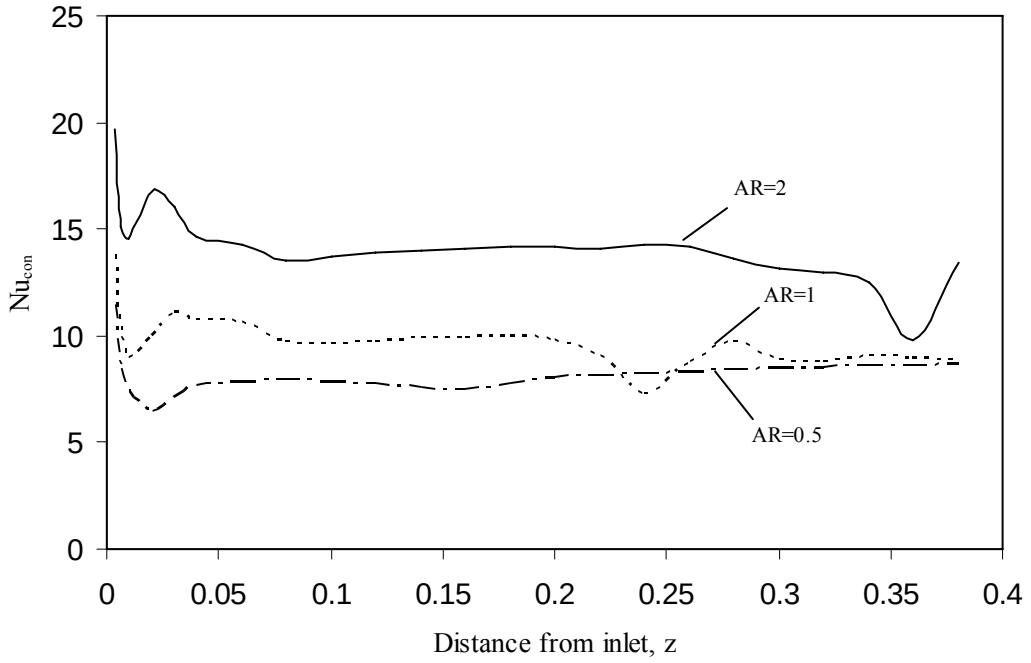

Figure 5.14 Effect of aspect ratio on the average convective Nusselt number at heated wall (Gr = 1,000,000, ε = 0.85)

In general, for every Grashof number, aspect ratio of 2 results in highest heat transfer rates. On the other hand, aspect ratio of 0.5 offers the lowest heat transfer rates. The difference between weak and strong radiation can be seen only from the case where Grashof number is high (such as Gr = 1,000,000).

In the case of high Grashof number where the onset of heat transfer instability is seen, as in Figure 5.14, increasing the aspect ratio helps delay the onset of thermal instability, but results in having higher fluctuation amplitude in the graphs of Nusselt number. Lower aspect ratio duct has less bottom wall area, and thus results in having less bottom wall heating effect. Higher aspect ratio duct gets higher effect of thermal instability. However, having larger distance between the heated and cooled walls results in having less wall heating effects caused by radiation heat exchange between the heated and cooled walls, which delays the onset of thermal instability.

5.4 Comparison of Heating Configuration CS2 with CS1

Figure 5.15 shows schematic diagrams of the cross section of a rectangular duct which is heated by uniform temperature (CS1), and linearly varying temperature

(CS2). Note that the hot and cold temperatures (T_h and T_c) of both cases share the same maximum and minimum values.

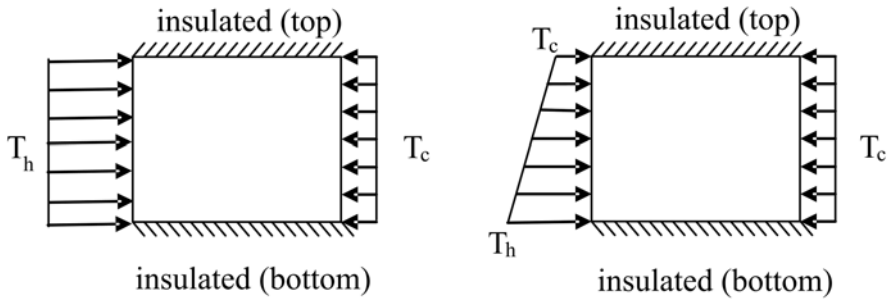

(i) (ii)

Figure 5.15 Heating configuration: (i) uniform temperature (CS1), and (ii) linearly varying temperature (CS2)

Due to both cases having the same maximum value of hot temperature, T_h, configuration CS1 applies hot temperature uniformly over the heated wall, while CS2 has temperature decreasing linearly along the height of the duct. Figure 5.16 shows the comparison of patterns of transverse average convective Nusselt number at the heated wall between these two heating configurations.

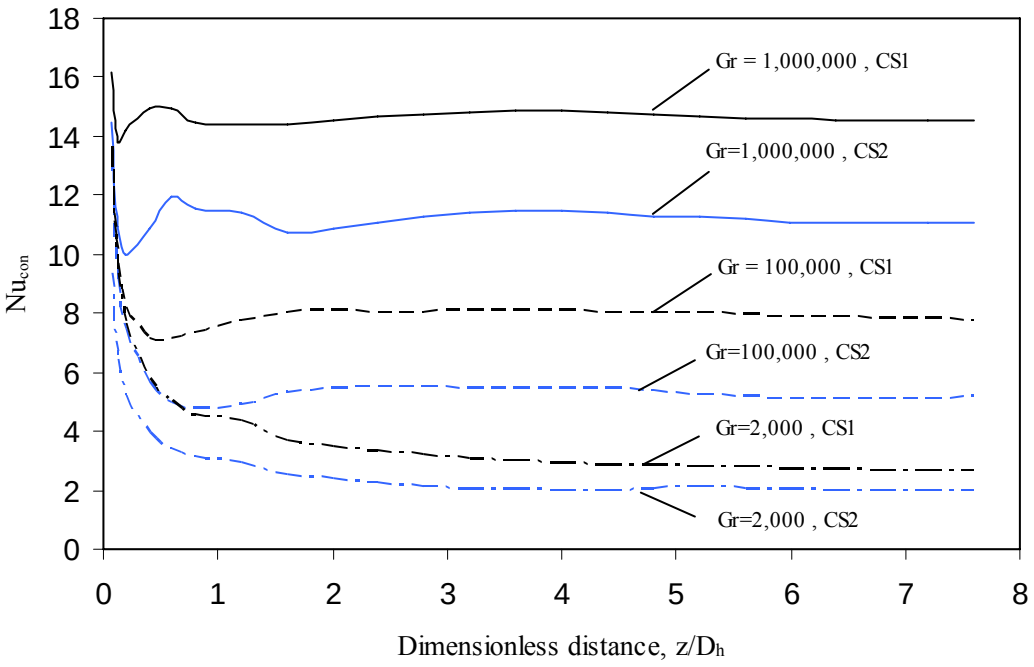

Figure 5.16 Comparison of the effect of Grashof number on the average convective Nusselt number at heated wall between CS1 and CS2 (AR = 1, ε = 0.05)

From the above figure, it can be seen that the patterns of Nusselt number between CS1 and CS2 follow the same trend. However, CS1 has generally higher the Nusselt number values than CS2 as expected. CS2 has lower convective Nusselt number values than CS1. The percentage differences in the Nusselt number values lie in the range of 25 - 40%.

Considering the case where radiation heat transfer effect is dominated. Figure 5.17 shows the comparison of transverse average convective Nusselt number between configuration CS1 and CS2 in the presence of high emissivity (ε = 0.85).

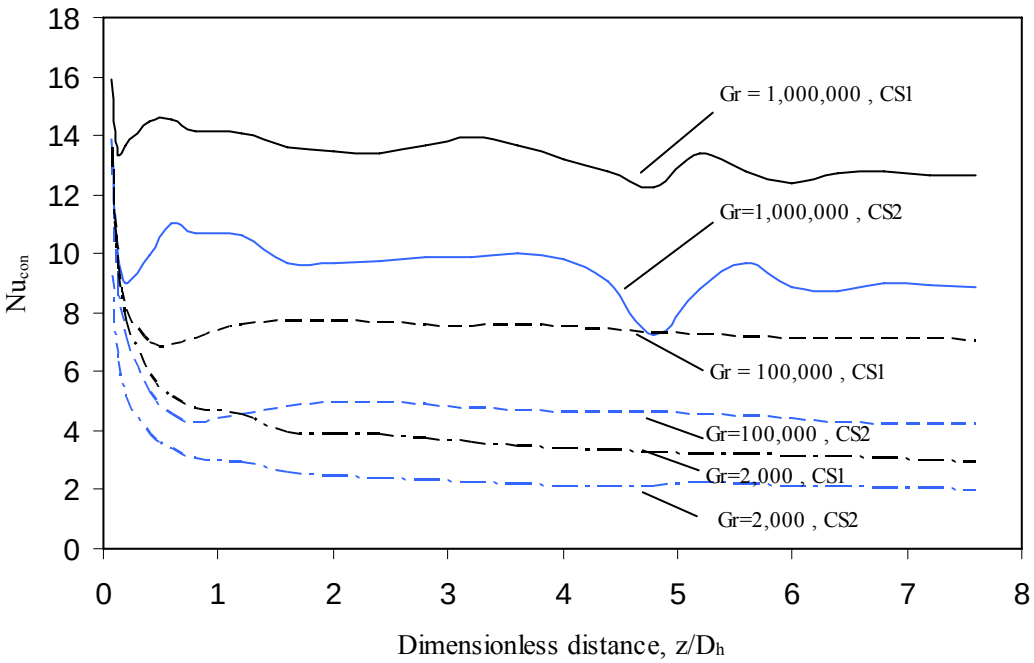

Figure 5.17 Comparison of the effect of Grashof number on the average convective Nusselt number at heated wall between CS1 and CS2 (AR = 1, ε = 0.85)

The graphs of heating configuration CS2 also follow the same trends as configuration CS1. CS2 has Nusselt number values lower than CS1. The difference is approximately between 30 - 45%. The fluctuation of Nusselt number values in the case of Grashof number = 1,000,000 due to effect of bottom wall heating seems to have a higher amplitude in the configuration CS2 than CS1.

Figure 5.18 shows the comparison between CS1 and CS2 for different aspect ratios. The figure shows the results of the variation of transverse average convective

Nusselt number at the heated wall for the case of Grashof number equal to 1,000,000 and emissivity equal to 0.85.

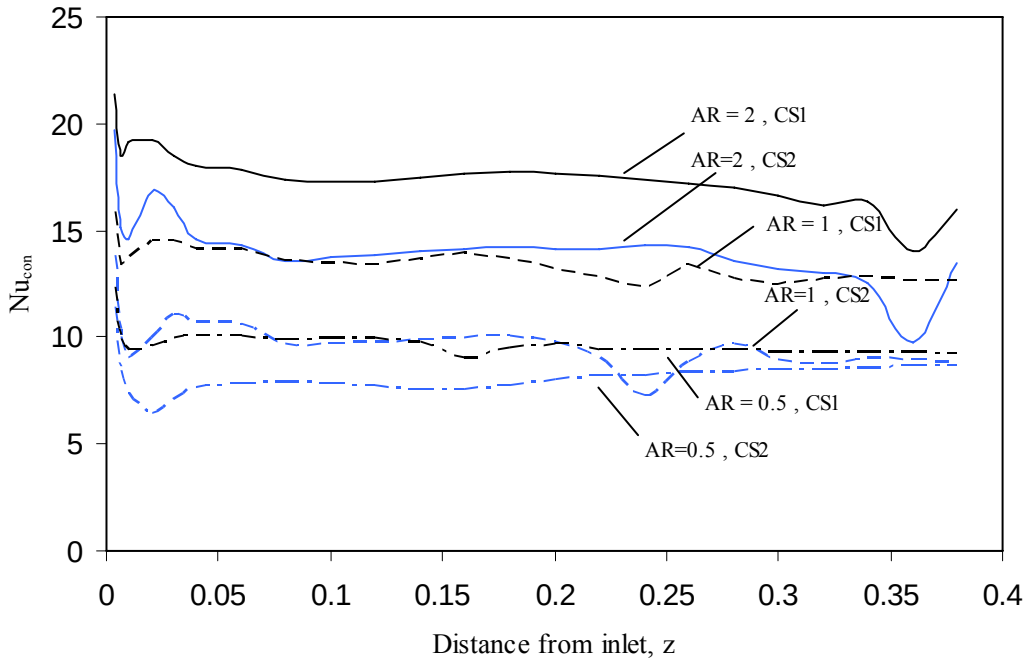

Figure 5.18 Comparison of the effect of aspect ratio on the average convective Nusselt number at heated wall between CS1 and CS2 (Gr = 1,000,000, ε = 0.85)

The trends in the figure show that CS1 has the same trend as CS2. Configuration CS1 generally has higher Nusselt number values than CS2. The percentage differences in the Nusselt number values between these two heating configurations are approximately 15 - 35%. For both CS1 and CS2, in the presence of strong radiation, decreasing the aspect ratio helps decrease the level of fluctuation of the Nusselt number values.

5.5 Closure

In this chapter, the flow patterns mechanism and heat transfer characteristics of heating configuration CS2 have been presented and discussed. The results are also compared with the case of uniform heating (configuration CS1) in order to explain the differences in heat transfer characteristics between these two heating configurations.

In the next chapter, the results of another case study in linearly varying temperature heating (configuration CS3) will be presented and discussed. Later on, the heat transfer characteristics of CS3 will be compared with CS1 and CS2.

CHAPTER 6
CASE STUDY CS3 - LINEARLY VARYING WALL TEMPERATURE

6.1 Introduction

In this chapter, the heating configuration CS3 is considered. In this configuration, the maximum temperature (T_h) is imposed at the top of the heated wall. The temperature decreases linearly down to cold temperature (T_c) at the bottom of the heated wall. The problem statement is presented first, followed by the results and discussion. The results obtained for this heating configuration is then compared with the cases of uniform temperature CS1, and linearly varying temperature heating CS2 to give a complete description and understanding of the heat transfer characteristics.

Figure 6.1 illustrates a schematic diagram of the heating configuration CS3. It is different from CS2 only in the way in which the temperature profile is applied on the heated wall. CS3 has opposite heating orientation as compared to CS2.

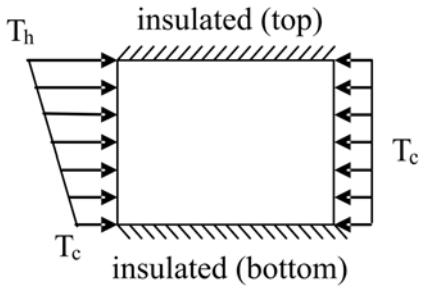

Figure 6.1 Schematic diagram of heating configuration CS3

6.2 Problem Statement

Due to this case study being a variable temperature case, as discussed earlier in section 5.2, the Grashof number has the same definition as equation (5-1). The local Nusselt number for this case is calculated from equation (5-2).

The simulation parameters in this case study remain the same as in the previous heating configurations. The Grashof number ranges from 2,000 to

1,000,000, while the radiative emissivity has two values: 0.05 and 0.85. The aspect ratio is varied from 0.5, 1 and 2.

6.3 Results and Discussion

6.3.1 Combined Forced and Natural Convection Heat Transfer

The variation of convective Nusselt numbers at the heated wall with effect from Grashof numbers, and low surface emissivity (ε = 0.05) is presented in Figures 6.2 to 6.4 for aspect ratios 0.5, 1 and 2, respectively. The effect of Grashof number on transverse average convective Nusselt number is investigated.

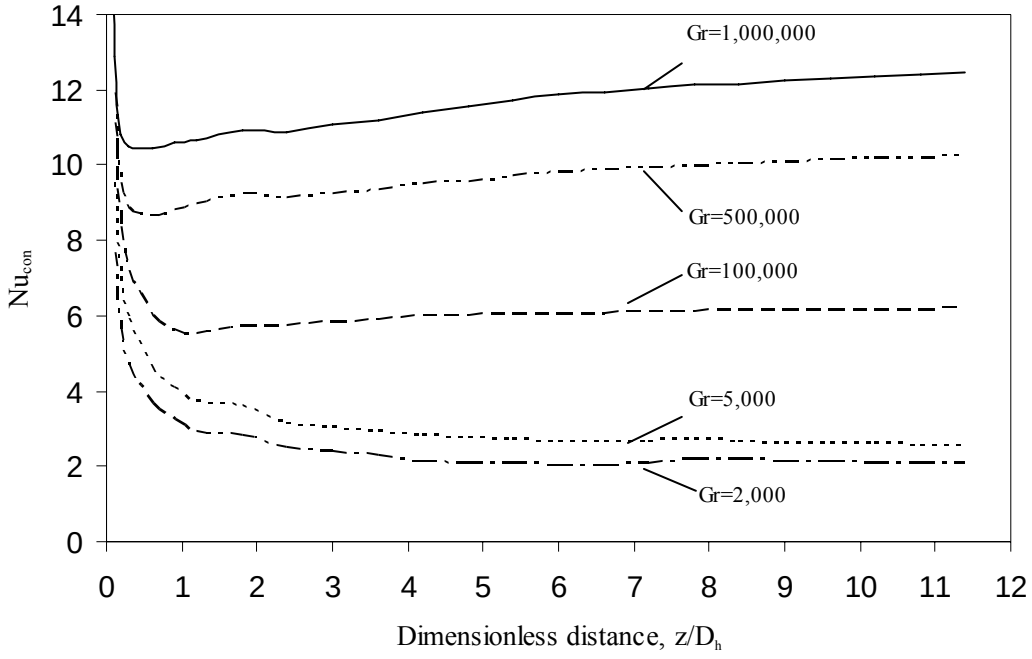

Figure 6.2 Effect of Grashof number on the average convective Nusselt number at heated wall (AR = 0.5, ε = 0.05)

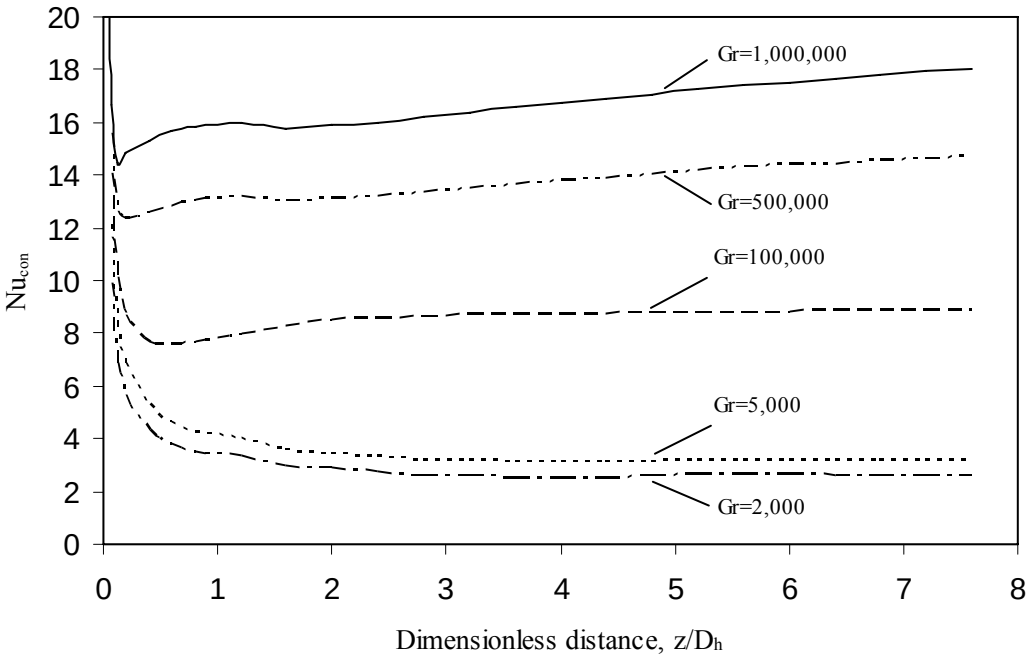

Figure 6.3 Effect of Grashof number on the average convective Nusselt number at heated wall (AR = 1, ε = 0.05)

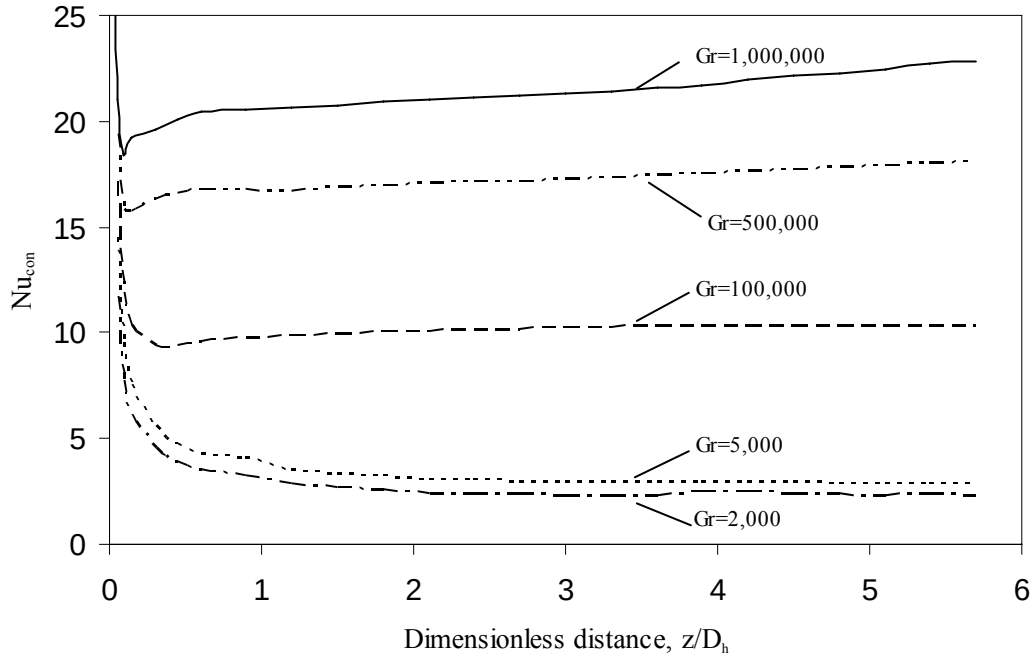

Figure 6.4 Effect of Grashof number on the average convective Nusselt number at heated wall (AR = 2, ε = 0.05)

From the above graphs, for each aspect ratio, at low Grashof numbers (2,000, 5,000), the average convective Nusselt numbers show the flow is dominated by the influence of forced convection heat transfer. Nusselt numbers decrease rapidly after the flow enters the duct. Thermal boundary layers are developing at this stage. Then, as the flow passes along the duct, Nusselt numbers decrease at a lower rate as thermal boundary layers are approaching the fully developed state. Once they reach the fully developed condition, Nusselt numbers reach a certain value and remain almost constant.

For Grashof numbers higher than 100,000, the heat transfer characteristics are more dominated by natural convection heat transfer. The augmentation of Nusselt number values indicates the onset of flow circulation created by natural convection, which promotes heat transfer. This natural convection induced flow circulates circumferentially in the rectangular duct and moves toward the outlet. Thermal boundary layers due to natural and forced convection heat transfer modes are present in the duct. The flow reaches the thermally fully developed stage at a duct length approximately 2 - 4 times the hydraulic diameter of the duct. However, in the case of high Grashof number (Gr = 500,000 and above), the increment of Nusselt number values still exists but at very low rates. With additional information from numerical flow visualization and results data, it is found that the thermal boundary layers have reached the fully developed stage at the region located along the duct approximately 2 times the hydraulic diameter. Meanwhile, the heat fluxes are decreasing at a lower rate than T_b. From equation (5-2), this contributes to the slight increment for Nusselt number values.

The heating configuration CS3 has the highest temperature T_h at the top of the heated wall. The air near the heated wall is heated non-uniformly by the varying temperature of the wall. Due to the buoyancy effect from natural convection heat transfer, the heated air rises to the upper part where the heated wall temperature increases linearly. Since air receives more energy as the flow rises up to the upper part, it does not create the flow separation as in the case of heating configuration CS2. The circulation caused by natural convection occurs around the circumference of the rectangular duct, which is regarded as secondary flow.

The heated air rises and accumulates around the top wall area. It has slower velocity compared to the cooler air at the bottom part of the duct. This accumulated air causes the air at the bottom part to be accelerated to satisfy the continuity equations. As the air at the bottom part is cooler and has higher velocity, it can then enhance the heat transfer at the heated wall because of the circulation created by natural convection effect pushing this cooler air toward the heated wall.

Figure 6.5 shows contours of fluid temperature of the cross section at a distance of one hydraulic diameter from the inlet, where the flow is still under thermally developing stage. The duct has aspect ratio of 1, and the hydraulic diameter is equal to 0.05 mm. The temperature contour indicates T_h at the top left corner of the figure. The temperature distribution shows areas of heated and cooled air. The heated air is accumulated at the top. It has slower velocity compared to the cooled air at the bottom, which can be seen from Figure 6.6. The enhancement of heat transfer occurs when cooled air from the bottom moving to the heated wall, which is illustrated by vector contour in Figure 6.7.

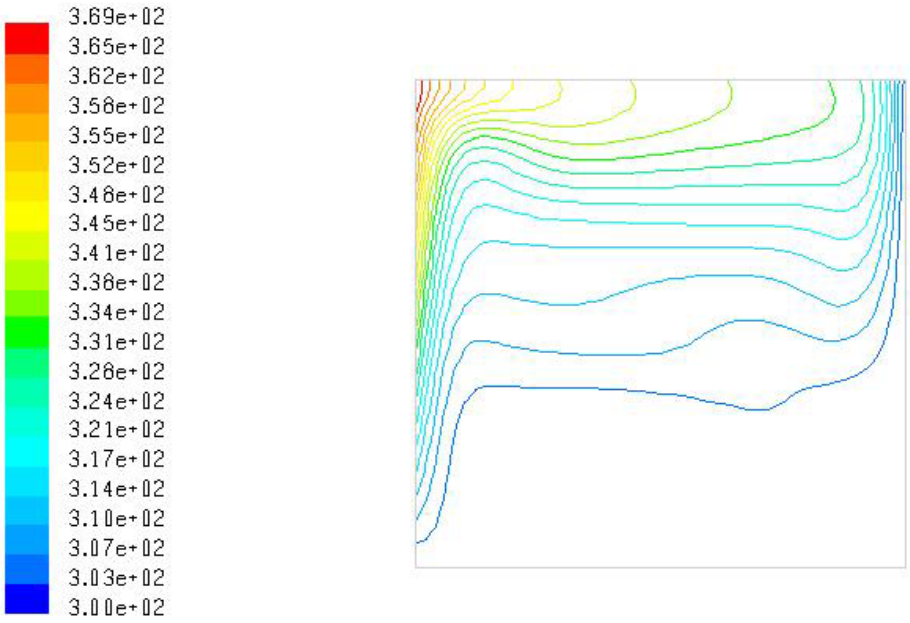

Figure 6.5 Cross sectional temperature contours (K) of air in the rectangular duct at a distance of 1 hydraulic diameter from inlet
(AR = 1, Gr = 1,000,000 , ε = 0.05)

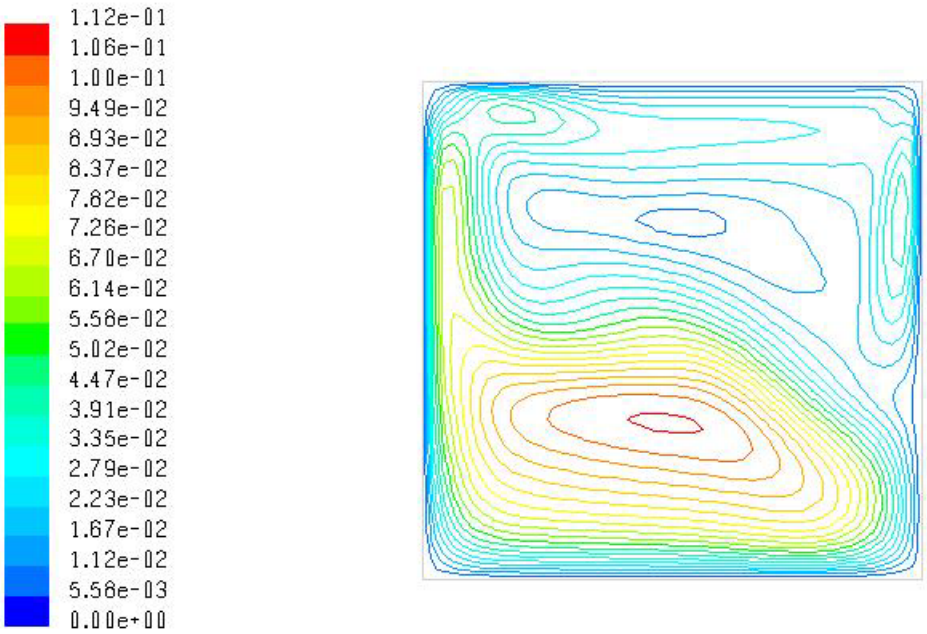

Figure 6.6 Cross sectional velocity contours (m/s) of air in the rectangular duct at a distance of 1 hydraulic diameter from inlet
(AR = 1, Gr = 1,000,000 , ε = 0.05)

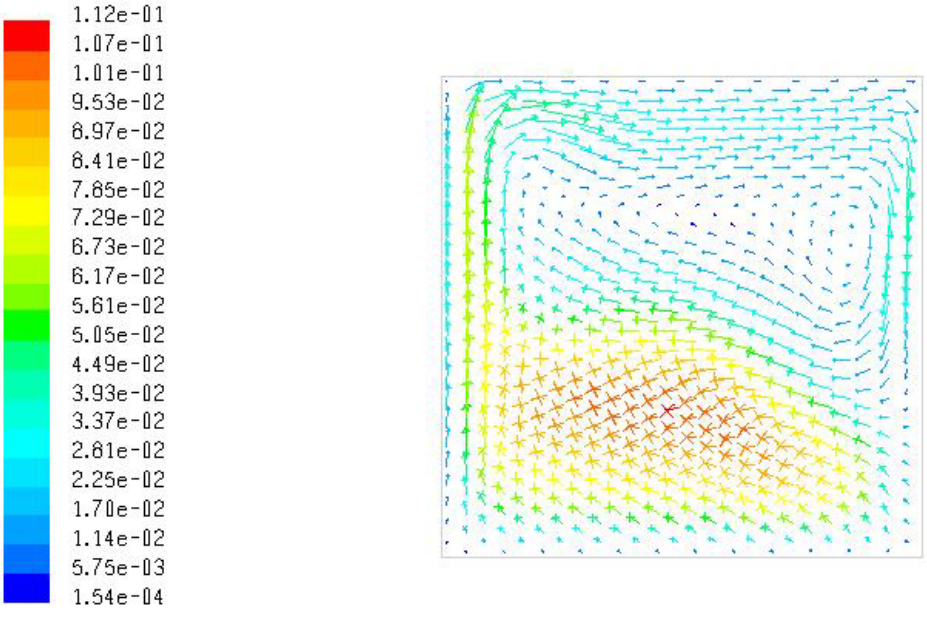

Figure 6.7 Cross sectional velocity vectors (m/s) of air in the rectangular duct at a distance of 1 hydraulic diameter from inlet
(AR = 1, Gr = 1,000,000 , ε = 0.05)

The flow patterns for this configuration are different from the heating configuration CS2. The heating configuration CS2 was found to have regions of

flow separation, where there is no flow separation taking place on CS3. This suggests that the present heating configuration may offer better heat transfer enhancement than heating configuration CS2. The heat transfer characteristics between heating configuration CS2 and CS3 will be compared in a later section.

6.3.2 Radiation Heat Transfer

The effect of radiation heat transfer influences the heat transfer characteristics when wall surface emissivity is equal to 0.85. Figures 6.8 to 6.10 present the variation of transverse average convective Nusselt number at heated wall for different Grashof numbers in the case of wall emissivity equal to 0.85 for the aspect ratios 0.5, 1 and 2, respectively. The convective Nusselt numbers in the figures indicate the transverse average convective heat transfer due to combined forced and natural convection.

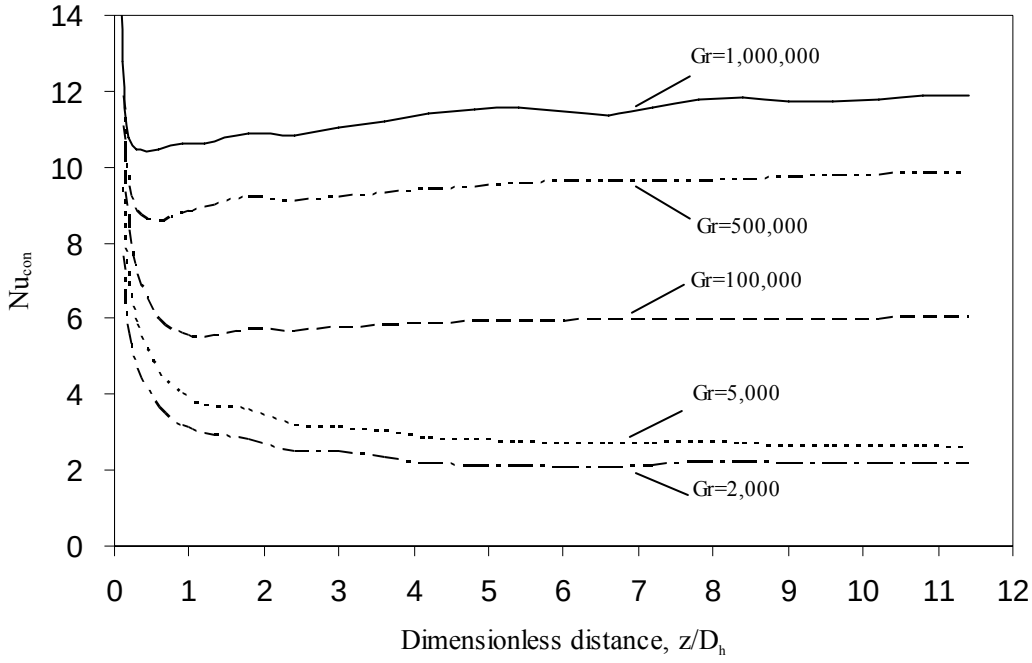

Figure 6.8 Effect of Grashof number on the average convective Nusselt number at heated wall (AR = 0.5, ε = 0.85)

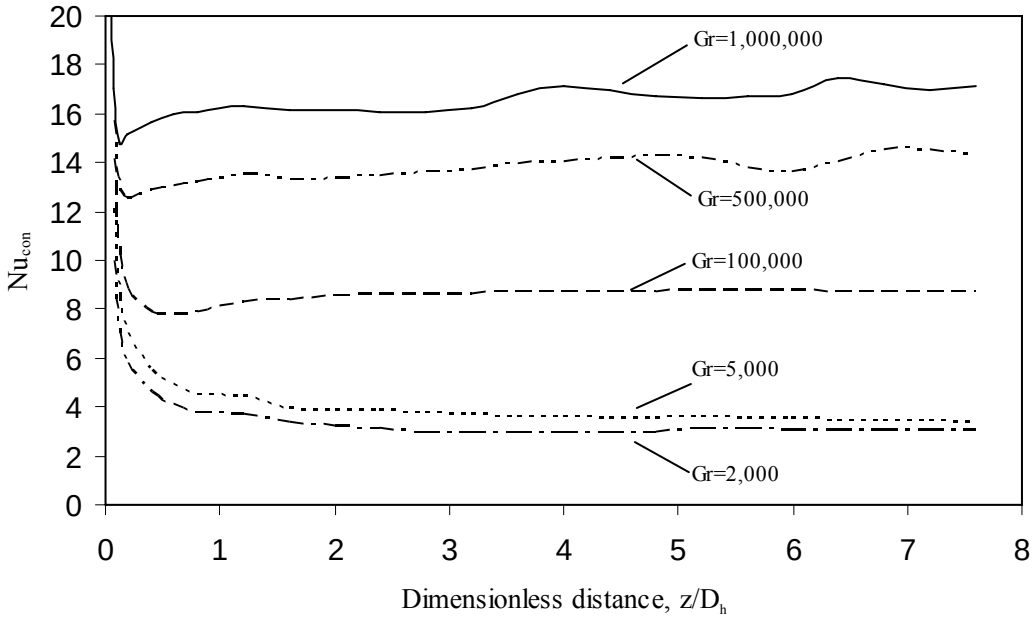

Figure 6.9 Effect of Grashof number on the average convective Nusselt number at heated wall (AR = 1, ε = 0.85)

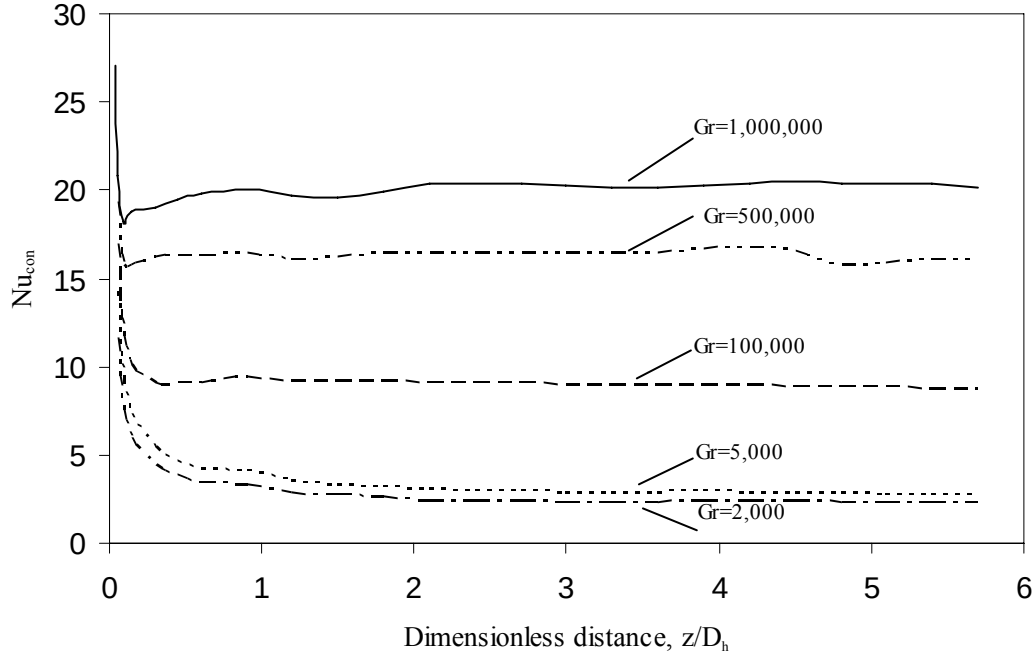

Figure 6.10 Effect of Grashof number on the average convective Nusselt number at heated wall (AR = 2, ε = 0.85)

From the above figures, the patterns and values of convective Nusselt numbers are comparable with the case of low surface emissivity (Figures 6.2 to 6.4).

The heat transfer characteristics of the flow for low and high emissivity cases remain almost the same. However, in the case of Gr = 500,000 and above, the fluctuations of the values of convective Nusselt number can be seen from all aspect ratios. The reason for these fluctuations can be explained on the same explanation as the case CS2, where radiation from the heated wall builds up the temperature on both top and bottom walls. Then, heat is being further transferred to the flow by means of convection heat transfer between the walls and the nearby fluid. The energy transfer at the bottom wall influences the effect of natural convection heat transfer as in the bottom wall heating phenomena. The onset of thermal instability is then noticed downstream from the inlet. However, the fluctuations of the Nusselt number values on configuration CS3 have very slight amplitude. This is because configuration CS3 contains the high temperature regions at the top of the heated wall. The distance between top part and the bottom wall areas reduces radiation intensities, and hence results in only small amount of radiation energy to be transferred to the bottom wall. Therefore, it lessens the effect of bottom wall heating.

For high surface emissivity conditions, the radiative Nusselt number presents the characteristics of radiation heat transfer. Figure 6.11 shows the variation of transverse average radiative Nusselt number (Nu_{rad}) at the heated wall as a function of duct length in the case of AR = 1 and $\varepsilon = 0.85$. Grashof number is varied from the domination influenced by forced convection, to natural convection flow.

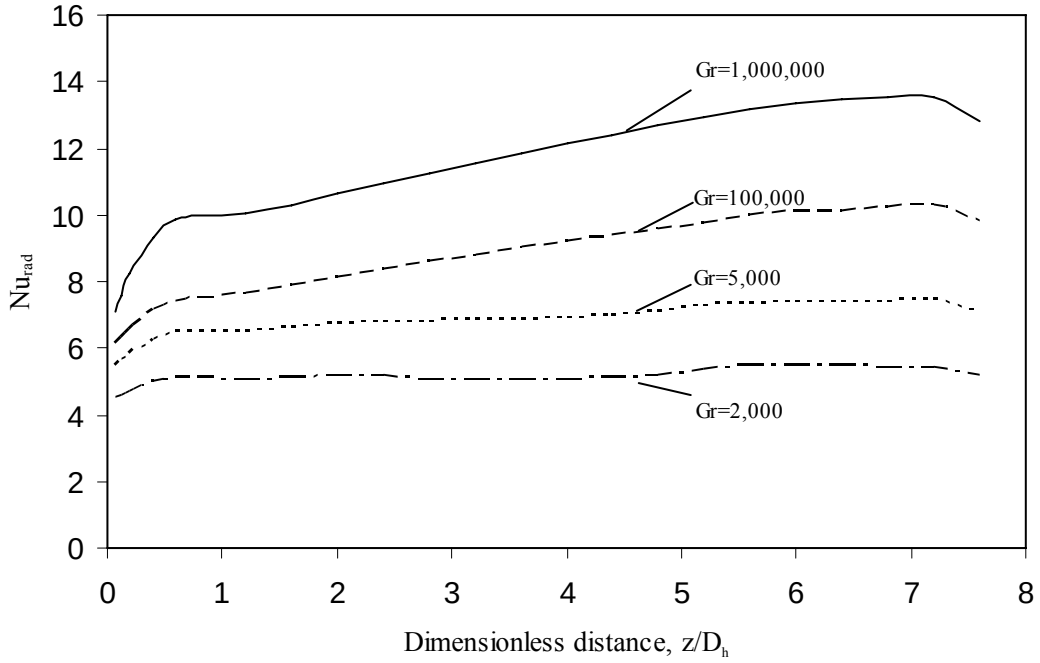

Figure 6.11 Effect of Grashof number on the average radiative Nusselt number at heated wall (AR = 1, $\varepsilon = 0.85$)

The graphs follow the same pattern as in the cases of uniform temperature (CS1) and varying temperature (CS2). Radiative Nusselt number increases slightly along the length of the duct, except only at the areas near the inlet and outlet where each graph increases and decreases respectively at high rates. From the analysis, the radiative heat flux values are almost constant for an entire length of the duct except only at the inlet and outlet where radiative heat flux is lost to the surroundings and makes the slope being changed in the graph of radiative Nusselt number. The slight increment of the graph along most part of duct length is attributed to bulk mean fluid temperature (T_b) values, which are used to calculate the radiative Nusselt number in equation (5-2).

The ratios of convective and radiative Nusselt numbers to the total Nusselt number are presented in Figure 6.12 (i) and (ii). For all high emissivity cases, strong natural convection (high Grashof number) has made convective part to be higher than the radiative part, while strong forced convection (low Grashof number) is dominated by radiation heat transfer.

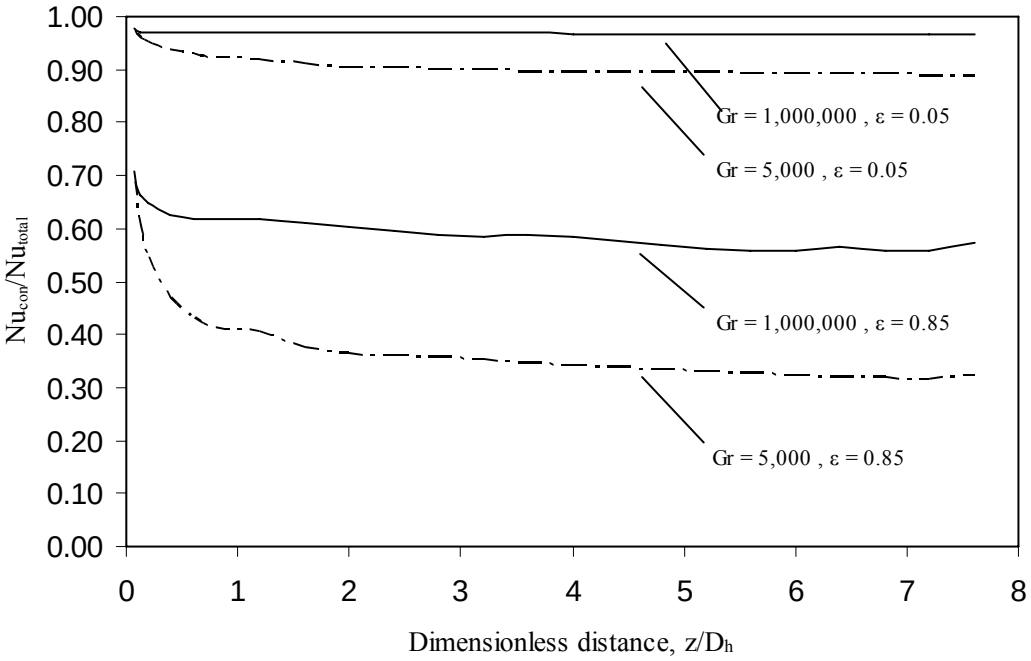

(i)

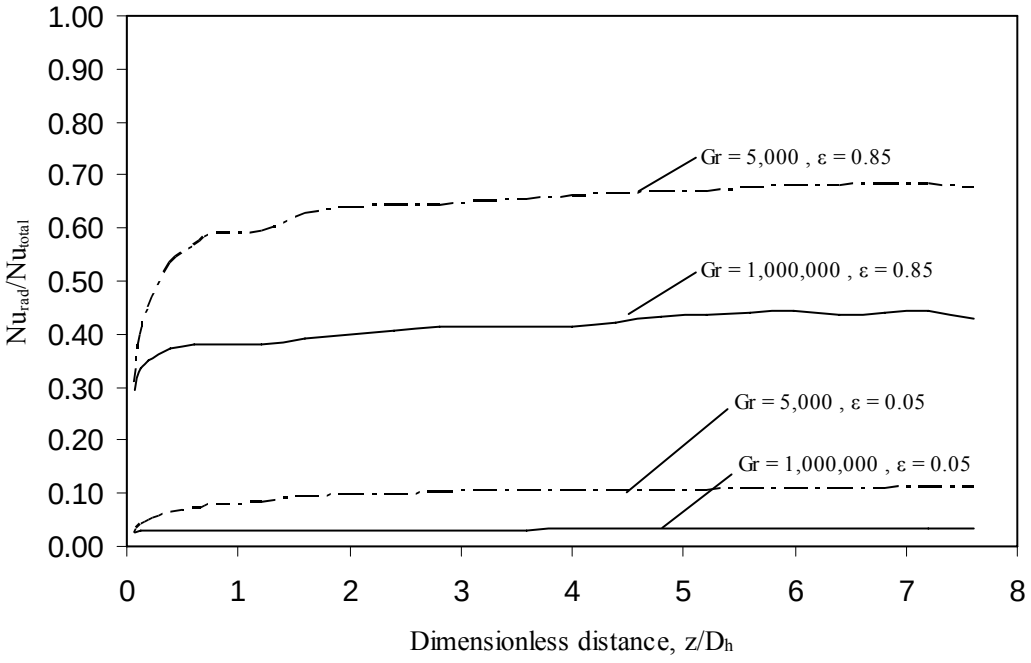

(ii)

Figure 6.12 Ratio of (i) convective to total Nusselt number and (ii) radiative to total Nusselt number (AR = 1)

6.3.3 Duct Aspect Ratio

Generally, higher aspect ratio results in higher of both convective and radiative Nusselt number values. Figure 6.13 shows the difference of transverse average convective Nusselt numbers between each aspect ratio.

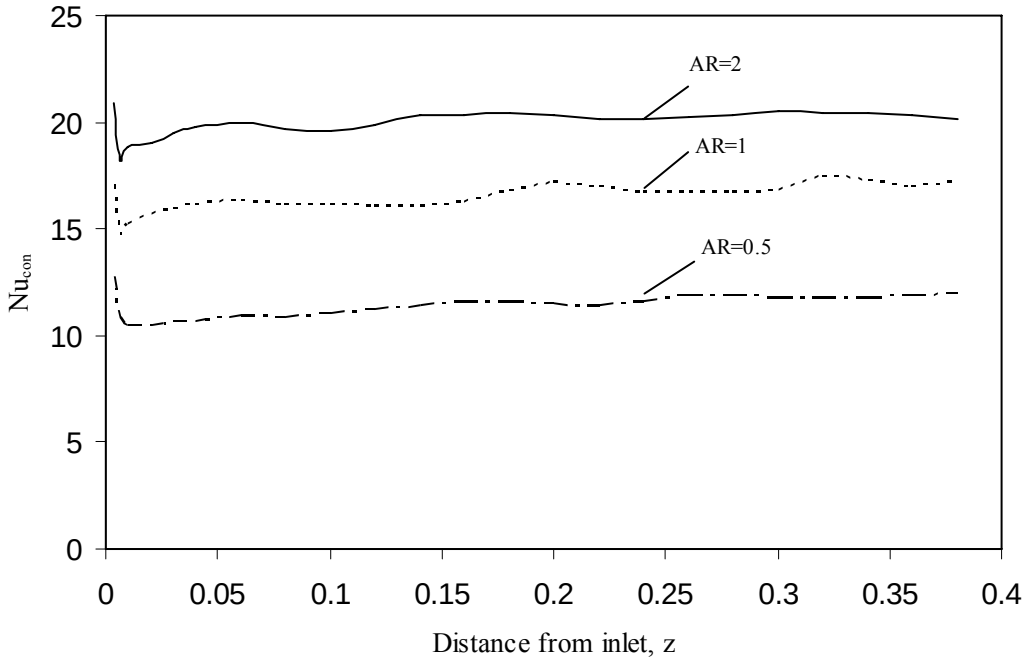

Figure 6.13 Effect of aspect ratio on the average convective Nusselt number at heated wall (Gr = 1,000,000, ε = 0.85)

Like the previous heating configurations, higher aspect ratio means having higher duct volume, and allows more cooling air to flow through it. As a consequence, a higher aspect ratio duct has a better heat transfer rate than a lower aspect ratio duct.

However, for the low value of Grashof number, Nusselt number values of aspect ratio of 1 is found to be higher than those of aspect ratio of 2 for most part of the duct. Figure 6.14 shows the comparison of transverse average convective Nusselt number values at heated wall from three aspect ratios in the case of Gr = 5,000 , and ε = 0.05.

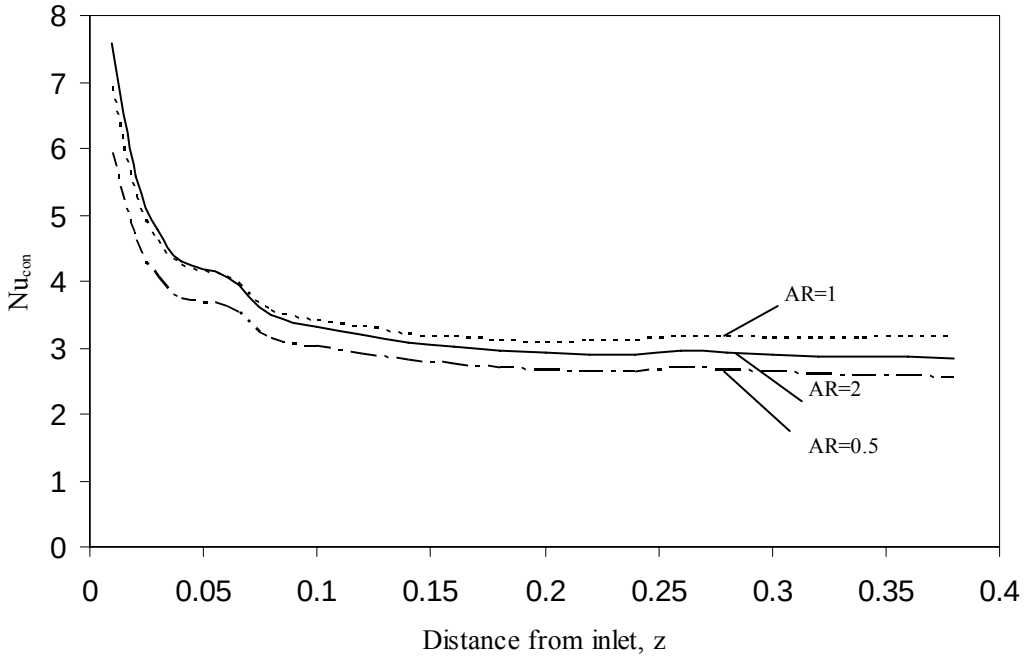

Figure 6.14 Effect of aspect ratio on the average convective Nusselt number at heated wall (Gr = 5,000, ε = 0.05)

6.4 Comparison of Configuration CS3 with CS1 and CS2

6.4.1 Heating Configuration CS1 and CS3

The schematic diagrams of heating configuration CS1 and CS3 are reproduced in Figure 6.15.

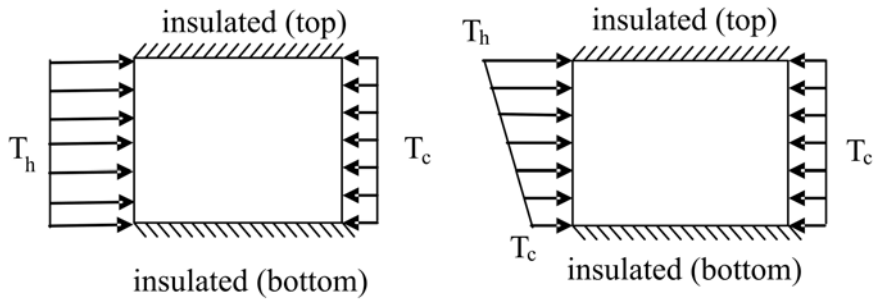

(i) (ii)

Figure 6.15 Schematic diagrams of (i) CS1, and (ii) CS3

The comparison is mainly made for convective Nusselt number. Combined natural and forced convection is the main mechanism that enhances heat transfer in this study. Therefore, it is significant to compare convective heat transfer characteristics between each heating configurations.

Figure 6.16 shows transverse average convective Nusselt numbers for both CS1 and CS3.

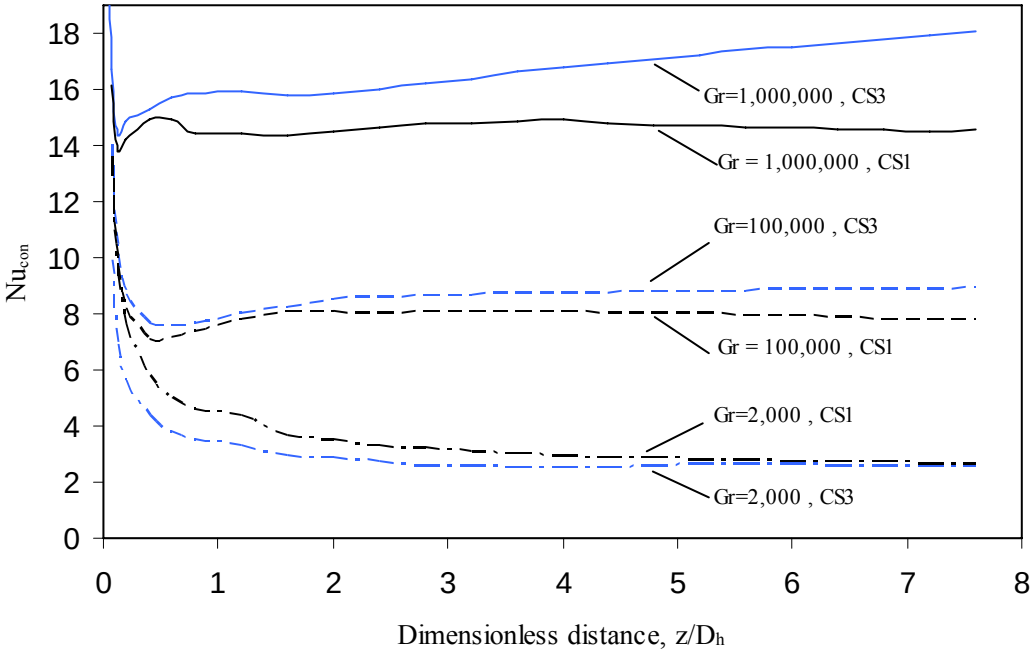

Figure 6.16 Comparison of average convective Nusselt number between heating configuration CS1 and CS3 (AR = 1 and $\varepsilon = 0.05$)

From the above figure, the heating configuration CS3 offers higher convective Nusselt number values than configuration CS1 for flows dominated by natural convection heat transfer. The difference in magnitude of Nusselt number between CS1 and CS3 increases as Grashof number increases. However, when the flow is dominated by forced convection, as in the case of Gr = 2,000, the convective Nusselt number values of configuration CS1 are higher than CS3. This is due to the fact that the main mechanism that drives heat transfer at low Grashof number of CS3 is contributed by radiation heat transfer.

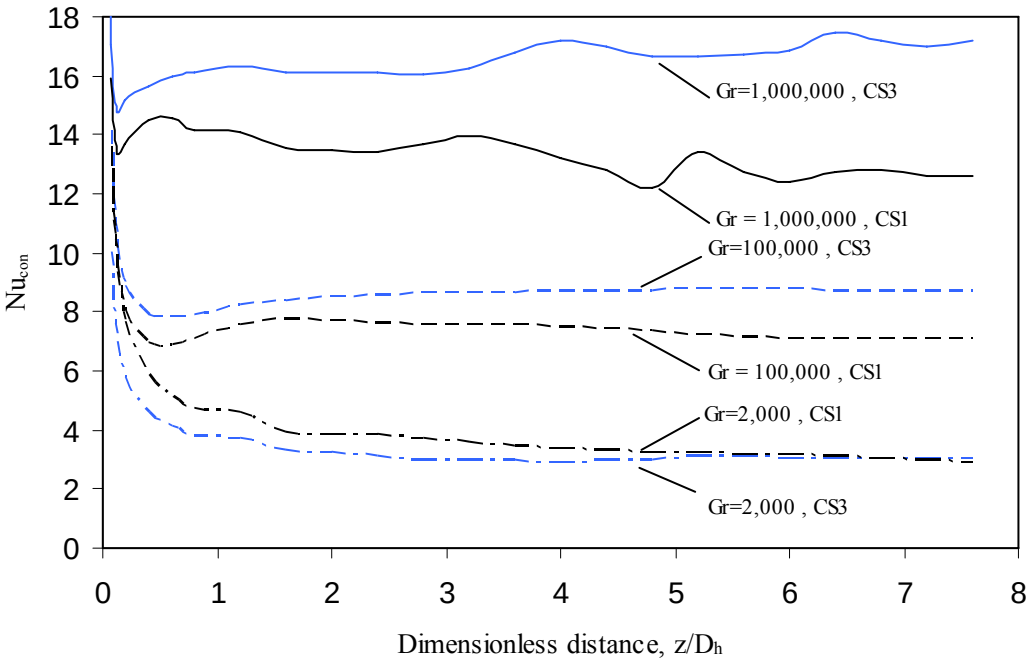

Figure 6.17 Comparison of average convective Nusselt number between heating configuration CS1 and CS3 (AR = 1 and ε = 0.85)

Figure 6.17 presents the variation of the transverse average convective Nusselt number at the heated wall with walls having high surface emissivity (ε = 0.85). Similar to Figure 6.16, the convective Nusselt number values in the case of CS3 are higher than CS1 when the flow is dominated by natural convection. On the other hand, the convective Nusselt number values of CS3 are lower than CS1 when the flow is under low Grashof number.

The effect of bottom wall heating in the case of Grashof equal to 1,000,000 can be seen for both CS1 and CS3 from the fluctuations on the convective Nusselt values. However, configuration CS3 has resulted in lower fluctuation amplitude levels compared to CS1.

When comparing the effect of aspect ratio between CS1 and CS3, Figure 6.18 presents the variation of transverse average convective Nusselt number at heated wall for all aspect ratios in the case of Gr = 1,000,000, and ε = 0.85. The heat transfer characteristics in this figure are dominated by natural convection. From the graphs, it can be seen that the convective Nusselt number values of CS3 are higher than those of CS1 for all aspect ratios. CS3 also results in lower levels of fluctuations than CS1.

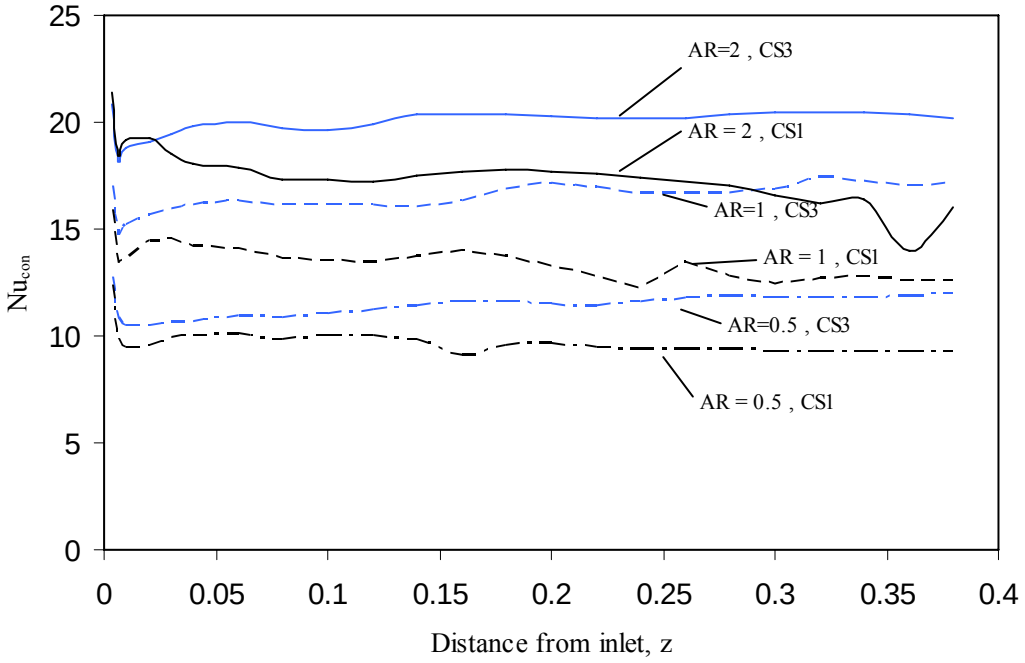

Figure 6.18 Comparison of average convective Nusselt number between heating configuration CS1 and CS3 for different aspect ratios
(Gr = 1,000,000 , ε = 0.85)

6.4.2 Heating Configuration CS2 and CS3

Figure 6.19 illustrates the schematic diagrams that show the heating configurations CS2 and CS3.

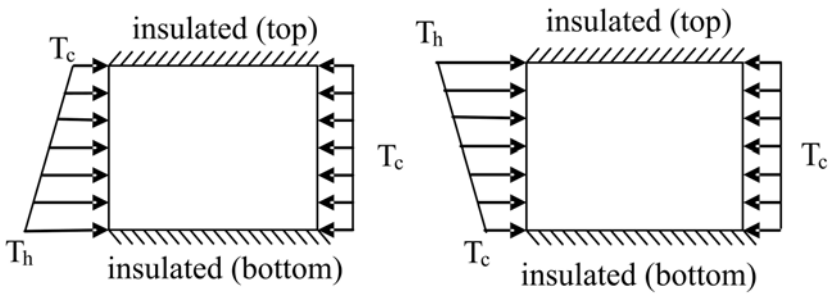

(i) (ii)

Figure 6.19 Schematic diagrams of heating configurations of (i) CS2 and (ii) CS3

Both heating configurations share the same maximum and minimum values of T_h and T_c when they are compared to each other.

Figure 6.20 compares the graphs of transverse average convective Nusselt number between CS2 and CS3 for a set of Grashof numbers with AR = 1, and ε = 0.05.

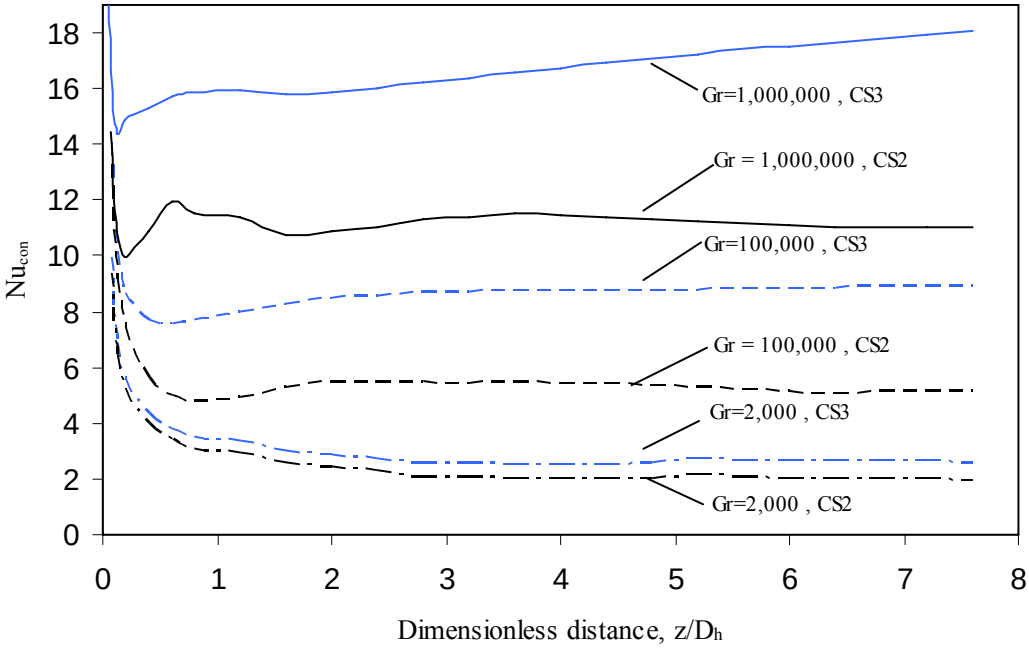

Figure 6.20 Comparison of average convective Nusselt number between heating configuration CS2 and CS3
(AR = 1 and ε = 0.05)

From the figure, it is obvious that the heating configuration CS3 shows better heat transfer than CS2, because all convective Nusselt values of CS3 are higher than CS2 all over the heated wall of the duct. The difference in Nusselt number values between CS2 and CS3 becomes larger for a higher Grashof number. The graph patterns are comparable to each other, except for Gr = 1,000,000, where the convective Nusselt values of CS3 still increase while those of CS2 slightly decrease.

Figure 6.21 compares both configurations at the same conditions as in Figure 6.20 except with emissivity values of 0.85. The Nusselt number fluctuations caused by bottom wall heating effect can be seen in the case of Gr = 1,000,000 for both CS2 and CS3. However, the amplitude of the fluctuations in CS3 is much less than CS2.

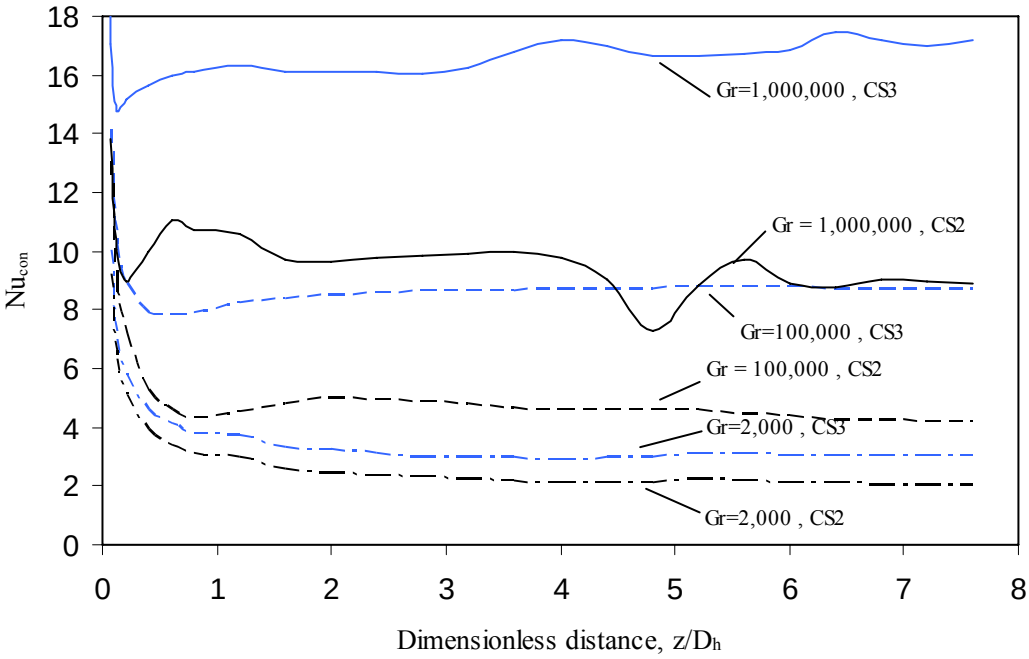

Figure 6.21 Comparison of average convective Nusselt number between heating configuration CS2 and CS3
(AR = 1 and ε = 0.85)

When comparing both heating configurations in terms of aspect ratio, Figure 6.22 shows that the variation of convective Nusselt number at the heated wall of the duct for all aspect ratios. From the graphs, it can be seen that the configuration CS3 offers better heat transfer than CS2 for all aspect ratios. The convective Nusselt number values of CS3 at AR = 1 are even higher than CS2 at AR = 2.

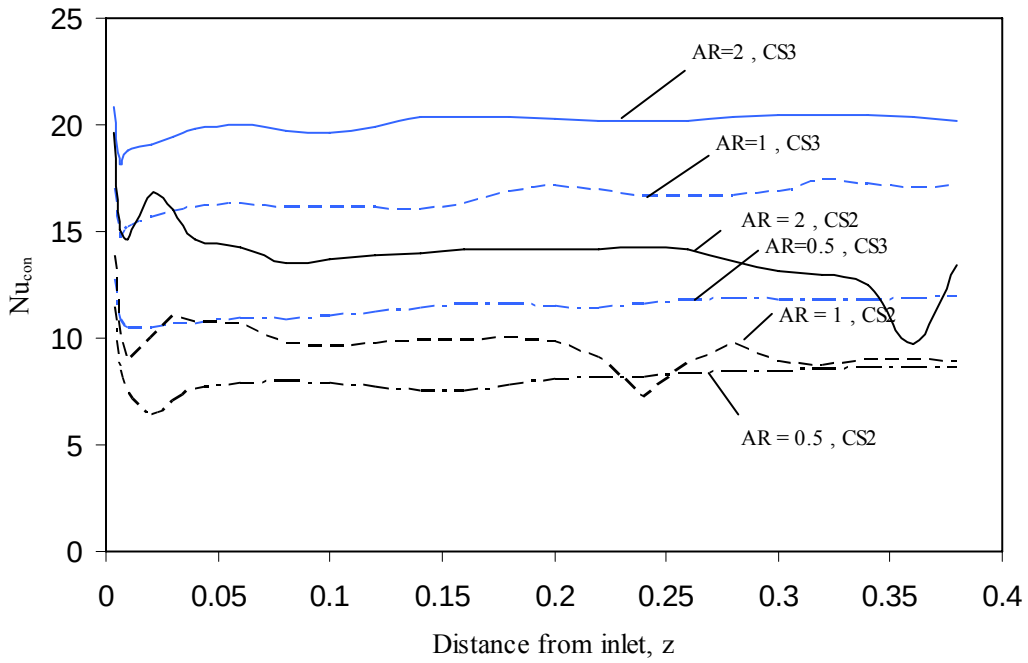

Figure 6.22 Comparison of average convective Nusselt number between heating configuration CS2 and CS3 for different aspect ratios
(Gr = 1,000,000, ε = 0.85)

6.5 Closure

In this chapter, the results and discussion of heating configuration CS3 have been presented. The discussion included the effect of considering the flow condition from forced convection-dominated to natural convection-dominated flow, the effect of interaction of the surface radiation heat transfer to the flow, and the influence of duct aspect ratio. A series of graphs containing variation of both convective and radiative Nusselt numbers under some selected important conditions have been presented throughout the chapter to show the relative importance of each of the effects on the heat transfer characteristics of the flow.

Comparison of the heat transfer characteristics of heating configuration CS3 has also been made with heating configuration CS1 and CS2. It has given a clear picture of what is different between them in terms of the heat transfer performance. This completes the results and discussion on case study CS3.

In the next chapter, conclusions of the entire work done will be presented.

CHAPTER 7
CONCLUSIONS

7.1 Introduction

A detailed analysis of three heating configurations was presented in Chapters 4, 5 and 6. The emphasis was on the heat transfer characteristics of flow in the duct influenced by combined forced and natural convection heat transfer, radiation heat transfer, and duct aspect ratio. The results and discussion presented in the earlier chapters are concluded in this chapter. The significant conclusions from the present work are presented in the next section followed by suggestions for future work.

The present study applied a numerical approach to solve the problem of laminar airflow in a differentially-heated horizontal rectangular duct in the presence of convection and radiation heat transfer. The formulated numerical model successfully solved the three case study problems, and provided valuable results which were analysed and discussed in this study. The conclusions for all the three cases are given below.

7.2 Conclusions

7.2.1 Uniform Wall Temperature Heating (CS1)

It was found that the effect of natural convection heat transfer in the mixed convection region helps promote overall heat transfer enhancement. The heat transfer enhancement occurs irrespective of whether the flow is under strong or weak radiation heat transfer. The amount of enhancement depends on the levels of temperature difference between the two heated vertical walls.

For certain cases, the effect of radiation heat transfer influences the convective heat transfer characteristics on the heated wall by inducing the bottom wall heating effect, which results in fluctuations on heat transfer. It occurs when temperature difference between the heated and cooled walls are sufficiently high. In the present study, radiation heat transfer becomes important when Grashof number is 500,000 and above.

The duct aspect ratio affects the heat transfer rates on the heated wall. A higher duct aspect ratio provides a higher heat transfer rate than a lower duct aspect ratio.

7.2.2 Linearly Varying Wall Temperature Heating (CS2 and CS3)

Under the linearly varying wall temperature heating condition, two heating configurations were studied. The following are the conclusions for both types:

The effect of natural convection heat transfer enhances the heat transfer rates on the heated wall for both CS2 and CS3. The heat transfer enhancement occurs for both strong and weak radiation conditions as long as mixed convection is dominated by natural convection heat transfer. CS2 has less heat transfer enhancement compared to CS3 due to its flow separation behaviour.

For both configurations, strong radiation heat transfer creates fluctuations on the convective heat transfer coefficient when Grashof number is high. Otherwise, the convective heat transfer coefficients have comparable characteristics for both strong and weak radiation effect. Between the two types, CS3 has less fluctuation.

In general, increasing the duct aspect ratio results in having higher heat transfer rates. However, for conditions when the flow is dominated more by forced convection heat transfer (low Grashof number), increasing the duct aspect ratio does not help enhance heat transfer.

Heating configuration CS3 offers better heat transfer rates than heating configuration CS2. Moreover, CS3 has the benefit of having lower heat transfer fluctuations. It can be concluded that heating configuration CS3 offers the best heat transfer performance between the two variable wall temperature heating cases considered in the present study.

7.2.3 Heating Configurations CS1 and CS3

Even though the total heat transfer rate for CS1 is higher than CS3, when considering in terms of dimensionless parameter, CS3 has higher Nusselt number values than CS1. Furthermore, CS3 has less effect from radiation-induced bottom

wall heating. Therefore, CS3 has promising heat transfer characteristics in terms of heat transfer enhancement over CS1, especially for conditions where radiation effect is significant.

7.3 Suggestions for Future Work

The present study considered only a linear variation of wall temperature along the heated wall. Future studies can be conducted using various types of temperature profiles, for instance, polynomial, exponential, or sinusoidal profiles. This would help extend the knowledge of the effect of variable heating profiles to some applications, because isothermal wall is quite an ideal situation in real world applications. In addition to the variable temperature profiles, variable heat flux profiles can also be part of the study.

The Grashof number was defined based on previous studies reported in published literature. However, this definition of Grashof number only provides an approximate value, which is not capable of fully reflecting the real physical meaning of the natural convection effect associated in Grashof number for a varying wall temperature. A further study is required to give more meaningful definition on how to define Grashof number in the case of variable heating.

REFERENCES

[1] E. Naito *Laminar heat transfer in the entrance region between parallel plates - the case of uniform heat flux*, Heat Transfer - Japan. Res., 4 (1975), pp. 63-74.

[2] H. Ozoe, H. Sayama and S. W. Churchill, *Natural convection in an inclined rectangular channel at various aspect ratios and angles-experimental measurements*, International Journal of Heat and Mass Transfer, 18 (1975), pp. 1425-1431.

[3] J. R. Maughan and F. P. Incropera, *Experiments on mixed convection heat transfer for airflow in a horizontal and inclined channel*, International Journal of Heat and Mass Transfer, 30 (1987), pp. 1307-1318.

[4] Kuan-Cheng Chiu and F. Rosenberger, *Mixed convection between horizontal plates-I. Entrance effects*, International Journal of Heat and Mass Transfer, 30 (1987), pp. 1645-1654.

[5] Kuan-Cheng Chiu, J. Ouazzani and F. Rosenberger, *Mixed convection between horizontal plates-II. Fully developed flow*, International Journal of Heat and Mass Transfer, 30 (1987), pp. 1655-1662.

[6] R. Smyth and Y. K. Salman, *Combined free and forced convection heat transfer in a rectangular duct*, International Communications in Heat and Mass Transfer, 18 (1991), pp. 669-680.

[7] T. A. Nyce, J. Ouazzani, A. Durand-Daubin and F. Rosenberger, *Mixed convection in a horizontal rectangular channel-experimental and numerical velocity distributions*, International Journal of Heat and Mass Transfer, 35 (1992), pp. 1481-1494.

[8] C. C. Huang and T. F. Lin, *Buoyancy induced flow transition in mixed convective flow of air through a bottom heated horizontal rectangular duct*, International Journal of Heat and Mass Transfer, 37 (1994), pp. 1235-1255.

[9] W. M. Yan, *Combined buoyancy effects of thermal and mass diffusion on laminar forced convection in horizontal rectangular ducts*, International Journal of Heat and Mass Transfer, 39 (1996), pp. 1479-1488.

[10] W. L. Lin and T. F. Lin, *Experimental study of unstable mixed convection of air in a bottom heated horizontal rectangular duct*, International Journal of Heat and Mass Transfer, 39 (1996), pp. 1649-1663.

[11] M. Corcione, *Effects of the thermal boundary conditions at the sidewalls upon natural convection in rectangular enclosures heated from below and cooled from above*, International Journal of Thermal Sciences, 42 (2003), pp. 199-208.

[12] Q. Wang, H. Yoo and Y. Jaluria, *Convection in a horizontal rectangular duct under constant and variable property formulations*, International Journal of Heat and Mass Transfer, 46 (2003), pp. 297-310.

[13] J. J. M. Sillekens, C. C. M. Rindt and A. A. van Steenhoven, *Development of laminar mixed convection in a horizontal square channel with heated side walls*, International Journal of Heat and Fluid Flow, 19 (1998), pp. 270-281.

[14] C. Gau, Y. C. Jeng and C. G. Liu, *An experimental study on mixed convection in a horizontal rectangular channel heated from a side*, Transactions of the ASME Journal of Heat Transfer, 122 (2000), pp. 701-707.

[15] J. R. Maughan and F. P. Incropera, *Regions of heat transfer enhancement for laminar mixed convection in a parallel plate channel*, International Journal of Heat and Mass Transfer, 33 (1990), pp. 555-570.

[16] K. H. Im and R. K. Ahluwalia, *Combined convection and radiation in rectangular ducts*, International Journal of Heat and Mass Transfer, 27 (1984), pp. 221-231.

[17] J. M. Huang , J. D. Lin and F. C. Chou, *Combined radiation and laminar mixed convection in the thermal entrance region of horizontal isothermal rectangular channels*, Numerical Heat Transfer, Part A, 18 (1990), pp. 113-125.

[18] G. Yang, M. A. Ebadian and A. Campo, *A numerical study of convective and radiative transfer in ducts of rectangular and equilateral cross sections*, International Journal of Heat and Mass Transfer, 34 (1991), pp. 1319-1322.

[19] G. Yang and M. A. Ebadian, *Analysis of heat transfer in arbitrary shaped ducts: Interaction of forced convection and radiation*, International Communications in Heat and Mass Transfer, 19 (1992), pp. 103-115.

[20] A. S. Krishnan, C. Balaji and S. P. Venkateshan, *An Experimental Correlation for Combined Convection and Radiation Between Parallel Vertical Plates*, ASME Journal of Heat Transfer, 126 (2004), pp. 849-851.

[21] S. Ostrach, *Combined natural and forced convection laminar flow and heat transfer of fluids with and without heat sources in channels with linearly varying wall temperatures*, National Advisory Committee for Aeronautics, Technical note 3141 (1954).

[22] T. S. Chen, H. C. Tien and B. F. Armaly, *Natural convection on horizontal, inclined, and vertical plates with variable surface temperature or heat flux*, International Journal of Heat and Mass Transfer, 29 (1986), pp. 1465-1478.

[23] T. Basak, S. Roy and A. R. Balakrishnan, *Effects of thermal boundary conditions on natural convection flows within a square cavity*, International Journal of Heat and Mass Transfer, 49 (2006), pp. 4525-4535.

[24] G. Colomer, M. Costa, R. Consul and A. Oliva, *Three-dimensional numerical simulation of convection and radiation in a differentially heated cavity using the discrete ordinates method*, International Journal of Heat and Mass Transfer, 47 (2004), pp. 257-269.

[25] S. M. Marco and L. S. Han, *A note on limiting laminar Nusselt number in ducts with constant temperature gradient by analogy to thin-plate theory*, ASME Journal of Heat Transfer, 77 (1995), pp. 625-630.

[26] A. Bejan, *Mass and heat transfer by natural convection in a vertical cavity*, International Journal of Heat and Fluid Flow, 6 (1985), pp. 149-159.

[27] GAMBIT 2.2 User's Guide, Fluent Inc., Lebanon, NH, 2004.

[28] FLUENT 6.1 User's Guide, Fluent Inc., Lebanon, NH, 2003.

[29] F. P. Incropera, *Introduction to Heat Transfer*, 4th Edition, John Wiley & Sons Inc., New York, 2002, pp. 831.

[30] J. D. Anderson Jr., *Computational Fluid Dynamics, The Basics with Applications*, McGraw-Hill Inc., Singapore, 1995.

[31] A. Bejan, *Heat Transfer*, John Wiley & Sons, Inc., New York, 1993, pp. 299-302.

[32] R. Siegel and J. R. Howell, *Thermal Radiation Heat Transfer*, Hemisphere, Washington, DC, 1992, pp. 421-422.

[33] S. V. Patankar, *Numerical Heat Transfer and Fluid Flow*, Hemisphere, Washington, DC, 1980.

[34] M. N. Ozisik, *Radiative Transfer*, John Wiley & Sons Inc., New York, 1973.

APPENDIX 1 MATRIX OF PARAMETERS

APPENDIX 1
MATRIX OF PARAMETERS

Duct Length 400 mm

Density of air at 300 K (inlet) [29] 1.1614 kg/m^3

Kinematic viscosity of air at 300 K (inlet) [29] 1.589×10^{-5} m^2/s

Heating configuration CS1

Case No.	Aspect Ratio	Duct Height(mm)	Duct Width(mm)	D_h(mm)	Re	Mean inlet Velocity(m/s)	Gr/Re^2	Gr	Heated wall temp(K)	Cooled wall temp(K)	Emissivity
AR=0.5											
1	0.5	50	25	33.33	100	0.048	0	0	300.000	300	0.05
2	0.5	50	25	33.33	100	0.048	0	0	300.000	300	0.85
3	0.5	50	25	33.33	100	0.048	0.2	2000	300.124	300	0.05
4	0.5	50	25	33.33	100	0.048	0.2	2000	300.124	300	0.85
5	0.5	50	25	33.33	100	0.048	0.5	5000	300.309	300	0.05
6	0.5	50	25	33.33	100	0.048	0.5	5000	300.309	300	0.85
7	0.5	50	25	33.33	100	0.048	10	100000	306.239	300	0.05
8	0.5	50	25	33.33	100	0.048	10	100000	306.239	300	0.85
9	0.5	50	25	33.33	100	0.048	50	500000	332.585	300	0.05
10	0.5	50	25	33.33	100	0.048	50	500000	332.585	300	0.85
11	0.5	50	25	33.33	100	0.048	70	700000	346.599	300	0.05
12	0.5	50	25	33.33	100	0.048	70	700000	346.599	300	0.85
13	0.5	50	25	33.33	100	0.048	100	1000000	368.773	300	0.05
14	0.5	50	25	33.33	100	0.048	100	1000000	368.773	300	0.85
AR=1											
15	1	50	50	50.00	100	0.032	0	0	300.000	300	0.05
16	1	50	50	50.00	100	0.032	0	0	300.000	300	0.85

Case No.	Aspect Ratio	Duct Height(mm)	Duct Width(mm)	D_h(mm)	Re	Mean inlet Velocity(m/s)	Gr/Re^2	Gr	Heated wall temp(K)	Cooled wall temp(K)	Emissivity
17	1	50	50	50.00	100	0.032	0.2	2000	300.124	300	0.05
18	1	50	50	50.00	100	0.032	0.2	2000	300.124	300	0.85
19	1	50	50	50.00	100	0.032	0.5	5000	300.309	300	0.05
20	1	50	50	50.00	100	0.032	0.5	5000	300.309	300	0.85
21	1	50	50	50.00	100	0.032	10	100000	306.239	300	0.05
22	1	50	50	50.00	100	0.032	10	100000	306.239	300	0.85
23	1	50	50	50.00	100	0.032	50	500000	332.585	300	0.05
24	1	50	50	50.00	100	0.032	50	500000	332.585	300	0.85
25	1	50	50	50.00	100	0.032	70	700000	346.599	300	0.05
26	1	50	50	50.00	100	0.032	70	700000	346.599	300	0.85
27	1	50	50	50.00	100	0.032	100	1000000	368.773	300	0.05
28	1	50	50	50.00	100	0.032	100	1000000	368.773	300	0.85
AR=2											
29	2	50	100	66.67	100	0.024	0	0	300.000	300	0.05
30	2	50	100	66.67	100	0.024	0	0	300.000	300	0.85
31	2	50	100	66.67	100	0.024	0.2	2000	300.124	300	0.05
32	2	50	100	66.67	100	0.024	0.2	2000	300.124	300	0.85
33	2	50	100	66.67	100	0.024	0.5	5000	300.309	300	0.05
34	2	50	100	66.67	100	0.024	0.5	5000	300.309	300	0.85
35	2	50	100	66.67	100	0.024	10	100000	306.239	300	0.05
36	2	50	100	66.67	100	0.024	10	100000	306.239	300	0.85
37	2	50	100	66.67	100	0.024	50	500000	332.585	300	0.05
38	2	50	100	66.67	100	0.024	50	500000	332.585	300	0.85
39	2	50	100	66.67	100	0.024	70	700000	346.599	300	0.05
40	2	50	100	66.67	100	0.024	70	700000	346.599	300	0.85
41	2	50	100	66.67	100	0.024	100	1000000	368.773	300	0.05
42	2	50	100	66.67	100	0.024	100	1000000	368.773	300	0.85

Heating configuration CS2

Case No.	Aspect Ratio	Duct Height(mm)	Duct Width(mm)	D_h(mm)	Re	Mean inlet Velocity(m/s)	Gr/Re^2	Gr	Heated wall max. temp(K)	Heated wall min. temp(K)	Emissivity
AR=0.5											
43	0.5	50	25	33.33	100	0.048	0.2	2000	300.124	300	0.05
44	0.5	50	25	33.33	100	0.048	0.2	2000	300.124	300	0.85
45	0.5	50	25	33.33	100	0.048	0.5	5000	300.309	300	0.05
46	0.5	50	25	33.33	100	0.048	0.5	5000	300.309	300	0.85
47	0.5	50	25	33.33	100	0.048	10	100000	306.239	300	0.05
48	0.5	50	25	33.33	100	0.048	10	100000	306.239	300	0.85
49	0.5	50	25	33.33	100	0.048	50	500000	332.585	300	0.05
50	0.5	50	25	33.33	100	0.048	50	500000	332.585	300	0.85
51	0.5	50	25	33.33	100	0.048	70	700000	346.599	300	0.05
52	0.5	50	25	33.33	100	0.048	70	700000	346.599	300	0.85
53	0.5	50	25	33.33	100	0.048	100	1000000	368.773	300	0.05
54	0.5	50	25	33.33	100	0.048	100	1000000	368.773	300	0.85
AR=1											
55	1	50	50	50.00	100	0.032	0.2	2000	300.124	300	0.05
56	1	50	50	50.00	100	0.032	0.2	2000	300.124	300	0.85
57	1	50	50	50.00	100	0.032	0.5	5000	300.309	300	0.05
58	1	50	50	50.00	100	0.032	0.5	5000	300.309	300	0.85
59	1	50	50	50.00	100	0.032	10	100000	306.239	300	0.05
60	1	50	50	50.00	100	0.032	10	100000	306.239	300	0.85
61	1	50	50	50.00	100	0.032	50	500000	332.585	300	0.05
62	1	50	50	50.00	100	0.032	50	500000	332.585	300	0.85
63	1	50	50	50.00	100	0.032	70	700000	346.599	300	0.05
64	1	50	50	50.00	100	0.032	70	700000	346.599	300	0.85
65	1	50	50	50.00	100	0.032	100	1000000	368.773	300	0.05
66	1	50	50	50.00	100	0.032	100	1000000	368.773	300	0.85

Case No.	Aspect Ratio	Duct Height(mm)	Duct Width(mm)	D_h(mm)	Re	Mean inlet Velocity(m/s)	Gr/Re^2	Gr	Heated wall max. temp(K)	Heated wall min. temp(K)	Emissivity
AR=2											
67	2	50	100	66.67	100	0.024	0.2	2000	300.124	300	0.05
68	2	50	100	66.67	100	0.024	0.2	2000	300.124	300	0.85
69	2	50	100	66.67	100	0.024	0.5	5000	300.309	300	0.05
70	2	50	100	66.67	100	0.024	0.5	5000	300.309	300	0.85
71	2	50	100	66.67	100	0.024	10	100000	306.239	300	0.05
72	2	50	100	66.67	100	0.024	10	100000	306.239	300	0.85
73	2	50	100	66.67	100	0.024	50	500000	332.585	300	0.05
74	2	50	100	66.67	100	0.024	50	500000	332.585	300	0.85
75	2	50	100	66.67	100	0.024	70	700000	346.599	300	0.05
76	2	50	100	66.67	100	0.024	70	700000	346.599	300	0.85
77	2	50	100	66.67	100	0.024	100	1000000	368.773	300	0.05
78	2	50	100	66.67	100	0.024	100	1000000	368.773	300	0.85

Heating configuration CS3

Case No.	Aspect Ratio	Duct Height(mm)	Duct Width(mm)	D_h(mm)	Re	Mean inlet Velocity(m/s)	Gr/Re^2	Gr	Heated wall max. temp(K)	Heated wall min. temp(K)	Emissivity
AR=0.5											
79	0.5	50	25	33.33	100	0.048	0.2	2000	300.124	300	0.05
80	0.5	50	25	33.33	100	0.048	0.2	2000	300.124	300	0.85
81	0.5	50	25	33.33	100	0.048	0.5	5000	300.309	300	0.05
82	0.5	50	25	33.33	100	0.048	0.5	5000	300.309	300	0.85
83	0.5	50	25	33.33	100	0.048	10	100000	306.239	300	0.05
84	0.5	50	25	33.33	100	0.048	10	100000	306.239	300	0.85
85	0.5	50	25	33.33	100	0.048	50	500000	332.585	300	0.05
86	0.5	50	25	33.33	100	0.048	50	500000	332.585	300	0.85
87	0.5	50	25	33.33	100	0.048	70	700000	346.599	300	0.05
88	0.5	50	25	33.33	100	0.048	70	700000	346.599	300	0.85
89	0.5	50	25	33.33	100	0.048	100	1000000	368.773	300	0.05
90	0.5	50	25	33.33	100	0.048	100	1000000	368.773	300	0.85
AR=1											
91	1	50	50	50.00	100	0.032	0.2	2000	300.124	300	0.05
92	1	50	50	50.00	100	0.032	0.2	2000	300.124	300	0.85
93	1	50	50	50.00	100	0.032	0.5	5000	300.309	300	0.05
94	1	50	50	50.00	100	0.032	0.5	5000	300.309	300	0.85
95	1	50	50	50.00	100	0.032	10	100000	306.239	300	0.05
96	1	50	50	50.00	100	0.032	10	100000	306.239	300	0.85
97	1	50	50	50.00	100	0.032	50	500000	332.585	300	0.05
98	1	50	50	50.00	100	0.032	50	500000	332.585	300	0.85
99	1	50	50	50.00	100	0.032	70	700000	346.599	300	0.05
100	1	50	50	50.00	100	0.032	70	700000	346.599	300	0.85
101	1	50	50	50.00	100	0.032	100	1000000	368.773	300	0.05
102	1	50	50	50.00	100	0.032	100	1000000	368.773	300	0.85

Case No.	Aspect Ratio	Duct Height(mm)	Duct Width(mm)	D_h(mm)	Re	Mean inlet Velocity(m/s)	Gr/Re^2	Gr	Heated wall max. temp(K)	Heated wall min. temp(K)	Emissivity
AR=2											
103	2	50	100	66.67	100	0.024	0.2	2000	300.124	300	0.05
104	2	50	100	66.67	100	0.024	0.2	2000	300.124	300	0.85
105	2	50	100	66.67	100	0.024	0.5	5000	300.309	300	0.05
106	2	50	100	66.67	100	0.024	0.5	5000	300.309	300	0.85
107	2	50	100	66.67	100	0.024	10	100000	306.239	300	0.05
108	2	50	100	66.67	100	0.024	10	100000	306.239	300	0.85
109	2	50	100	66.67	100	0.024	50	500000	332.585	300	0.05
110	2	50	100	66.67	100	0.024	50	500000	332.585	300	0.85
111	2	50	100	66.67	100	0.024	70	700000	346.599	300	0.05
112	2	50	100	66.67	100	0.024	70	700000	346.599	300	0.85
113	2	50	100	66.67	100	0.024	100	1000000	368.773	300	0.05
114	2	50	100	66.67	100	0.024	100	1000000	368.773	300	0.85